NUMERICAL IMPLEMENTATION AND MODELING OF EARTHQUAKE INDUCED LANDSLIDES FOR SLOPES WITH SOFT AND SENSITIVE CLAY LAYERS

by

© **NAVEEL ISLAM**

A thesis submitted to the

School of Graduate Studies

in partial fulfillment of the requirements for the degree of

Master of Engineering (Civil)

Faculty of Engineering and Applied Science

Memorial University of Newfoundland

May, 2017

St. John's   Newfoundland and Labrador   Canada

ABSTRACT

Earthquake induced landslides pose a significant threat to many communities, environment and infrastructure. The potential damages could be severe in sensitive clay slope failures because the post-peak softening behaviour could cause retrogressive failure of soil blocks resulting in large-scale landslides. The failed soil blocks generally displace over a large distance during earthquake and post-quake stages. Therefore, upslope retrogression and downslope runout are two important phenomena need to be studied for better understanding of risks associated with landslides in sensitive clays.

The traditional limit equilibrium methods, commonly used in slope stability analysis, cannot model retrogressive failure or deformation of slopes. The present study concentrates on development of large deformation finite element (FE) models using a Coupled Eulerian-Lagrangian (CEL) approach to simulate the failure of soft and sensitive clay slopes triggered by earthquakes. Analyses are performed for pseudostatic and dynamic loading conditions modeling the undrained behaviour of clay as elasto-plastic material with and without post-peak degradation of shear strength. A nonlinear post-peak strength degradation model as a function of accumulated plastic shear strain is implemented in FE analysis. In addition to CEL, FE analyses are performed using Lagrangian-based FE techniques to show the advantages of CEL to simulate large landslides. The CEL approach can successfully simulate the formation of shear bands (zone of accumulated shear strains), type of failure commonly observed after earthquake, upslope retrogression and downslope runout for varying geometry and soil properties.

ACKNOWLEDGEMENTS

Table of Contents

List of Figures

List of Tables

List of Symbols

As the thesis is written in manuscript format, list of symbols or notations used in the study are listed at the end of Chapter 3 and 4.

Chapter 1

Introduction

1.1   General

Historical records and case studies indicate that numerous large scale landslides can be triggered by earthquakes that may sometimes extend over vast areas. For example, the 1663 Charlevoix earthquake (magnitude M_M greater than 7), Québec in eastern Canada triggered large earthflows in sensitive clay that extended over a wide region of the Saguenay Fjord basin (Desjardins, 1980; Filion et. al., 1991; Syvitski and Schafer, 1996). In general, large-scale earthflows or flowslide type landslides begin with an initial rotational slide followed by succession of rapid rotational failures under undrained conditions. During this process, part of the clayey deposit along the failure planes is transformed into a more or less liquid state that carries the overlying clay materials along the direction of the flow. Therefore, the failure extends over a large area from the initial zone of failure (Tavenas, 1984; Lefebvre, 1996; Demers et al., 2014).

Small-scale landslides can also be triggered by smaller magnitude of earthquakes. Lefebvre et al. (1992) documented nine such landslides in eastern Canada triggered by the 1988 Saguenay earthquake (M_M=5.9). Two of them were reported to have occurred in sensitive clay slopes. The very recent Notre-Dame-de-la-Salette and Mulgrave & Derry

slides were caused by the 2010 Val des-Bois earthquake, Québec (M_M=5.2). The failure was characterized as flowslide and spread type (Perret et al. 2013).

Not only in onshore, massive landslides in offshore environments were also triggered by earthquakes. In eastern Canada, the 1929 Grand Banks earthquake (M_M=7.2) caused a huge submarine landslide in offshore Newfoundland that resulted in a deadly tsunami along the southern coast and killed 28 people (Fine et al., 2005; Lamontagne, 2008).

Some of the most devastating landslides in clay soils have occurred during the 1964 Alaska earthquakes (M_M=9.2). Among them the Fourth Avenue, L-Street, Government Hill and Turnagain Heights slides were widely spread that caused significant damage. Post-slide investigations show that most of these slides were caused by post-peak strength degradation of the highly sensitive Bootlegger Cove clay formation (Stark and Contreras, 1998).

Figure 1.1 shows the air photographs and interpreted shear zones for some of the historical earthquake induced landslides in sensitive clay slopes from the literature.
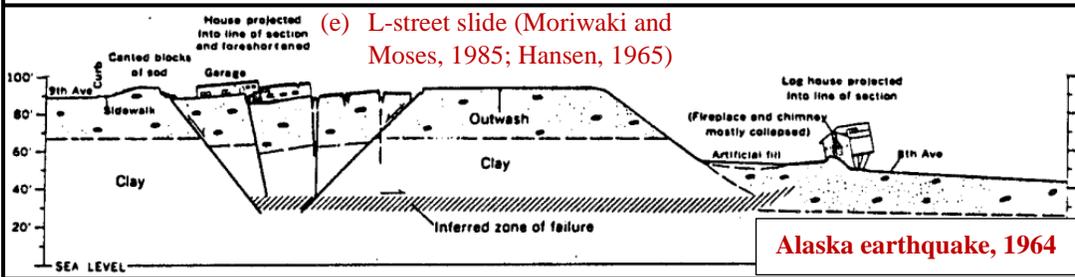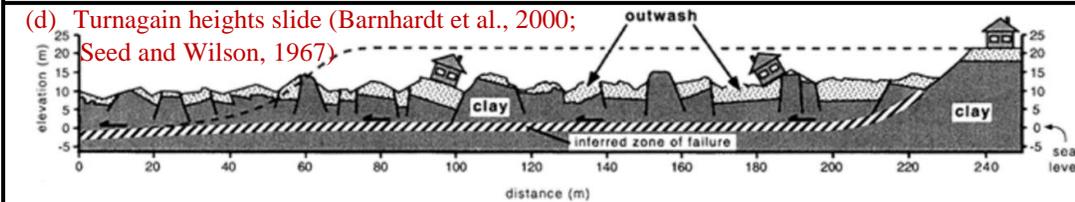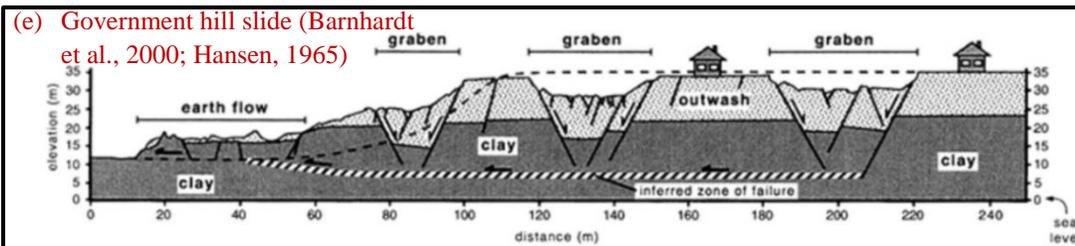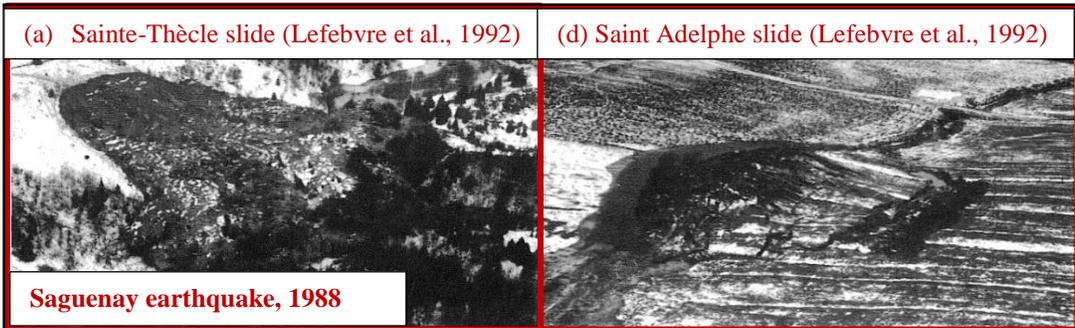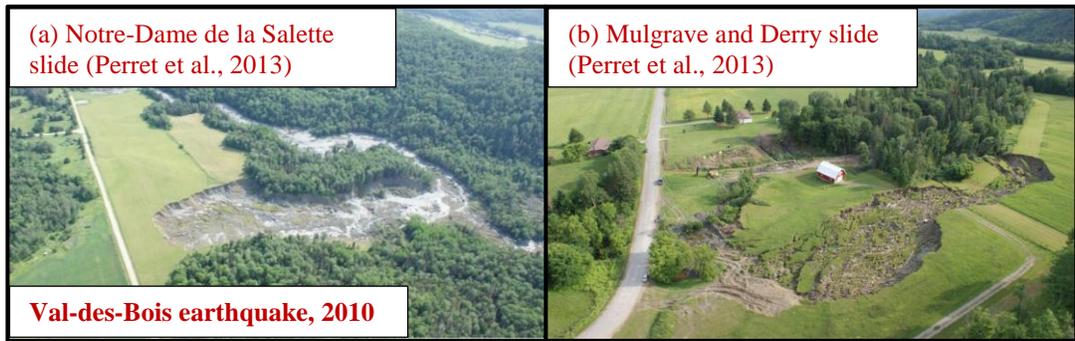
Figure 1.1: Some air photographs and interpreted shear zones for historical earthquake induced landslides in sensitive clay slopes

1.2   Scope of the research

Slope stability analyses are generally performed using the traditional limit equilibrium (LE) method. To check the stability of a slope subjected to earthquake loading, in the LE framework, a static horizontal inertial force is applied at the center of the soil mass above the potential failure plane. This is commonly referred as the "pseudostatic" method of analyses. The computer programs, such as SLOPE/W (GeoStudio 2016), developed in the LE principle has made the calculation process easier. It is also possible to accommodate complex geometries and varying soil properties in the LE analysis. However, LE methods cannot model the progressive development of failure planes as commonly observed in large landslides (Fig. 1.1). Moreover, LE method cannot accommodate post-peak softening of sensitive clays and strain localization along the failure planes.

A number of researchers suggested Finite Element (FE) analysis as an alternative approach to the LE method. The FE methods provide the information about displacement of soil and a priori definition of failure plane is not required. With advancement of modern computing tools in the last few decades, various FE software packages have been developed that can simulate complex geotechnical problems. FE techniques have been also used to perform seismic slope stability analyses. Most of the available FE analyses could not handle very large deformations because of numerical issues resulted from mesh distortions. The numerical issues become very severe when soil has strain softening behaviour because extremely large strain concentration occurs around the narrow zone of failure (shear band). Moreover, most of the FE programs do not have any built-in model

4

that represents strain softening behaviour of sensitive clays, although this type of model could be implemented in FE program using user defined subroutines.

1.3 Objectives

The main purpose of this study is to perform pseudostatic and dynamic FE analyses to examine the failure mechanisms in earthquake induced landslides in soft and sensitive clay. Analyses are performed using three difference FE approaches available in Abaqus FE software: Coupled Eulerian Lagrangian (CEL), explicit and implicit solution schemes. FE simulations are performed for varying geometries, soil conditions, existence of surcharge in the upslope area and different earthquake–time histories. The stress–strain behaviour of soft and sensitive clay is implemented through the user defined subroutine VUSDFLD writing a code in FORTRAN.

The following are the main objectives of this research:

- Develop a large deformation FE modeling technique for pseudostatic seismic stability analyses of soft clay slopes.
- Develop a large deformation FE technique for modeling comprehensive dynamic response of clay slopes during earthquake and post-quake stages.
- Perform parametric studies to explain typical failure patterns, topography and extent of earthquake induced landslides zones.

1.4   Outline of thesis

The thesis consists of five chapters. The outline is as follows:

- **Chapter 1** highlights the backgrounds, scope and objectives of the research work.

- **Chapter 2** contains a brief literature review. However, as the thesis is prepared in manuscript format, detailed literature review is provided in Chapters 3 and 4 and also in Appendix-A.

- **Chapter 3** presents FE model development for pseudostatic and dynamic analyses of clay slopes. This chapter is prepared as a manuscript for publication in an international journal. A part of this research work has been published in the 69th Canadian Geotechnical Conference, Geovancouver2016, Vancouver, B.C, Canada, October 2–5, 2016 (Appendix A).

- **Chapter 4** presents dynamic FE analyses of sensitive clay slope failure due to earthquake. This chapter is also prepared as a manuscript for publication in an international journal.

- **Chapter 5** summarizes the outcomes of the research and recommendations for future studies.

The thesis has been arranged in manuscript format. The reference cited in Chapters 1 and 2 are listed in the reference list at the end of the thesis. Conclusions and references of Chapters 3 and 4 are presented at the end of each chapter as in technical papers. Overall discussions and concluding remarks are provided in Chapter 5. The conference paper is included in Appendix A.

1.5   Co-authorships

Research works presented in Chapters 3, 4 and Appendix-A have been conducted by the author of this thesis. He also prepared the draft manuscripts. The supervisor and co-authors reviewed the manuscripts and provided technical comments, which has been also addressed by the author.

Chapter 2

Literature Review

2.1   Introduction

Different techniques have been used in the past to study the initiation and propagation/extent of earthquake induced landslides. However, most of the traditional slope stability analyses techniques cannot explain large-scale landslides. The aim of the present study is to present large deformation dynamic finite element (FE) analyses of clay slopes, more specifically sensitive clay slopes.

The literature review presented in the following sections focuses mainly on clay slope failure, although it is understood that earthquake could cause the failure of other types of soil such as loose sand. This chapter has been divided into two sections: (i) stress–strain behaviour of clay under cyclic loading, and (ii) modeling of clay slope failure due to earthquake. As the thesis has been written in manuscript format, problem specific literature review is presented in Chapters 3, 4 and Appendix-A. This chapter provides a brief overview of previous research relevant to the present study.

2.2   Behaviour of clay under dynamic loading

Dynamic behaviour of cohesive soils was studied from laboratory tests, such as triaxial and direct simple shear, by applying loading/unloading cycles at a range of shear stress or

shear strains. Damping and stiffness variation at small strains, cyclic softening and strength loss of saturated clay soils were the main foci of most of these studies.

Post-peak strength reduction has been considered as one of the causes of many earthquake induced large-scale landslides (Stark and Contreras, 1998). Shannon and Wilson (1964) and Woodward-Clyde (1982) conducted a series of triaxial compressions tests on the slightly overconsolidated Bootlegger Cove Clay that experienced undrained strength loss during the 1964 Alaskan earthquake. They found that the undrained peak shear strength normalized by the vertical consolidation pressure ranges between 0.26 and 0.28. Woodward-Clyde (1982) conducted a series of monotonic and cyclic loading tests using direct simple shear (DSS) apparatus. The peak undrained shear strength ratio in DSS varies from 0.18 to 0.24, which is less in cyclic loading condition. Lade et al. (1988) conducted cyclic triaxial compression tests on Bootlegger Cove Clay and showed the ratio of cyclic to static undrained shear strength greater than unity. They also concluded that cyclic loading and the generation of excess pore water pressure may not be the prime cause of shear strength reduction, rather large shear displacements along the failure plane during landslide could be the cause of shear strength reduction in clay soil. Idriss (1985) also suggested that sufficient shear deformations during an earthquake event could reduce undrained shear strength to a residual value. Stark and Contreras (1998) showed that triaxial, direct shear or direct simple shear tests may not be suitable for estimating the undrained residual strength, because these apparatuses cannot accommodate large strains and therefore they used constant volume ring shear and field vane shear tests.

Reviewing published dynamic experimental data, Díaz-Rodríguez and Lopez-Molina (2008) suggested four cyclic strain thresholds for clay type soils. Firstly, the linear threshold shear strain (γ_{tl}) that separates the very small from small strain regime, which is 0.001–0.005% for most of the clayey soils. Secondly, the limit that separates small and medium strain regime is termed as the volumetric cyclic threshold strain (γ_{tv}) where the strengths are below the peak undrained shear strength. For silts and clay, the γ_{tv}=0.024–0.06% (Hsu and Vucetic, 2004, 2006).

Thirdly, the degradation threshold (γ_{td}) represents the boundary of the medium and large strain regime. It separates the critical level of repeated loading in which soil failure will not occur. Below γ_{td}, the clay structure remains relatively unaltered. Typical value of γ_{td} includes 0.5% to 3% (Lefevbre, 1989; Houston and Herrmann, 1980; Díaz-Rodríguez and Santamarina, 2001). Lastly, the boundary of the large strain and residual strain regime is represented by flow threshold (γ_{tf}) where the de-structuring of initial fabric occurs. Okur and Ansal (2007) defined γ_{tf} as the point where the stiffness is approximately 10% of the initial value.

Very limited laboratory tests are available at large strain levels that can lead to residual shear strengths. Stark and Contreras (1996) presented the use of constant volume ring shear apparatus and field vane shear to determine the mobilized and residual undrained shear strength for the sensitive clay samples that was responsible for the Fourth Avenue slide during the 1964 Alaskan earthquake. Based on their analysis, they suggested that 80% of the peak undrained shear strength may be conservatively used to evaluate the seismic stability of slopes in sensitive clay soils for a shear displacement less than 0.15

m. However, the undrained residual shear strength should be used if the shear displacement exceeds 0.15 m.

2.3   Seismic slope stability

2.3.1   Analytical and empirical methods

Seismic slope stability assessment started in the early 1920's based on the pseudostatic approach, where a pseudostatic force due to earthquake acceleration is added to the driving force due to gravitational acceleration and then solved the problem using limit equilibrium method. The pseudostatic approach is available in many commercial software packages such as Slope/W (GeoStudio, 2016). Many authors criticized this approach, although it is very simple for practical application, and reported that this approach is over-conservative in many situations but there are also some conditions where it is unconservative (Jibson, 1993, 2011; Bray and Travasarou, 2009). Kramer (1996) mentioned that the pseudostatic approach may not be applicable if the soil undergoes post-peak shear strength degradation greater than 15% or build up significant dynamic pore water pressures. Moreover, the limit equilibrium approaches do not provide any information about the progressive development of failure planes. It only provides the factor of safety (F_S) considering that a complete failure planes have developed. However, due to the fact that this method has long been used as a state-of-practice by engineers, several researchers attempted to advance it further. Among them, new approaches for selection of horizontal pseudostatic coefficients (k_h) based on updated case histories and

level of acceptable deformation, and implementation in FE models are notable. A comprehensive review of this pseudostatic approach is available in Jibson (2011). Table 2.1 shows several recommendations on selection of k_h.

Table 2.1: Recommended values on selecting pseudostatic coefficient (k_h)

k_h	Description & Reference	
0.1	"severe" earthquakes (Rossi-Forel IX)	Terzaghi (1950), FOS >1
0.2	"violent, destructive" earthquakes (Rossi-Forel X)	
0.5	"catastrophic" earthquakes (Rossi-Forel >X)	
0.1	Major Earthquake, FOS > 1.0	Corps of Engineers (1970)
0.15	Great Earthquake, FOS > 1.0	
0.12 - 0.25	For Japan, Seed (1979)	
0.1-0.15 (M_M=6.5-8.25)	Seed (1979), FOS >= 1.15, <1m displacements earthdams	
0.13-0.20 of PGA/g		
0.33 -0.50 X PGA/g	Marcuson (1981); Marcuson and Franklin (1983), FOS >1.0	
0.50 X PGA/g	Hynes-Griffin and Franklin (1984), FOS > 1.0 and SR > 20%, <1m displacements earthdams	
0.65X PGA/g	Matsuo et al. (1984); Taniguchi and Sasaki (1985)	
0.15	California Divisions of Mines and Geology (1997), based on <1m displacement in earth dams	
0.05 - 0.15	In United States (California), Abramson et al. (2002)	
0.1-0.15	Ghobrial et. al. (2015)	

The limit equilibrium analyses using pseudostatic approach do not provide any information about displacement of soil. Seismic displacement is normally calculated using Newmark's Sliding Block method (Newmark, 1965) in which the sliding soil mass is assumed as a rigid body that slides over the basal plane if downslope acceleration exceeds a critical acceleration. The shear resistance along the sliding plane is assumed to be constant. However, this method has been thought to be overly simplified and may not be applicable to different types of failure and soil conditions as it does not account for the effect of internal deformation of the failed soil mass (Seed and Martin, 1966; Seed et al., 1978; Jibson, 1993). Kramer and Smith (1997) modified Newmark's method considering a discrete system of two or more blocks connected by springs and dashpots instead of one rigid block.

One of the very first attempts for estimating earthquake induced shear stresses has been presented by Seed and Idriss (1969). Their simplified procedure is mainly applicable to the liquefaction in sand. Later, Makdisi and Seed (1977) provided a detailed procedure for estimating earthquake induced deformation in dams and embankments of compacted cohesive and cohesionless soils. This method is based on the concept of Newmark's sliding block analysis and dynamic response evaluation proposed by Seed and Martin (1966). A well-defined slip surface is assumed as a potential failure plane. Soil behaves elastically at stress level below the yield acceleration and as perfectly plastic material above the yield acceleration. For a given potential sliding mass, the stages at which acceleration exceeds the yield acceleration, movement will occur along the failure plane.

Similar to Newmark (1965), double integration rule is used to determine the magnitude of the displacement.

Ambraseys and Srbulov (1994) presented simple semi-empirical predictive relations based on their proposed sliding block model to determine earthquake induced ground displacements as a function of critical acceleration ratio (ratio of maximum horizontal acceleration beyond which yield will occur to the maximum predicted acceleration), earthquake magnitude and source distance. Cai and Bathurst (1995) presented an overall review and quantitative comparison of existing deterministic sliding block methods in accordance to case studies for predicting permanent displacement. They concluded that most of the predicted displacements from the different empirical methods fall in a narrow range.

Bray and Travasarou (2007) presented a simplified semi-empirical probabilistic based seismic slope displacement model based on the nonlinear coupled stick–slip deformable sliding block model originally proposed by Rathje and Bray (2000), to account for the deformability of the sliding mass as an advancement of the Newmark model. The performance of their probabilistic model for estimating seismic displacement has been compared with documented cases of earth dam and solid-waste landfills. Bray and Travasarou (2009) revised their probabilistic model to develop a rational method for selecting seismic coefficient (k_h) depending on the expected seismic demand at the site and the desired level of seismic performance.

A summary of major achievements and advancements in the state-of-practice of seismic slope stability analysis and design of earthen dams and embankments of cohesionless soils could be found in Marcuson et al. (1992, 2007). However, as the focus of the present study is clay slope, these studies are not discussed here.

Most of the analytical and empirical relationships available in the literature are for seismic stability of dams, based on the assumption that maximum 1 m of seismic displacement is acceptable and the soil does not experience significant strength loss due to earthquake (<15% of its initial value) (Bray and Travasarou, 2009). Therefore, these approaches may not be applicable to large displacement failures that are commonly observed in landslides in soft and sensitive clays.

2.3.2 Physical tests

Very limited physical model tests on sensitive clay slope failure are available in the literature. One of the main reasons is that large extent of failure is very difficult to accommodate in experimental setup.

Seed and Wilson (1967) presented a series of model tests to explain the failure mechanisms involved in the Turnagain Heights landslide due to the 1964 Alaskan earthquake. The slopes were composed of an extremely weak layer at the level of toe, overlain by layers of stronger clays, to understand large-scale landslides in Turnagain Heights area. A series of retrogressive rotational slides were found in model tests (Fig. 2.1).
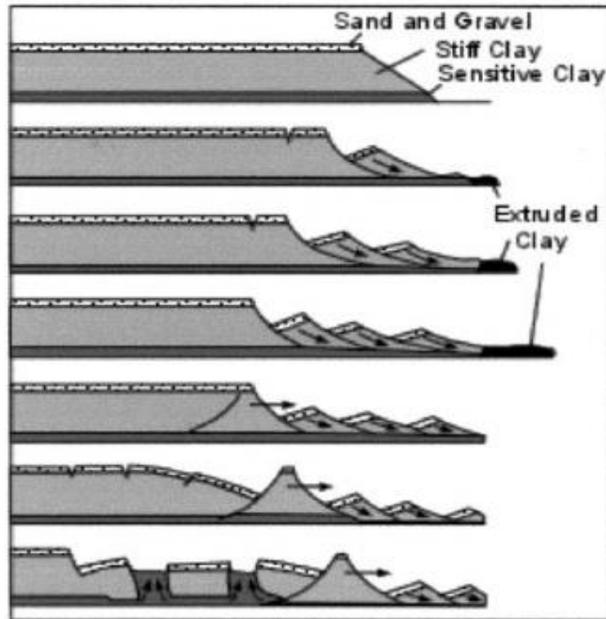
Figure 2.1: Typical failure in model test slopes for Turnagain Heights landslide

(after Abbott, 1996)

Wartman (2005) performed four 1g shaking table tests on clay slope models to investigate the mechanisms of earthquake induced permanent deformations. Vane shear tests were conducted to measure the undrained shear strength of the clay used in tests. Deep rotational and translational sliding occurred in the model slopes at the interface between soft and stiff soil layers. The measured deformations in model tests have been compared with calculated deformation using Newmark's sliding block method.

Park and Kutter (2015) performed a total of 4 static and 8 dynamic centrifuge experiments at 50 times gravitational acceleration for different earthquake input motions to study the effects of soil sensitivity on slope failure mechanisms. Vane shear and uniaxial compression tests were also conducted to obtain strength and sensitivity of tested

soils. Deeper failure with a diffused plastic zone was found in dynamic tests while shallow and distinct shear bands were obtained in static tests.

2.3.3   Numerical analyses

Numerical analysis could be an alternative approach for modeling dynamic response of slopes. Different numerical techniques—finite element, finite difference, discrete element and material point methods—have been used in the past for modeling slope failure. Again, keeping in mind the focus of the present study, literature review related to clay slope failure due to earthquake is mainly discussed.

Loukidis et al. (2003) conducted pseudostatic FE analysis to study homogeneous soil slopes using Abaqus/Standard (implicit) FE software. For one case, they used the SNAC FE code (Abbo and Sloan, 2000) to incorporate pore pressure effect. The in situ stress condition has been achieved by applying gravitational acceleration. A horizontal pseudostatic acceleration is then applied to calculate the critical seismic coefficient (k_c) that causes failure. Tan and Sarma (2008) also presented a series of pseudostatic FE analyses to study homogeneous soil slope failure using the Imperial College Finite Element program (ICFEP) (Potts and Zdravković, 1999). Li (2007) conducted pseudostatic FE analysis using a nonlinear shear strength criterion defined as a power-law.

Aryal (2006) conducted pseudostatic analysis using the LE based Slope/W software and dynamic analysis using the Plaxis FE software (PLAXIS,2004) and showed that LE analyses gives 5–14% higher factor of safety than FE analysis.

Azizian and Popescu (2003) conducted three-dimensional seismic FE analyses of submarine slopes using a multi-yield surface plasticity model implemented in DYNAFLOW (Prevost, 1981). The selection of appropriate boundary conditions and its effects on slope failure has been discussed.

Kourkoulis et al. (2010) studied the combined effects of earthquake triggered landslide and ground shaking on foundation-structure system near the slope using Abaqus/Standard FE software. A post-peak softening with accumulated plastic shear strain has been also considered in this study. FE analysis shows gradual formation of failure planes. The yield acceleration obtained from FE analysis is comparable to LE results. Note that, Abaqus FE software has been also used for rock slope analyses (Mitani et al., 2013).

Melo and Sharma (2004) used a two-dimensional explicit finite difference program FLAC to study static and dynamic response of an embankment. Parametric studies were performed for varying geometry and soil properties for three different strong ground motions. It is shown that, critical seismic coefficients that causes the failure are proportional to embankment height and the peak horizontal acceleration of the input ground motion.

Taiebat et al. (2010) used the nonlinear finite difference code, FLAC^{3D} to simulate dynamic response of a mild saturated clay slope. SANICLAY—a simplified anisotropic

clay plasticity model that has been extended from the modified Cam-Clay (MMC) model (Roscoe and Burland 1968)—has been used to define the constitutive behaviour of clay. The influence of anisotropy and destructuration—related to earthquake-induced strains— have been presented. Numerical results have been also compared with the modified Newmark sliding block analysis.

Clay slopes, more specifically sensitive clay slopes, might experience significant strength degradation due to cyclic loading. In additions, extremely large strains generate along the failure planes due to large movement of the failed soil blocks. However, very limited studies are available in the literature for modelling large deformation behaviour of slope failure due to earthquake. Some of the preliminary studies available in the literature are discussed below.

Chen and Qiu (2014) presented the use of smooth particle hydrodynamics (SPH) method to model earthquake induced large slope deformation under undrained conditions. A constitutive model combining the isotropic strain softening, viscoplasticity and rate dependent stiffness has been implemented in the numerical model. Figure 2.2 shows a comparison of numerical results (Fig. 2.2(a) with shake table test result (Fig. 2.2(b)) conducted by Wartman (2005). As shown, the failure of only one soil block is modeled both in numerical analysis and model tests. However, in the field a number of soil blocks fail in earthquake triggered large-scale landslides (Fig. 1.1).

(a) Numerical (SPH) model

(b) Physical (Shake table) model
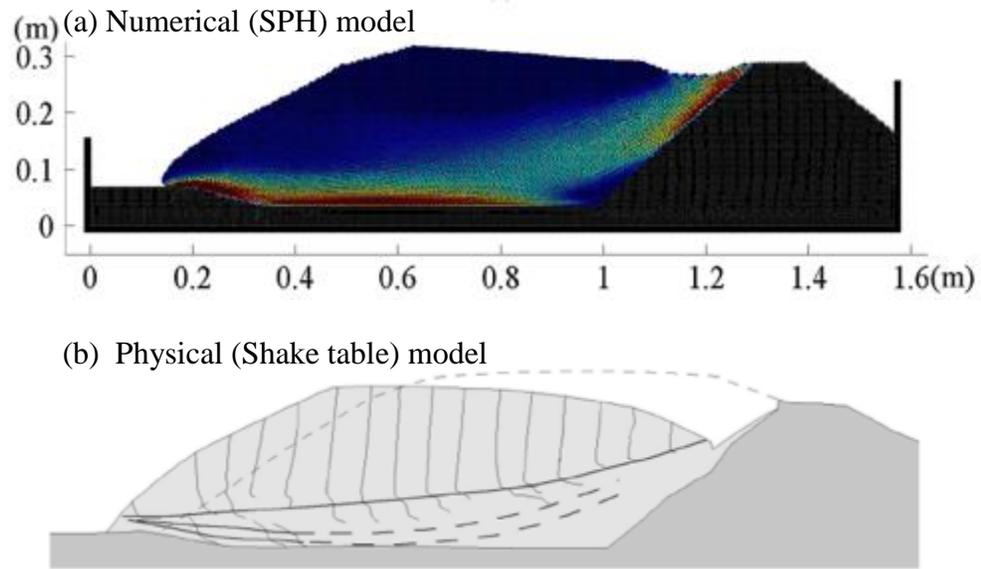
Figure 2.2: Comparison of simulated failure surface and deformed shape with shake

table model slope test by Wartman (2005) (after Chen and Qiu, 2014).

Moormann and Hamad (2015) used two large deformation continuum based modeling techniques namely Material Point Method (MPM) and Coupled Eulerian Lagrangian (CEL) approach to simulate sliding mass over a rock joint due to earthquake. The Mohr-Coulomb failure criterion was used for the analyses. The authors demonstrated reasonably good agreement in sliding mechanisms obtained from these two numerical methods (Fig. 2.3).
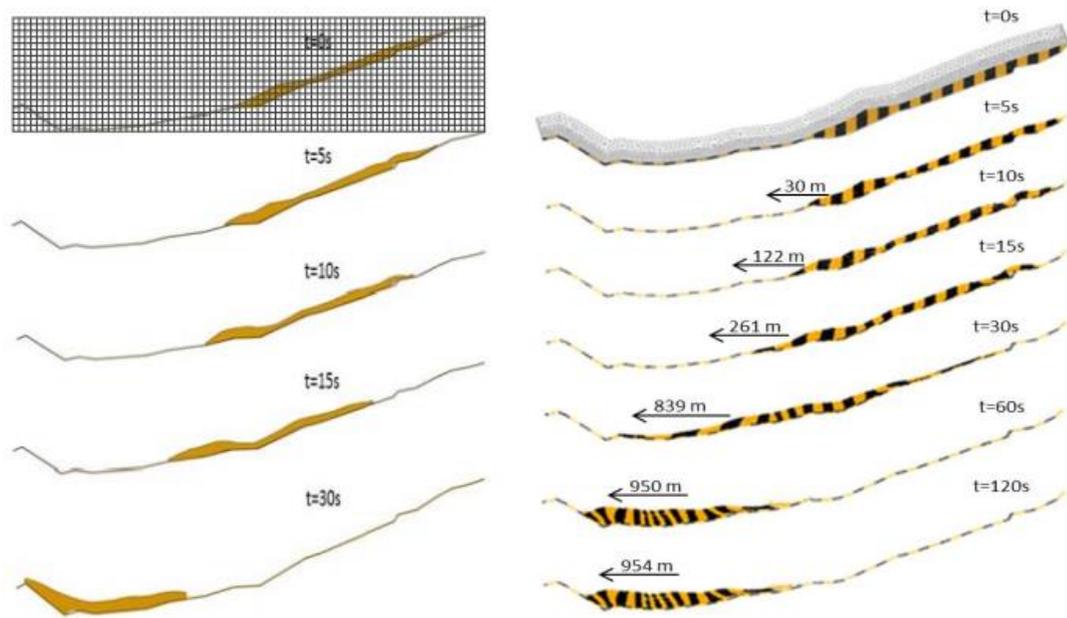
Figure 2.3: Progression of landslide: (left) CEL and (right) MPM

(after Moormann and Hamad, 2015)

2.4 Summary

Most of the available analytical and empirical techniques for earthquake induced slope stability analyses have been developed for idealized and simplified conditions. Very limited number physical model tests are available in the literature on stability of sensitive clay slope subjected to earthquake. In most of the physical models, the dimensions are not sufficiently large to model large-scale landslides and also the failure surface is somehow predefined.

Numerical modeling could provide better insights into the mechanisms of large-scale landslides. Limit equilibrium analysis with pseudostatic approach does not provided any

information about displacement of soil mass. Finite element and finite difference are the two commonly used methods for dynamic slope stability. In sensitive clay slope failures, significantly large strain accumulations occur in the narrow shear band. However, most of the finite element and finite difference methods cannot handle very large deformation.

Therefore, in the present study, large deformation finite element modeling of clay slope failures due to earthquakes are presented.

Chapter 3

Implementation of a Large Deformation Finite Element Modeling Technique for Seismic Slope Stability Analyses

3.1   Abstract

Post-slide investigations show that large displacement of failed soil mass occur in many earthquake-triggered landslides. Finite element (FE) modeling of progressive formation of failure planes in clay slopes subjected to earthquake loading is presented in this study. Pseudostatic and dynamic FE analyses are performed using the Coupled Eulerian Lagrangian (CEL) approach in Abaqus FE software to investigate large displacement behaviour. Compared with FE simulation results using pure explicit and implicit approaches; Abaqus CEL can successfully model the failure processes even at large displacements which cannot be done using the other two FE approaches. The dynamic FE analyses for nine earthquake acceleration–time histories show that multiple failure surfaces could be formed in the slope, which cannot be modeled using the traditional limit equilibrium method (LEM). The similarity and differences between the results of dynamic and pseudostatic FE analyses based on estimated pseudostatic coefficient from acceleration–time records are presented. The duration of earthquake influences the failure process and displacement of the failed soil mass.

3.2　Introduction

The pseudostatic approach is commonly used in geotechnical engineering practice to evaluate the stability of slopes in which a destabilizing horizontal body force representing the earthquake induced force is included in the conventional static limit equilibrium method (LEM). The factor of safety (F_s) can be calculated from pseudostatic analysis; however, it does not provide any information about displacement. Depending upon severity of earthquake and peak ground acceleration, a wide range of horizontal pseudostatic coefficients (k_h) has been recommended. In some cases, the k_h is recommended calibrating against acceptable displacement—for example, less than 1 m in earth dams (Seed, 1979; Hynes-Griffin and Franklin, 1984). The selection of k_h is further rationalized in a number of studies (Bray and Rathje, 1998; Stewart et al., 2003; Bray and Travasarou, 2009). Jibson (2011) suggested that, although it is simple, the pseudostatic approach stems from crude characterization of dynamic response of the slope.

The permanent deformation of the slope is generally calculated using the Newmark sliding block method (Newmark 1965) assuming the failed soil mass as a rigid block that slides downslope on a basal shear surface when its acceleration exceeds the critical acceleration. A number of studies also attempted to improve this method and proposed empirical relations calibrating against post-slide field data (Seed and Martin, 1966; Seed et al., 1978;

24

Ambraseys and Srbulov, 1994; Kramer and Smith, 1997; Rathje and Bray, 2000; Bray and Travasarou, 2007, 2009).

Post-slide investigations show that earthquake induced landslides involve the failure of a number of soil blocks. All the failure planes may not develop at the same time, instead the failure occurs progressively. The pseudostatic and Newmark block type models cannot explain the progressive landslides. Therefore, numerical modeling such as finite element method (FEM) can be used.

The FEM developed in Lagrangian framework has been used in the past to model slope failure. Loukidis et al. (2003) conducted FE analysis using Abaqus/Standard (implicit) to calculate the limiting k_h required to fail a homogeneous slope. Tan and Sarma (2008) conducted pseudostatic FE analyses using the ICFEP FE program (Potts and Zdravkovic, 1999), where k_h is gradually increased until the failure of the slope. Kourkoulis et al. (2010) conducted dynamic FE analysis using Abaqus/Standard where the earthquake excitation is applied at the base of the model. They also considered the post-peak degradation of shear strength parameters with accumulated plastic shear strain. However, these studies did not investigate large deformation behaviour of failed soil mass as occurred in earthquake-triggered landslides.

The Lagrangian FE modeling suffers from numerical issues related to convergence and mesh distortion at large strains (Griffiths and Lane, 1999). In recent years, advanced FE modeling techniques have been developed to accommodate large strains, which has been used for static and quasi-static geotechnical problems (Hu and Randolph, 1998; Qiu et al,

2011; Dutta et al, 2015; Dey et. al., 2015, 2016). In addition, explicit finite difference method based on Lagrangian and updated Lagrangian procedure has been used in some computer programs to cope with some level of large deformation, such as FLAC (Itasca, 2012). The CEL approach in Abaqus can handle very large deformation during slope failure (Dey et al., 2015). However, except for some preliminary studies (e.g. Moormann and Hamad, 2015; Islam and Hawlader, 2016), these large deformation FE modeling techniques have not been used in dynamic slope stability analyses.

The focus of the present study is to show the performance of three FE modeling approaches in simulating clay slope failures. Analyses are performed using Abaqus/Standard, Abaqus/Explicit and Abaqus CEL, which are referred as implicit, explicit and CEL, respectively, in the following sections. Conducting a series of dynamic and pseudostatic FE analyses, the limitations of pseudostatic modeling, including the selection of k_h for assessing the likelihood of failure, are identified.

3.3 Problem statement

Figure 3.1 shows the geometry of the slopes considered in the present study. A 15 m high 2H:1V clay slope—stable under gravity load—is subjected to earthquake loading. A large soil domain of 400 m long (200 m in each side from the toe of the slope) is modeled in order to avoid boundary effects on slope failure. Analyses are performed for two slopes (Figs. 3.1(a & b)). In Slope-I, the soil profile consists of a 25 m thick upper clay layer of uniform undrained shear strength (s_{u0}) underlain by a 10 m thick strong base layer (Fig

26

3.1(a)). The soil profile in Slope-II consists of two clay layers and a strong base layer (Fig. 3.1(b)). In the upper clay layer, s_{u0} increases with depth, while it is constant in the bottom clay layer. As will be shown latter, the failure of the slope mainly occurs through the upper clay layer; however, to avoid boundary effects from the bottom surface where the dynamic acceleration is applied, the bottom boundary is placed at sufficiently large depth. The groundwater table is located at the ground surface.

3.4   Finite element modeling

A number of studies show the advantages of FEM over traditional LEM for slope stability analysis (Duncan, 1996; Griffiths and Lane, 1999). The main advantages of FEM are: (i) a priori definition of failure plane is not required as LEM, instead the failure occurs through the locations where shear stress reaches the shear strength, (ii) progressive formation of failure plane can be simulated and (iii) the deformation of failed soil mass can be calculated. Many slope stability problems involve large deformation of the failed soil mass. Most of the FEM used in previous studies have been developed in purely Lagrangian framework (Dawson et al., 1999; Swan and Seo, 1999; Zheng et al., 2005; Cheng et al., 2007; Liu et al., 2015) and therefore cannot simulate large deformation because of significant mesh distortion around the failure planes that causes numerical instabilities and non-convergences of the solutions (e.g. Griffiths and Lane, 1999). Recognizing the limitations of Lagrangian FEM, large deformation FE techniques have been used for modeling slope failure (Mohammadi and Taiebat, 2013, 2014; Wang et al., 2013).

27

The FE modeling becomes further complex if the soil has strain softening behaviour because large strain concentration occurs in narrow zones forming shear bands, which is one of the key factors in modeling progressive failure of slopes (Potts et al., 1990; Puzrin et al., 2004; Kvalstad et al., 2005; Gauer et al., 2005; Puzrin et al., 2015). The strain localization has been also modeled using other approaches such as Cosserat model (de Borst, 1991; de Borst et al., 1993), gradient or nonlocal theories (Troncone, 2005), computational fluid dynamics (Gauer et al., 2005), extended finite element (Thakur, 2007), material point method (Zabala and Alonso, 2011), and smoothed particle hydrodynamics (SPH) (Bui et al., 2011). The authors and their co-workers provided review of currently available large deformation FE modeling techniques for static and quasi-static problems elsewhere (Dutta et al., 2015; Dey et al., 2015, 2016; Soga et al., 2016). The application of these large deformation FEM techniques for earthquake-triggered landslides is very limited. Table 3.1 shows a summary of the advancement and use of FEM—together with some other numerical modeling techniques—for modeling slope failure due to earthquake.

3.5   Finite element model development

3.5.1   Coupled Eulerian-Lagrangian (CEL) approach

The CEL approach in Abaqus 6.14.2 FE software (Dassault Systèmes, 2013) is used for large deformation FE modeling of the slopes subjected to earthquake. One of the main advantages of CEL is that material (soil) flow through the fixed mesh and therefore numerical issues related to mesh distortion is not encountered. Further details of

28

mathematical formulation, its application to large deformation static and quasi-static geotechnical problems (e.g. onshore and offshore landslides, penetration of surface laid pipelines and spudcan foundation in seabed) and advantages of CEL over other FE formulations are available in previous studies (Benson, 1992 , 1995; Benson and Okazawa, 2004; Qiu et al., 2011; Henke et al., 2011; Tho et al., 2011; Dassault Systèmes, 2013; Dey et al., 2015 , 2016; Dutta et al., 2015; Hamann et al., 2015; Trapper et al., 2015).

Only three-dimensional modeling is allowed in CEL. Therefore, the analysis is performed with only one element length in the out-of-plane direction in order to simulate plane strain condition. The domain is discretized using 0.25 m cubical elements, except for the mesh sensitivity analyses. The soil is modeled as an Eulerian material using EC3D8R—eight-node brick elements. A void space above the ground surface is created in order to accommodate the displaced soil mass during landslide. The Eulerian volume fraction (EVF) tool in Abaqus is used to create the initial void and soil domains. For any element, EVF=1 means that the element is filled with soil and EVF=0 means the element is void. Fractional value of EVF means that the element is partially filled with soil.

Zero velocity boundary conditions are applied normal to the bottom and all the vertical faces in pseudostatic analysis. In other words, the bottom of the model is restrained from any vertical movement while these vertical faces are restrained from any lateral movement. However, for dynamic analysis, non-reflecting boundary conditions are applied to the left and right vertical faces as discussed in Section 3.7.2.2. No boundary condition is applied along the soil-void interface to allow the displaced soil to move in the void space when needed.

3.5.2 Implicit and Explicit approaches

In Abaqus/Standard and Abaqus/Explicit, the 8-noded brick elements with reduced integration (C3D8R) are used. The bottom of the domain is restrained from vertical movements. In pseudostatic analysis, the two vertical faces are restrained from any lateral movement using roller supports. However, for dynamic FE analysis, infinite elements are used to avoid wave reflection from lateral boundaries as discussed in Section 3.7.2.2.

3.5.3 FE modeling steps

FE modeling consists of following three consecutive steps:

    i.   Gravity loading: The geostatic load is applied to establish in-situ stress condition. The slope is stable at the end of this loading step.

    ii.   Earthquake loading: Two approaches are used for seismic loading. First, in the pseudostatic analysis, the horizontal component of body force is increased gradually with time. Second, in "dynamic analysis," a horizontal excitation (acceleration–time history) is applied at the base of the model. For the Slope-I (Fig. 3.1(a)), only pseudostatic analysis is performed.

    iii.   Post-quake simulation: After earthquake loading, the analysis is continued for a period of time to investigate post-quake behaviour.

3.6   Modeling of soil

The analyses are performed for undrained loading condition because the earthquake loading and failure occur in a short period of time. The clay layers are modeled as elastic-perfectly plastic material adopting von Mises yield criteria. For Slope-I, uniform s_{u0}=60 kPa is used for the upper clay layer. For Slope-II, analyses are performed for two types of stress–strain behaviour of the upper clay layer. Firstly, in the no-softening case, s_{u0} of the upper clay layer is increased linearly with depth from 15 kPa at the ground surface at the level of crest to 95 kPa at 30 m depth. For the stiff clay layer, uniform undrained shear strength 150 kPa is used. The base layer is modeled as elastic material. Secondly, in the softening case, in addition to linear variation of s_{u0}, a post-peak degradation of mobilized undrained shear strength (s_u) is incorporated using Eq. (3.1).

$$s_\mathrm{u} = \left[\frac{1}{S_\mathrm{t}} + \left(1 - \frac{1}{S_\mathrm{t}} \right) \mathrm{e}^{-\frac{3\delta}{\delta_{95}}} \right] s_{\mathrm{u}0} \qquad\qquad (3.1)$$

where, δ is the accumulated plastic shear displacements from loading and unloading; sensitivity $S_\mathrm{t} = s_{u0}/s_{uR}$ in which s_{uR} is the remolded s_u at large plastic shear displacement; and δ_{95} is the value of δ at which 95% reduction of (s_{u0}-s_{uR}) occurs. Equation (3.1) is a modified form of strength degradation equation proposed by Einav and Randolph (2005), but in terms of plastic shear displacement. Note that, a linear degradation of post-peak shear strength with accumulated plastic shear strain during cyclic loading has been used in previous studies (Nadim, 1998; Pestana and Nadim, 2000).

The pseudostatic slope stability analysis generally provides reasonable results if the strength degradation due to earthquake loading is not very significant (Bray and Travasarou, 2007, 2009). For example, Kramer (1996) recommended that this procedure could be used if strength degradation is less than 15% of the peak shear strength. Therefore, in the present study, the post-peak strength degradation model is not used in pseudostatic analysis. The soil parameters used in pseudostatic analysis are shown in Table 3.2.

3.6.1 Numerical implementation

Uniform s_{u0} for the upper clay layer in Slope-I and stiff layer in Slope-II is given as an input in Abaqus. However, the linear variation of s_{u0} in the upper clay layer in Slope-II cannot be given directly as an input, and therefore it is defined using the temperature as a dummy variable. The post-peak degradation of s_u with plastic shear strain is implemented in Abaqus using the user subroutine VUSDFLD. During loading, a soil element might displace to different locations from its initial depth. In VUSDFLD, a computer program is written to ensure that the displaced soil elements carry the initial value of s_{u0}. The equivalent plastic shear strain (PEEQVAVG in CEL, PEEQ in implicit and explicit analyses) is called in the subroutine in each time increment. In CEL analysis, PEEQVAVG=PEEQ, when an element is completely filled with clay. For brevity, PEEQVAVG or PEEQ is replaced by ϵ_q^p in this paper, which represents the integration of plastic deviatoric strain rate tensor ($\dot{\epsilon}_{ij}^p$) over the period of analysis (i.e. $\int_0^t \sqrt{\frac{2}{3}\dot{\epsilon}_{ij}^p\dot{\epsilon}_{ij}^p}dt$) . Note that, ϵ_q^p is a scaler variable that represents generalized plastic strain. When ϵ_q^p is zero,

only undrained elastic deformation occurs. Assuming simple shear condition, the plastic

shear strain (γ^p) can be calculated as δ/t_{FE}, where t_{FE} is the length of the cubical elements

(EC3D8R) used in this study. The variation of yield strength is defined as a function of

ϵ_q^p ($= \gamma^p/\sqrt{3}$).

3.7   Numerical simulation results

In the following sections, the development of failure planes is explained by the formation

of shear bands where the concentration of ϵ_q^p occurs due to earthquake loading.

3.7.1   Pseudostatic FE analyses results

Similar to previous studies (Loukidis et al., 2003; Tan and Sarma, 2008), the pseudostatic

load is applied in FE modeling by increasing the horizontal body force F_b ($=k_h\gamma$) per unit

volume of soil, where γ is the bulk unit weight of soil. Except for some implicit analyses

where the solution is stopped because of numerical issues due to mesh distortion, k_h is

increased to a maximum value of 0.1, which represents a severe earthquake as per Rossi-

Forel IX (Terzaghi, 1950, Corps of Engineers, 1970). To maintain quasi-static condition,

k_h is increased slowly.

3.7.1.1 Pseudostatic simulation results for Slope-I

The left column of Fig. 3.2 shows the simulation results using Abaqus CEL for Slope-I

(Fig. 3.1(a)). At the end of geostatic step (k_h=0), very small plastic shear strains develop at

the interface between the upper clay and base layer below the middle of the slope (Figs. 3.2(a–c)). However, the slope is globally stable under this load. Limit equilibrium analysis (Spencer's method) is also performed using the Slope/W software (GeoStudio, 2016), which gives F_s=1.24 for the geostatic loading condition. The circular dashed line in the first column of Fig. 3.2 shows the critical circle (minimum F_s) obtained from Slope/W. The critical circle also passes through the interface between clay and base layer. For clarity, the critical circles are shown only on CEL simulation results.

With increase in k_h, the shear band propagation occurs mainly in the left side of point A and reaches the downslope ground surface (Fig. 3.2(d)). The equivalent plastic shear strain distribution for k_h=0.03 shows that a triangular wedge develops by the formation of another shear band from the toe of the slope (Figs. 3.2(j–l)).

From FE results, the failure of a slope can be defined based on several criteria such as bulging of slope profile, limiting shear stress on the failure plane, non-convergence of the solution, and formation of a complete shear band for global failure of a soil block (Griffith and Lane, 1999; Loukidis et al., 2003). In the present study, the last criteria is used to define failure.

The accumulation of plastic strains in the shear band and its propagation in the right side of point A continues with increase in k_h (Figs. 3.2(g & j)). A curved shear band forms from the horizontal shear band and reaches the ground surface (Fig. 3.2(m)). Figures 3.2(j & m) show that the global failure of the soil mass M1 occurs at k_h=0.07–0.08. The LEM gives F_s=1.0 at this level of k_h. The value of k_h that gives F_s=1 is known as the yield coefficient (k_y) (Jibson, 2011). In other words, k_y obtained from Abaqus CEL and LEM are

comparable. For $k_h > k_y$, the magnitude of ϵ_q^p increases in the shear bands and also the length of the horizontal shear band increases.

In order to compare the performance of Abaqus CEL for large deformation modeling of slopes, analyses are also performed with Abaqus/Explicit and Abaqus/Standard (implicit). The first three rows of Fig. 3.2 show that simulation results are very comparable for these three types of FE analysis for $k_h < 0.05$ where ϵ_q^p is not significantly high. However, at $k_h = 0.05$–0.07, a complete sliding surface develops causing a global failure of soil mass M1 in implicit analysis. Considerable heave near the toe and settlement in the upslope area occur at this stage. The FE mesh along the failure planes becomes extremely distorted (inset of Fig. 3.2(l)). Figures 3.2(k & n) show that the failure pattern in Abaqus/Explicit is similar to Abaqus CEL, although ϵ_q^p in Explicit is higher than CEL. At a very large k_h (=0.1), the zone of accumulated ϵ_q^p widens in Explicit (Fig. 3.2(p)) while ϵ_q^p mainly concentrates relatively in a narrow band in CEL analysis (Fig. 3.2(o)). At this level of large displacements, significant mesh distortion also occurs in Explicit, which is discussed further in the following sections.

Unlike limit equilibrium analysis, FEM provides information about deformation/strains in soil elements. Figure 3.3 shows the increase in ϵ_q^p with k_h at point A in Figs. 3.2(a–c). The calculated ϵ_q^p using all three approaches are comparable for low k_h (<0.05). However, at $k_h \approx 0.07$, ϵ_q^p increases abruptly in Abaqus/Standard when significant mesh distortion occurs. However, in Explicit and CEL, ϵ_q^p increases gradually and, at $k_h \approx 0.1$, the rate of increase of ϵ_q^p becomes high.

In summary, Abaqus CEL can successfully simulate the failure of a clay slope even at large deformation. Failure occurs at lower k_h in implicit analysis than that of in Explicit and CEL analyses. The FE modeling provides deformation while the LEM gives only the decrease in F_s with increase in k_h.

3.7.1.2 Pseudostatic simulation results for Slope-II

In Slope-I, because uniform s_{u0} in the upper clay layer, failure initiates from the interface between the clay and base layers (Figs. 3.2(a–c)). In order to investigate the effects of shear strength of the upper clay layer on failure patterns, pseudostatic FE and LE analyses are performed for the Slope-II. Figure 3.4 shows the progressive development of failure planes with k_h using three FE modeling approaches. As the linearly increasing s_{u0} profile is used, the failure plane does not reach the bottom of the upper clay layer. Only the curved failure planes develop without formation of any horizontal shear band as in Fig. 3.2. The critical circles obtained from LE analysis using Slope/W is comparable to FE analysis as shown in the 1st column of Fig. 3.4. The maximum depth of the failure plane from the toe is 3~4 m. Similar to Slope-I, the yield coefficient k_y (i.e. value of k_h when ϵ_q^p generates along a complete failure plane) is lower in implicit analysis than the other two FE methods— $k_y \approx 0.04$ in implicit while $k_y \approx 0.06$ in Explicit and CEL. Figure 3.4(l) shows that extremely large mesh distortion occurs after k_y, which implies that the solution obtained from Lagrangian based implicit FE approach is not acceptable at large deformations. However, mesh distortion issue is completely avoided in Abaqus CEL.

3.7.1.3 <u>Effect of FE mesh size</u>

Figure 3.5 shows the formation of failure planes with k_h for four mesh sizes. The width of ϵ_q^p accumulation zone increases with increase in mesh size. At large k_h, a number of distinct shear bands form in the upslope area near the ground surface for small meshes (e.g. 0.125 m, Fig. 3.5(c)). However, ϵ_q^p accumulates in a thick zone for large mesh (e.g. 1.0 m, Fig. 3.5(l)). Overall, the failure pattern is very similar for these mesh sizes; however, the computational cost increases significantly for small mesh. Therefore, in the present study, all the other analyses are performed using 0.25 m cubical elements.

3.7.2 Dynamic FE analyses

The pseudostatic analysis may not provide actual response of the slope in many cases (Jibson, 1993, 2011; Bray and Travasarou, 2009). In addition to uncertainty in the selection of appropriate value of k_h, generally it tends to provide over-conservative solution while in some cases it is unconservative (Jibson, 2011). Dynamic analysis is presented in this section aiming to show the similarities and differences between the results from pseudostatic and dynamic FE models. Dynamic analysis is also performed considering post-peak degradation of shear strength due to earthquake loading.

The following are some of the challenging issues in dynamic FE modeling: (i) modeling of stress–strain behaviour of soil including the degradation of shear strength due to earthquake loading; (ii) modeling of large deformation without numerical issues (iii) selection of a suit of input ground motion; and (iv) modeling of boundary conditions. The

advantages of Abaqus CEL for modeling large deformation are discussed in previous sections. The dynamic analyses are performed for the Slope-II (Fig. 3.1b) with and without post-peak degradation of s_u (Fig. 3.6).

3.7.2.1 <u>Input motions</u>

The intensity of earthquake excitation could significantly affect slope failure mechanisms. Figure 3.7 shows the horizontal acceleration–time histories of 9 reference earthquake input motions used in the present numerical simulations, which are obtained from the Pacific Earthquake Engineering Research Center (PEER) ground motion database (PEER, 2010). These earthquakes are considered because they cover a wide range of peak ground accelerations (a_{peak}=0.183g–0.821g) and significant durations (t_{sig}=4.34–24.91 sec). The moment magnitude (M_M) varies between 6.0 and 7.6, which can cause widespread landslides (Keefer, 1984). All these motions are baseline corrected, which is verified using DEEPSOIL software (Hashash et al., 2015) and therefore unexpected velocity and displacement are avoided. The input earthquake excitation is applied as an acceleration–time history at the base of the model, which is similar to previous dynamic FE analysis of slopes (Ghosh and Madhabushi, 2003; Melo, 2004; Azizan and Popescu, 2003, 2006; Aryal, 2006; Kourkoulis et al., 2010; Taiebat et al., 2010; Kaynia and Saigili, 2014; Mitani et al., 2015).

3.7.2.2 <u>Boundary conditions</u>

The selection of appropriate boundary conditions is a challenging task in dynamic FE modeling. In pseudostatic FE analysis, fixed boundary conditions at a sufficiently large distance from the slope—defined by velocity or fixity—does not affect the simulation results. However, in dynamic FE analysis, energy radiation and wave reflection from the boundary plays a major role. Different approaches have been used in the past, which includes the placement of lateral boundary very far from the slope, infinite elements at the end, the use of absorbent, transmitting or non-reflecting lateral boundaries to minimize undesirable parasitic boundary effect due to the seismic reflection to the zone of concern (Melo and Sharma, 2004; Azizan and Popescu, 2003, 2006; Aryal 2006; Refahi, 2006; Kourkoulis et al., 2010; Taiebat et al., 2010; Wakai, 2010, 2012; Mitani et al, 2013; Nielsen, 2014).

In the present analysis, the lateral boundary effects are minimized by placing them at large distance from the slope (cf. § II) together with appropriate boundary conditions. For Implicit and Explicit analyses, infinite elements are used at the two lateral ends of the model. However, infinite elements cannot be used in CEL analysis. Hence, a nonreflecting Eulerian outflow boundary condition is used in CEL modeling. The mathematical formulations of inflow/outflow Eulerian boundaries for modeling non-reflecting boundary conditions could be found in previous studies (Cerjan et al., 1985; Atassi and Galan, 2007; Jiang et al., 2010). The effects of lateral boundary condition on slope failure are discussed later.

3.7.2.3 <u>Material Damping</u>

The energy dissipation primarily occurs due to frequency independent hysteretic behaviour of soil, which can be incorporated in dynamic FE analysis using nonlinear stress–strain relationship (Kwok et al., 2007; Mánica et al., 2014; Tsai et al., 2014). As elasto-plastic soil model is used in the present study, the plastic flow can simulate hysteretic damping when loading/unloading occurs from yield strength, and therefore additional damping is required only in elastic part (Zhai et al., 2004; Mánica et al., 2014). For cyclic loading inside yield surface, energy dissipation can be achieved by nonlinear variation of stiffness with Masing's rule (Masing, 1926; Chen and Qiu, 2014) and viscous damping. As the main interest of the present study is to investigate large deformation failure of slopes, pre-yield stiffness variation is not considered, which requires additional reliable soil models and is left for a future study. Mánica et al. (2014) compared the damping models available in FLAC (Itasca, 2012) and showed the best performance with the Rayleigh damping method for their problems. In the present study, the viscous damping is incorporated using Rayleigh damping, as previous studies (Martino and Mugnozza, 2005; Ju and Ni, 2007; Alipour and Zareian, 2008; Jehel et al., 2014; Lindberg and Sandvik, 2015). The default bulk viscosity is used to control high frequency oscillations. Abaqus CEL neglects mass proportional damping. The stiffness proportional damping $\beta=0.000375$ is used, which represents approximately 2–3% damping ratio for the problems analyzed in this study. This is verified by comparing the simulation results using Quake/W (GeoStudio 2016) for this range of damping ratio.

3.7.3   Dynamic FE results

3.7.3.1 Effects of lateral boundary condition

Figure 3.8 shows the simulation results with and without Eulerian nonreflecting lateral boundary conditions for Slope-II (Fig. 3.1(b)) subjected to the Parkfield earthquake loading (Fig. 3.7(c)), at t=30 s. In both cases, the lateral boundary is placed at 200 m from the toe of the slope. The analysis with nonreflecting boundary condition shows the development of small plastic shear strain only near the toe (Fig. 3.8(a)). However, in the analysis without nonreflecting boundary condition shows the development of a complete failure plane (Fig. 3.8(b)). This is because of considerable wave reflection from the lateral boundaries even though they are placed sufficiently far from the slope. As mentioned before, infinite elements have been successfully used in Lagrangian FE methods to avoid boundary effects. Dynamic analysis using Abaqus/Explicit is also performed with infinite elements at the lateral boundaries. The acceleration–time histories in soil elements and the development of ϵ_q^p are in good agreement with CEL results for Eulerian nonreflecting boundary condition. This implies that the nonreflecting boundary condition in CEL can successfully simulate the lateral boundary, in addition to its advantage of simulating large deformation.

3.7.3.2 Dynamic FE results for elastic-perfectly plastic clay

The soil parameters used in dynamic FE modeling are shown in Table 3.2. Figure 3.9 shows the development of failure planes in Slope-II using three FE approaches for the 9 earthquakes shown in Fig. 3.7. In order to investigate post-quake behaviour, the simulation

41

is continued after earthquake until the change in stress and deformation is negligible with time. For brevity, ϵ_q^p only at the end of simulation is shown in Fig. 3.9.

In order to compare the results of dynamic FE analysis (Fig. 3.9) with pseudostatic FE analysis (Fig. 3.4), the pseudostatic horizontal coefficient k_h for the earthquakes shown in Fig. 3.7 is estimated. As mentioned in the introduction, the estimation of k_h is a challenging task. Terzaghi (1950) recommended k_h simply based on severity of the earthquake. Considering a tolerable seismic displacement of 1 m for earth dams, k_h between 0.05 and 0.15 has been recommended (Abramson et al. 2002). Some studies suggested k_h as a percentage of the peak ground acceleration (a_{peak}) (Seed, 1979; Marcuson and Franklin, 1983; Matsuo et al., 1984; Taniguchi and Sasaki, 1985). Pyke (1991) proposed a chart for k_h/a_{peak} as a function earthquake magnitude M_M. As a_{peak} and M_M are known for the earthquakes shown in Fig. 3.7, k_h is calculated using Pyke's chart and the values are shown in Fig. 3.7 and in the first column of Fig. 3.9. Using this value of k_h, limit equilibrium analysis is performed using Slope/W. The location of the critical circle (dashed line) and corresponding F_s are shown in the second column of Fig. 3.9.

Figures 3.9(a–f) show the development of very small ϵ_q^p only near the toe for the Whitter Narrows and Northridge earthquakes. The LE analyses with corresponding k_h (=0.032 and 0.048) give F_s greater than 1. Compared with pseudostatic FE analysis for this range of k_h in Fig. 3.4 (3rd and 4th rows) shows similar ϵ_q^p in CEL and Explicit analyses. However, implicit analysis gives higher ϵ_q^p in pseudostatic analysis (Fig. 3.4(i)) than that of in dynamic FE analysis (Fig. 3.9(f)) for the Northridge earthquake.

42

The Parkfield earthquake was of short duration (t_{sig}=4.34 sec). The CEL and Explicit analyses do not show global failure (Figs. 3.9(g & h)) while the pseudostatic analysis with corresponding k_h (=0.065) show the formation of a complete failure planes (Figs. 3.4(j & k)). Calculated toe displacement for implicit analysis is less in the dynamic FE modeling (Fig. 3.9(i)) than that of in pseudostatic modeling (Fig. 3.4(l)). This simulation shows that the duration of earthquake influences the failure and displacement of the slope (Bray and Rathje, 1998; Kourkoulis et al., 2010; Chen and Qiu, 2014; Park and Kutter, 2015).

Global failure occurs for the other 6 earthquakes (see the last 6 rows of Fig. 3.9). The calculated F_s using Slope/W with k_h obtained from Pyke's chart is less than 1.0. The critical circle obtained from Slope/W is located along the shear band obtained from dynamic FE analysis using Abaqus CEL.

In implicit and explicit FE simulations of Chi-Chi earthquake, significantly high ϵ_q^p generates in a wide shear band in dynamic analysis (Figs. 3.9(k & l)) as compared to pseudostatic analysis with estimated k_h=0.065 (Figs. 3.4(k & l)). A potential reason for this difference is the long duration of earthquake (t_{sig}=24.91 sec). Once the failure is initiated, the displacement of the failed soil mass over a long period of cyclic loading widens the zone of plastic shear strain. However, in pseudostatic analysis the earthquake induced body force simply acts as a permanent force where loading period does not have any effect.

In case of Kocaeli, Mammoth Lake and Loma Gilroy earthquakes, dynamic analysis gives lower ϵ_q^p than pseudostatic analysis. Significantly large distortion of mesh occurs in pseudostatic implicit analyses for the estimated range of k_h=0.070–0.088, and therefore it

is not shown in Fig. 3.4. However, in dynamic analysis mesh distortion is relatively less

(Figs. 3.9(r, u & x)).

Finally, the Kobe is a very strong earthquake which could reduce the F_s significantly lower

than 1.0. Abaqus CEL simulation shows that ϵ_q^p generates over a large area; however, its

value is high along the critical failure plane obtained from LE analysis. Explicit and

implicit analyses also give a wide zone of ϵ_q^p. Extremely large distortion of mesh occurs in

these simulations (see the insets of Figs. 3.10(z & aa)), and therefore these solutions are

not reliable. However, it is shown here to demonstrate the limitations of these approaches.

In summary, the comparison between Figs. 3.4 and 3.9 reveals the following: (i) Abaqus

CEL can successfully simulate the failure of the slope, including the large deformation of

the failed soil mass, (ii) the pseudostatic FE modeling results may not be always consistent

with dynamic FE analysis results and (iii) the duration of earthquake loading also

influences the failure process.

3.7.3.3 Dynamic FEM results for post-peak softening of undrained shear strength of

upper clay

In addition to the soil parameters listed in Table 3.2, two additional parameters (S_t and δ_{95}

in Eq. 3.1) are required for modeling post-peak degradation of s_u of the upper clay layer in

Fig 1(b). In this study, S_t=1.5 and δ_{95}=250 mm are used. Note that, S_t in this paper is used

to represent the reduction of s_u of typical clay due to cyclic loading, which is very similar

to "remoulded sensitivity" used by Randolph and his coworkers (Randolph, 2004; Einav

44

and Randloph,2005). The remoulded sensitivity of typical clay such as kaolin or glacial clay is in the range of 1.5–3.0 (Dey et al., 2016), while the sensitivity of sensitive clay could be significantly higher than these values. A large amount of accumulated plastic shear strain is required to reach s_{uR} (Randolph, 2004; Einav and Randolph, 2005). For the value of δ_{95} and element size used in this study, the 95% reduction in s_u will occur at $\gamma^p=100\%$ (i.e. δ_{95}/t_{FE}).

Figures 3.10(a–c) show that the slope is globally stable for Whittier Narrows earthquake. As shown in Eq. (3.1), the s_u degradation occurs only if plastic shear strains develop. For this earthquake, very small plastic shear strain generates, which is not sufficient to reduce s_u significantly. Therefore, the post-peak degradation of s_u does not have significant effect on failure patterns.

Similarly, Figs. 3.10(d & e) show that slope is globally stable when the dynamic FE analyses are performed using CEL and Explicit. However, the implicit analysis shows the formation of a complete failure plane (Fig. 3.10(f)). As mentioned before, implicit analysis generally calculates higher ϵ_q^p than Explicit and CEL, especially around and after global failure (cf. Figs. 3.4(g–l)). The reduction of s_u at these ϵ_q^p causes redistribution of load and therefore a complete failure plane develops. A very similar response is found for the Parkfield earthquake in CEL and explicit simulations (Figs. 3.10(g & h)). However, very significant mesh distortion occurs in implicit analysis and therefore the results are not presented. Note that global failure is calculated from implicit analysis even without softening (Fig. 3.9(i)).

For the no softening cases (Fig. 3.9), the last six rows show the development of ϵ_q^p along the complete failures planes. As softening is considered in the simulations presented in Fig. 3.10, ϵ_q^p reduces s_u which generates additional ϵ_q^p along the failure planes. The following are the key observation from the last 6 rows of Figs. 3.9 and 3.10.

- Softening increases ϵ_q^p along the failure planes. Clear shear bands form in a narrow zone, as compared to no softening case, because of concentration of ϵ_q^p due to softening.

- In some cases, additional clear shear bands form when softening is considered (cf. Figs. 3.9(j) & 3.10(i)).

- The failed soil mass displaces significantly as observed from upslope ground settlement near the failure plane and heave at the toe (e.g. Fig. 3.10(k)).

- Extremely distorted mesh at large deformation is observed in implicit and explicit analyses. Therefore, in modeling of large deformation slope failure, implicit analysis is not suitable and explicit analysis is questionable. The CEL does not have any mesh distortion issue.

3.8   Conclusions

Large deformation FE modeling of clay slope failure due to earthquake loading is presented in this study. The coupled Eulerian Lagrangian (CEL) approach in Abaqus FE software is used for numerical simulation. The CEL models are developed through a systematic calibration of results against implicit and explicit FE simulations which have been used in

previous studies for slope stability analysis. Two approaches are used to incorporate earthquake effects in FE simulations: (i) in the pseudostatic method, the earthquake induced force is applied by a pseudostatic horizontal coefficient k_h, (ii) in dynamic analysis, the acceleration–time history is applied at the base of the model. The performance of CEL modeling, in terms of location of global failure plane and earthquake load required for slope failure, is compared with traditional limit equilibrium method. The following conclusions are drawn from this study.

a) The CEL approach in Abaqus can be used for modeling clay slope failures. The CEL results are comparable to implicit and explicit FE analyses at small deformation levels. However, the latter two FE modeling techniques cannot be used for large deformation because of significant mesh distortion.

b) The location of the global failure planes obtained from pseudostatic FE modeling is consistent with critical circle in pseudostatic limit equilibrium analysis. However, in FE modeling with uniform s_{u0} in the upper clay layer also shows horizontal (local) shear bands.

c) Dynamic FE simulation results does not always match with pseudostatic FE results based on estimated k_h using Pyke's chart. The duration of earthquake influences the deformation behaviour and thereby failure process, which cannot be captured using the pseudostatic coefficient.

d) Post-peak degradation of shear strength increases the propensity of failure initiation if the slope is in the verge of failure. The deformation of failure and plastic shear strains along the failure planes increase with degradation of strength.

47

Acknowledgements

Notations

β	Stiffness proportional damping
δ	Accumulated plastic shear displacement
δ_{95}	δ at which s_u reduced by 95% of (s_{up}-s_{uR})
$\dot{\epsilon}_{ij}^{p}$	Plastic deviatoric strain rate tensor
ϵ_{q}^{p}	Generalized plastic shear strain
γ^{p}	Plastic shear strain
ν_u	Undrained Poisson's ratio
a_{peak}	Peak acceleration
E_u	Undrained modulus of elasticity
F_b	Horizontal body force per unit volume
F_s	Factor of safety
k_h	Horizontal pseudostatic coefficient

k_y Yield pseuodstatic coefficient

M_M Moment magnitude of earthquake

PI Plasticity index

S_t Sensitivity of clay, s_{u0}/s_{uR}

s_u Mobilized undrained shear strength

s_{u0} Initial (peak) undrained shear strength

s_{uR} Remolded s_u at large plastic shear displacement

t_{FE} Length of cubical elements (thickness of FE mesh size)

t_{sig} Significant duration of earthquake ground motion

z Depth from upslope ground surface

(a) Slope-I

Void

c

d

15 m

1

2

Upper clay
(Uniform s_{u0})

25 m

a

b

200 m

200 m

10 m

y

Base
(Elastic)

x

400 m

(b) Slope-II

Void

c

d

15 m

1

2

Upper clay
(Linearly increasing s_{u0} with and
without softening)

30 m

a

b

200 m

200 m

Stiff clay
(Uniform s_{u0})

15 m

y

Base (Elastic)

2 m

x

400 m

Not in scale

Figure 3.1: Geometry of the slopes used in FE modeling
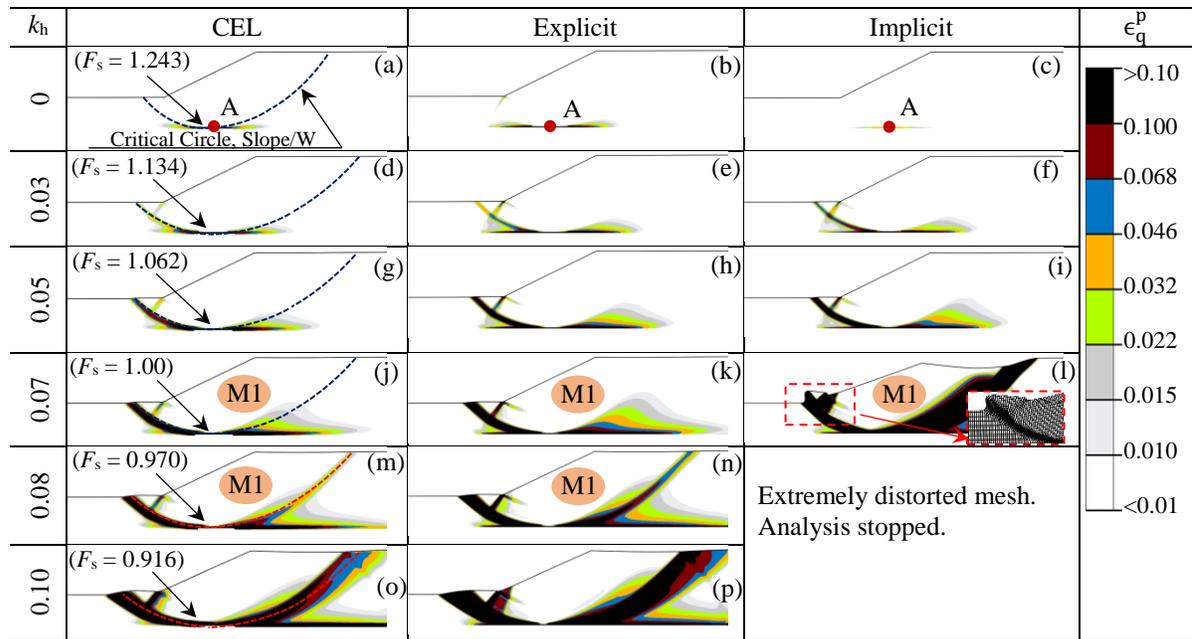
Figure 3.2: Pseudostatic analyses for Slope-I using three FE modeling approaches

51
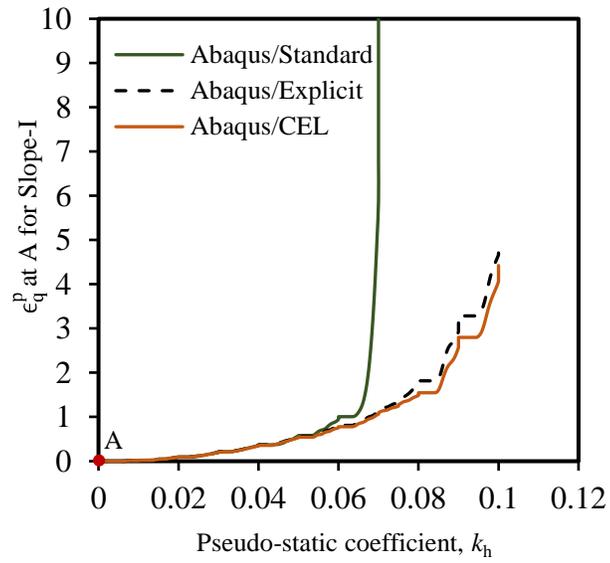
Figure 3.3: Comparison of ϵ_q^p at the integration point A with variations of pseudostatic coefficients (k_h)
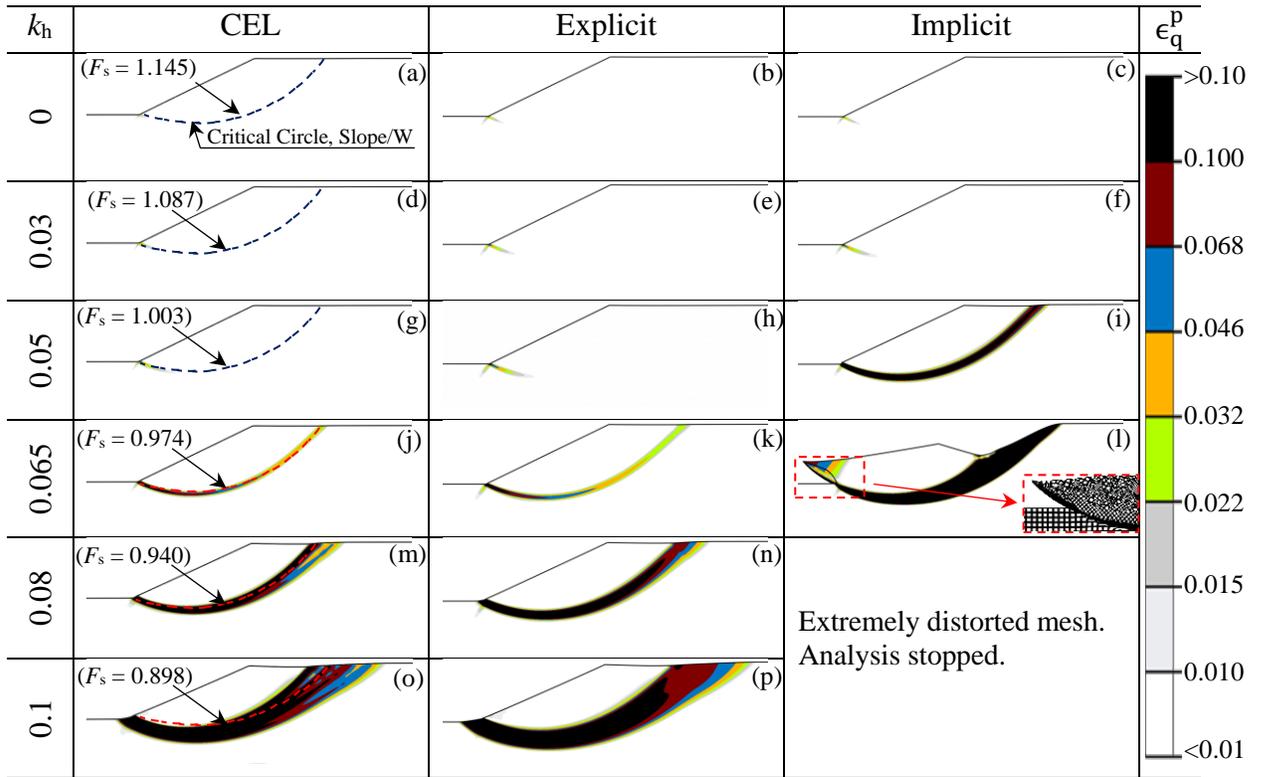
Figure 3.4: Pseudostatic analyses for Slope-II using three FE modeling approaches
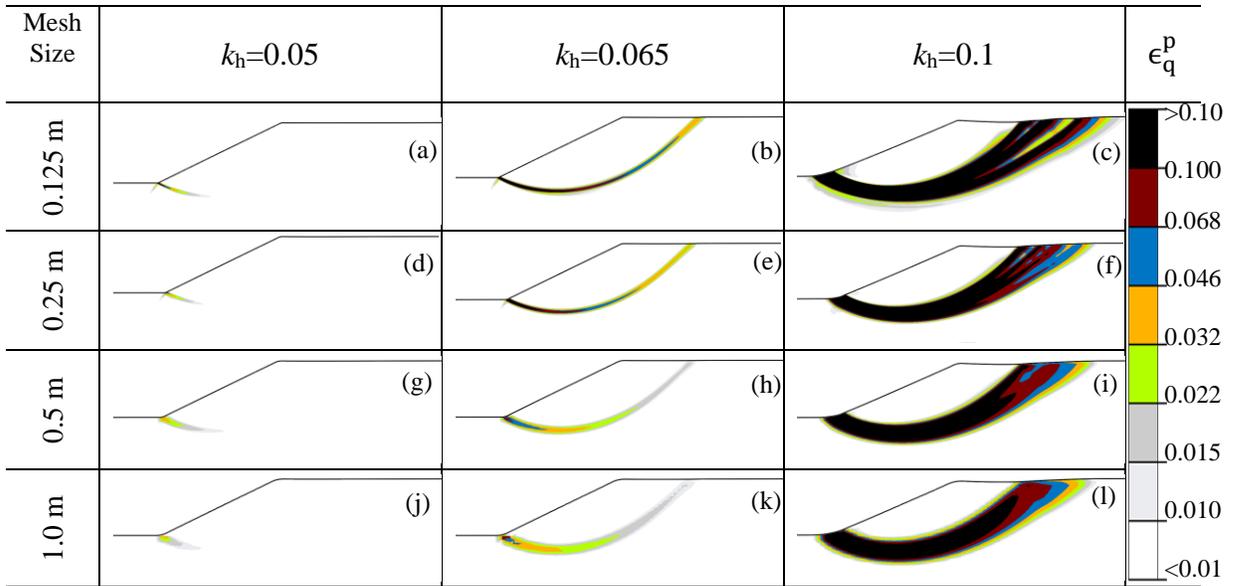
Figure 3.5: Mesh size effects on FE results based on pseudostatic analyses in Slope-II.
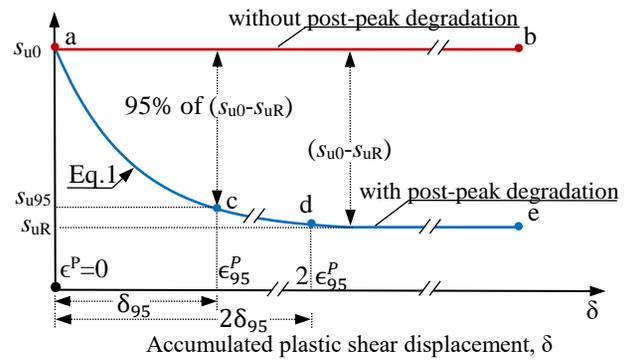
Figure 3.6: Stress strain behaviour used in FE modeling
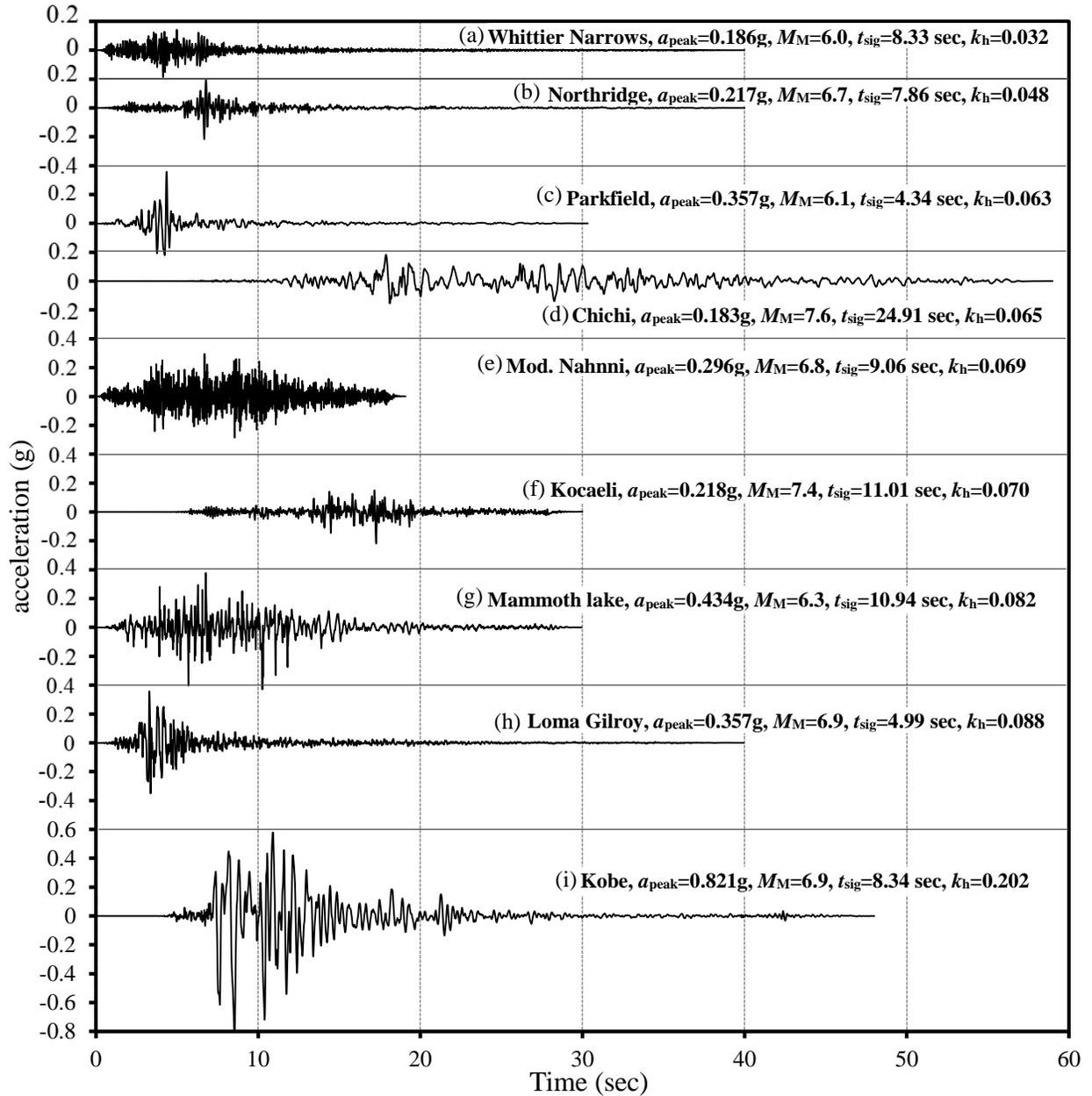
Figure 3.7: Acceleration time histories as reference earthquake input motions

used in numerical simulation

	ε_q^p	
	>0.10	
	0.100	
	0.068	
	0.046	
	0.032	
	0.022	
	0.015	
	0.010	
	<0.010	

CEL (With Eulerian non-reflecting boundary)	CEL (without Eulerian non-reflecting boundary)
(a)	(b)
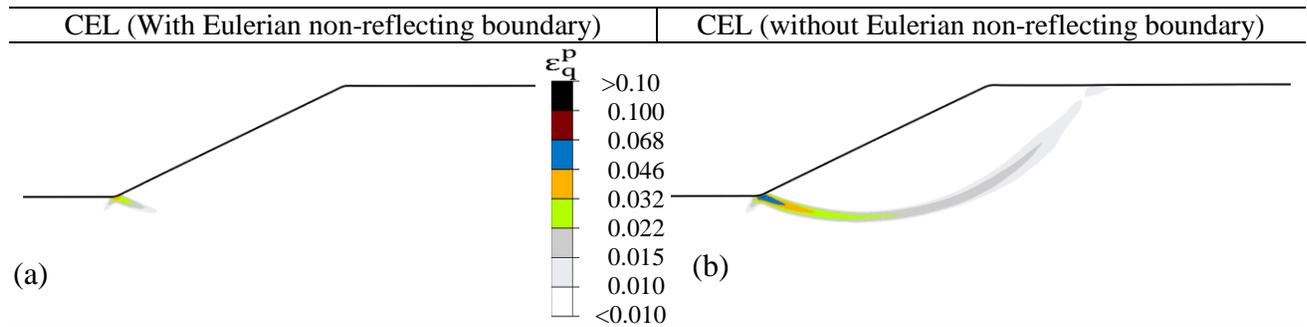
Figure 3.8: Effect of including non-reflecting outflow Eulerian boundary conditions in

Abaqus/CEL analyses (shown for Parkfield earthquake input motion)

Earthquake Input Motions	CEL	Explicit	Implicit	ϵ_q^p
Whittier Narrows (k_h=0.032)	(F_s = 1.055) (a) Critical Circle, Slope/W	(b)	(c)	>0.10
Northridge (k_h=0.048)	(F_s = 1.015) (d)	(e)	(f)	0.100
Parkfield (k_h=0.063)	(F_s = 1.001) (g)	(h)	(i)	0.068
Chichi (k_h=0.065)	(F_s = 0.973) (j)	(k)	(l)	0.046
Mod. Nahnni (k_h=0.069)	(F_s = 0.965) (m)	(n)	(o)	0.032
Kocaeli (k_h=0.070)	(F_s = 0.962) (p)	(q)	(r)	0.022
Mammoth lake (k_h=0.082)	(F_s = 0.936) (s)	(t)	(u)	0.015
Loma Gilroy (k_h=0.088)	(F_s = 0.923) (v)	(w)	(x)	0.010
Kobe (k_h=0.202)	(F_s = 0.724) (y)	(z)	(aa)	<0.01

Figure 3.9: Dynamic analysis for perfectly plastic soil condition by three FE modeling

approaches

Earthquake Input Motions	CEL	Explicit	Implicit	ϵ_q^p
Whittier Narrows (k_h=0.032)	(a)	(b)	(c)	>0.10
Northridge (k_h=0.048)	(d)	(e)	(f)	0.100
Parkfield (k_h=0.063)	(g)	(h)		0.068
Chichi (k_h=0.065)	(i)	(j)		0.046
Mod. Nahnni (k_h=0.069)	(k)	(l)		0.032
Kocaeli (k_h=0.070)	(m)	(n)	Extremely distorted mesh. Analysis stopped.	0.022
Mammoth lake (k_h=0.082)	(o)	(p)		0.015
Loma Gilroy (k_h=0.088)	(q)	(r)		0.010
Kobe (k_h=0.202)	(s)	(t)		<0.01
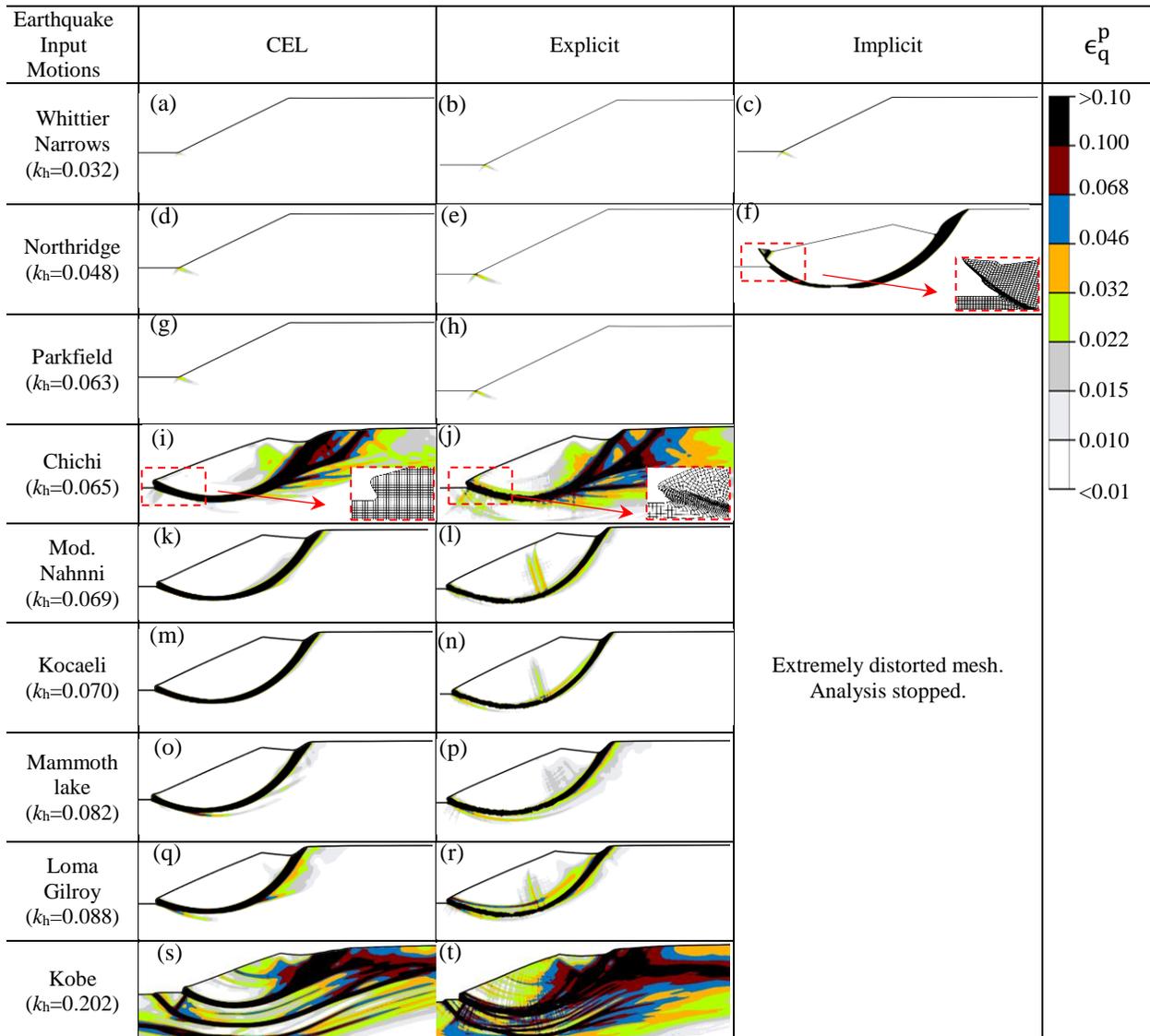
Figure 3.10: Dynamic analyses for post-peak softening soil condition by three FE modeling approaches.

Table 3.1: Advancement of numerical modeling technique

Numerical Technique	Analyzed Seismic Phenomenon	References
FE analysis using 2D dynamic stress analysis technique	Elastic, homogeneous and isotropic earth dam	Chopra et al. (1969)
FE analysis using FLUSH & NOLM	Elastoplastic clay embankment dam	Wu (1992)
FE analysis using SAP-IV	Gravity -dam reservoir system with Eulerian and Lagrangian approaches	Calayir et al. (1996)
FE analysis using DYNAFLOW	Simplified liquefaction assessment on embankment dam	Popescu (2002)
	Nonlinear submarine slope assessment in sand and silt	Azizan and Popescu (2006)
FE analysis using Quake/W & AMPLE	Case study on submarine sensitive clay slopes	Leynaud et al. (2004)
FE analysis using PLAXIS	Idealized, natural and man-made slopes	Aryal (2006)
	Pseudostatic analysis on simple slope	Loria (2014)
	Case study on submarine slope with weak clay layers	Rodríguez-Ochoa et al. (2015)
FE analysis using power law strength relation	Pseudostatic analysis on simple homogeneous slopes	Li (2007)
FE analysis using ICFEP	Pseudostatic analysis of homogenous slope	Tan and Sarma (2008)
	Case study on elastoplastic earth dam	Pelecanos et al. (2015)
FD analysis using FLAC	Pseudostatic analysis on homogeneous earth embankment slope	Melo and Sharma (2004)
	Case study on Calitri landslide	Martino and Mugnozza (2005)
	Stability analysis of Waba earth dam	Refahi (2006)
	Elastoplastic saturated clay slope	Taiebat et al. (2010)
FE analysis using Abaqus & SNAC	Pseudostatic analysis on simple homogeneous slope	Loukidis et al. (2003)
FE analysis using Abaqus	Stability analysis of homogeneous slope with interaction of foundation at the ground surface	Kourkoulis et al. (2010)
	Case study on tuffs and shale slopes	Mitani et al. (2013)
	Pseudostatic analysis on simple homogeneous slope	Khosravi et al. (2013)
Numerical analysis using QUIVER_slope	Infinite slopes with strain softening behavior	Kaynia and Saygili (2014)
Mesh free analysis using SPH method in Abaqus	Large deformation study on shake table test for clay slopes by Wartman (2005)	Chen and Qiu (2014)
FE analysis using Abaqus CEL & MPM method	Case study on sliding mass over a rock layer	Moorman and Hamad (2015)

Table 3.2: Geotechnical Parameters used in Finite Element Analyses

Parameters	Values		
	Soft Clay	**Stiff Clay**	**Base**
Undrained Young's Modulus, E_u: Mpa	10	10	100
Poisson ratio, v_u	0.495	0.495	0.495
Saturated unit weight, γ_{sat}: kN/m^3	20	20	20
Undrained shear strength for clay, s_u: kPa	60 (Slope-I)	-	-
	15+2.67z* (Slope-II)		-

* z is the depth from the ground surface

Bibliography

Abramson, L.W., Lee, T.S., Sharma, S. and Boyce, G.M., 2002. *Slope Stability and Stabilization Methods*, 2nd ed., John Wiley & Sons, Inc., New York, NY, USA.

Alipour, A. and Zareian, F., 2008. Study Rayleigh damping in structures; uncertainties and treatments. In *Proceedings of 14th World Conference on Earthquake Engineering, Beijing, China*.

Ambraseys, N.N. and Srbulov, M., 1994. Attenuation of earthquake-induced ground displacements. *Earthquake engineering & structural dynamics*, *23*(5), pp.467-487.

Aryal, K.P., 2006. *Slope stability evaluations by limit equilibrium and finite element methods*. Doctoral Thesis, NTNU, Trondheim, Norway.

Atassi, O.V. and Galán, J.M., 2008. Implementation of nonreflecting boundary conditions for the nonlinear Euler equations. *Journal of Computational Physics*, *227*(3), pp.1643-1662.

Azizian, A. and Popescu, R., 2003. Finite element simulation of retrogressive failure of submarine slopes. *Submarine Mass Movements and Their Consequences*. Springer Netherlands, pp. 11-20.

Azizian, A. and Popescu, R., 2006. Three-dimensional seismic analysis of submarine slopes. *Soil Dynamics and Earthquake Engineering*, *26*(9), pp.870-887.

Benson, D.J., 1992. Computational methods in Lagrangian and Eulerian hydrocodes. *Computer methods in Applied mechanics and Engineering*, *99*(2), pp.235-394.

Benson, D.J., 1995. A multi-material Eulerian formulation for the efficient solution of impact and penetration problems. *Computational Mechanics*, *15*(6), pp.558-571.

Benson, D.J. and Okazawa, S., 2004. Contact in a multi-material Eulerian finite element formulation. *Computer methods in applied mechanics and engineering*, *193*(39), pp.4277-4298.

Bray, J.D. and Rathje, E.M., 1998. Earthquake-induced displacements of solid-waste landfills. *Journal of Geotechnical and Geoenvironmental Engineering*, *124*(3), pp.242-253.

Bray, J.D. and Travasarou, T., 2007. Simplified procedure for estimating earthquake-induced deviatoric slope displacements. *Journal of Geotechnical and Geoenvironmental Engineering*, *133*(4), pp.381-392.

Bray, J.D. and Travasarou, T., 2009. Pseudostatic coefficient for use in simplified seismic slope stability evaluation. *Journal of Geotechnical and Geoenvironmental Engineering*, *135*(9), pp.1336-1340.

Bui, H.H., Fukagawa, R., Sako, K. and Wells, J.C., 2011. Slope stability analysis and discontinuous slope failure simulation by elasto-plastic smoothed particle hydrodynamics (SPH). *Geotechnique*, *61*(7), pp.565-574.

Dassault Systèmes 2013. Abaqus user manual, version 6.14-EF2.Waltham, MA, USA: Dassault Systèmes.

Calayir, Y., Dumanoğlu, A.A. and Bayraktar, A., 1996. Earthquake analysis of gravity dam-reservoir systems using the Eulerian and Lagrangian approaches. *Computers & structures*, *59*(5), pp.877-890.

Cerjan, C., Kosloff, D., Kosloff, R. and Reshef, M., 1985. A nonreflecting boundary condition for discrete acoustic and elastic wave equations. *Geophysics*, *50*(4), pp.705-708.

Cheng, Y.M., Lansivaara, T. and Wei, W.B., 2007. Two-dimensional slope stability analysis by limit equilibrium and strength reduction methods. *Computers and Geotechnics*, *34*(3), pp.137-150.

Chen, W. and Qiu, T., 2014. Simulation of earthquake-induced slope deformation using SPH method. *International Journal for Numerical and Analytical Methods in Geomechanics*, *38*(3), pp.297-330.

Chopra, A.K., Dibaj, M., Clough, R.W., Penzien, J. and Seed, H.B., 1969, Earthquake analysis of earth dams. In *Proc. 4th World Conf. on Earthq. Engrg., Santiago*.

Corps of Engineers, 1970. *Stability of earth and rock-fill dams*, Engineer Manual 1110-2-1902, U.S. Army Corps of Engineers, Washington D.C., USA.

Dawson, E. M., Roth, W. H., Drescher. A., 1999. Slope stability analysis by strength reduction. *Geotechnique*, *49*(6):835–840.

de Borst, R., 1991. Simulation of strain localization: a reappraisal of the Cosserat continuum. *Engineering computations*, *8*(4), pp.317-332.

de Borst, R., Sluys, L.J., Muhlhaus, H.B. and Pamin, J., 1993. Fundamental issues in finite element analyses of localization of deformation. *Engineering computations*, *10*(2), pp.99-121.

Dey, R., Hawlader, B., Phillips, R. and Soga, K., 2015. Large deformation finite element modeling of progressive failure leading to spread in sensitive clay slopes. *Géotechnique*, *65*(8), pp.657-668.

Dey, R., Hawlader, B., Phillips, R. and Soga, K., 2016. Modeling of large-deformation behaviour of marine sensitive clays and its application to submarine slope stability analysis. *Canadian Geotechnical Journal*, *53*, pp.1-18.

Duncan, J.M., 1996. State of the art: limit equilibrium and finite-element analysis of slopes. *Journal of Geotechnical engineering*, *122*(7), pp.577-596.

Dutta, S., Hawlader, B. and Phillips, R., 2015. Finite element modeling of partially embedded pipelines in clay seabed using Coupled Eulerian–Lagrangian method. *Canadian Geotech. Journal*, *52*(1), pp.58-72.

Einav, I. and Randolph, M.F., 2005. Combining upper bound and strain path methods for evaluating penetration resistance. *International Journal for Numerical Methods in Engineering*, *63*(14), pp.1991-2016.

Gauer, P., Kvalstad, T.J., Forsberg, C.F., Bryn, P. and Berg, K., 2005. The last phase of the Storegga Slide: simulation of retrogressive slide dynamics and comparison with slide-scar morphology. *Marine and Petroleum Geology*, *22*(1), pp.171-178.

GeoStudio 2016, GEOSLOPE International Ltd. Calgary, AB, Canada.

Ghosh, B. and Madabhushi, S.P.G., 2003. A numerical investigation into effects of single and multiple frequency earthquake motions. *Soil Dynamics and Earthquake Engineering*, *23*(8), pp.691-704.

Griffiths, D.V. and Lane, P.A., 1999. Slope stability analysis by finite elements. *Geotechnique*, *49*(3), pp.387-403.

Hamann, T., Qiu, G. and Grabe, J., 2015. Application of a Coupled Eulerian–Lagrangian approach on pile installation problems under partially drained conditions. *Computers and Geotechnics*, *63*, pp.279-290.

Hashash, Y.M.A., Musgrove, M.I., Harmon, J.A., Groholski, D.R., Phillips, C.A. and Park, D., 2015. DEEPSOIL 6.1, User manual. *Board of Trustees of University of Illinois at Urbana-Champaign, Urbana*.

Henke, S., Hamann, T. and Grabe, J., 2011. Coupled Eulerian-Lagrangian simulation of the deep vibration compaction process as a plastodynamic problem. In *Proceedings of the 8th international conference on structural dynamics, EURODYN* (pp. 482-489).

Hu, Y. and Randolph, M.F., 1998. A practical numerical approach for large deformation problems in soil. *International Journal for Numerical and Analytical Methods in Geomechanics*, *22*(5), pp.327-350.

Hynes-Griffin, M.E. and Franklin, A.G., 1984. *Rationalizing The Seismic Coefficient Method* (No. Wes/Mp/Gl-84-13). Army Engineer Waterways Experiment Station Vicksburg Ms Geotechnical Lab.

Islam, N. and Hawlader, B., 2016. Pseudostatic Seismic Slope Stability Analyses using a Large Deformation Finite Element Modeling Technique . *The 69th Canadian Geotechnical Conference, Geovancouver 2016*, Vancouver,B.C, Canada, Oct 2-5.

Itasca, 2012. FLAC3D. Fast lagrangian analysis of continua in 3-dimensions, version 5.0, manual. Itasca, Minnesota.

Jehel, P., Léger, P. and Ibrahimbegovic, A., 2014. Initial versus tangent stiffness-based Rayleigh damping in inelastic time history seismic analyses. *Earthquake Eng. & Structural Dynamics*, *43*(3), pp.467-484.

Jiang, Z., Bancroft, J.C. and Lines, L.R., 2010. Combining absorbing and nonreflecting boundary conditions for elastic wave simulation. In *SEG Int. Exposition and Eightieth Annual Meeting, Denver, Colorado.*

Jibson, R.W., 1993. Predicting earthquake-induced landslide displacements using Newmark's sliding block analysis. *Transportation research record*, pp.9-9.

Jibson, R.W., 2011. Methods for assessing the stability of slopes during earthquakes—A retrospective. *Engineering Geology*, *122*(1), pp.43-50.

Ju, S.H. and Ni, S.H., 2007. Determining Rayleigh damping parameters of soils for finite element analysis. *Int. Journal for Numerical and Analytical Methods in Geomechanics*, *31*(10), pp.1239-1255.

Kaynia, A.M. and Saygili, G., 2014. Predictive Models for Earthquake Response of Clay and Sensitive Clay Slopes. *Perspectives on European Earthquake Engineering and Seismology*, pp.557-584.

Keefer, D.K., 1984. Landslides caused by earthquakes. *Geological Society of America Bulletin*, *95*(4), pp.406-421.

Kramer, S.L., 1996. *Geotechnical earthquake engineering*. Pearson Education.

Kramer, S.L. and Smith, M.W., 1997. Modified Newmark model for seismic displacements of compliant slopes. *Journal of Geotechnical and Geoenvironmental Engineering*, *123*(7), pp.635-644.

Kourkoulis, R., Anastasopoulos, I., Gelagoti, F. and Gazetas, G., 2010. Interaction of foundation− structure systems with seismically precarious slopes: Numerical analysis with strain softening constitutive model. *Soil Dynamics and Earthquake Engineering*, *30*(12), pp.1430-1445.

Kvalstad, T.J., Nadim, F., Kaynia, A.M., Mokkelbost, K.H. and Bryn, P., 2005. Soil conditions and slope stability in the Ormen Lange area. *Marine and Petroleum Geology*, *22*(1), pp.299-310.

Kwok, A.O., Stewart, J.P., Hashash, Y.M., Matasovic, N., Pyke, R., Wang, Z. and Yang, Z., 2007. Use of exact solutions of wave propagation problems to guide implementation of nonlinear seismic ground response analysis procedures. *Journal of Geotech. and Geoenvironmental Eng.*, *133*(11), pp.1385-1398.

Leynaud, D., Mienert, J. and Nadim, F., 2004. Slope stability assessment of the Helland Hansen area offshore the mid-Norwegian margin. *Marine Geology*, *213*(1), pp.457-480.

Li, X., 2007. Finite element analysis of slope stability using a nonlinear failure criterion. *Computers and Geotechnics*, *34*(3), pp.127-136.

Lindberg, S. and Sandvik, P., 2015. *A comparison of finite element formulations for analysis of the converting process of packaging materials*. Master's Thesis, Chalmers University of Technology, Göteborg, Sweden.

Liu, S.Y., Shao, L.T. and Li, H.J., 2015. Slope stability analysis using the limit equilibrium method and two finite element methods. *Computers and Geotechnics*, *63*, pp.291-298.

Loria, L.C.S., 2014. *Prediction of co-seismic soil slope instability with finite element methods*. Doctoral dissertation, TU Delft, Delft, Netherlands.

Loukidis, D., Bandini, P. and Salgado, R., 2003. Stability of seismically loaded slopes using limit analysis. *Geotechnique*, *53*(5), pp.463-480.

Mánica, M., Ovando, E. and Botero, E., 2014. Assessment of damping models in FLAC. *Computers and Geotechnics*, *59*, pp.12-20.

Martino, S. and Mugnozza, G.S., 2005. The role of the seismic trigger in the Calitri landslide (Italy): historical reconstruction and dynamic analysis. *Soil Dynamics and Earthquake Eng.*, *25*(12), pp.933-950.

Marcuson, W.F. and Franklin, A.G., 1983. *Seismic design analysis and remedial measures to improve the stability of existing earth dams, Corps of Engineers Approach, Seismic Design of Embankments and Caverns*. TR Howard (ed) New York, ASCE.

Masing G., 1926.Eigenspannungen and verfertigung beim messing [Fundamental stresses and strengthening with brass]. In *Proceeding of 2nd International Congress on Applied Mechanics*, *Zurich*, 332–335.

Matsuo, M., Itabashi, K. and Sasaki, Y., 1984, March. Study on a seismicity of earth structures by inverse analyses of actual cases. In *Proceedings Of The Japan Society Of Civil Engineers* (Vol. 1984, No. 343, Pp. 25-33). Japan Society Of Civil Engineers.

Melo, C. and Sharma, S., 2004, August. Seismic coefficients for pseudostatic slope analysis. In *13th World Conference on Earthquake Engineering, Vancouver, BC, Canada, Paper* (No. 369).

Mitani, Y., Wang, F., Okeke, A.C. and Qi, W., 2013. Dynamic analysis of earthquake amplification effect of slopes in different topographic and geological conditions by using ABAQUS. *Progress of Geo-Disaster Mitigation Technology in Asia*, pp.469-490.

Moormann, C. and Hamad, F., 2015. MPM dynamic simulation of a seismically induced sliding mass. In *IOP Conference Series: Earth and Environmental Science* (Vol. 26, No. 1, p. 012024). IOP Publishing.

Mohammadi, S. and Taiebat, H.A., 2013. A large deformation analysis for the assessment of failure induced deformations of slopes in strain softening materials. *Computers and Geotechnics*, *49*, pp.279-288.

Mohammadi, S. and Taiebat, H., 2014. H-adaptive updated Lagrangian approach for large-deformation analysis of slope failure. *International Journal of Geomechanics*, *15*(6), 1943–5622.

Nadim, F. 1998. *Slope stability under Earthquake Loading*, appendix F in Seabead Project. NGI Report, 982512-2.

Newmark, N. M. 1965 Effects of earthquakes on dams and embankments. *Geotechnique, 15 (2)*, 139–160.

Nielsen, A.H., 2014. Towards a complete framework for seismic analysis in Abaqus. In *Proceedings of the Institution of Civil Engineers–Engineering and Computational Mechanics*, *167*(1), pp.3-12.

Park, D.S. and Kutter, B.L., 2015. Static and seismic stability of sensitive clay slopes. *Soil Dynamics and Earthquake Engineering*, *79*, pp.118-129.

PEER, 2010. Pacific Earthquake Engineering Research Center (PEER) ground motion database *http://peer.berkeley.edu/smcat/*

Pelecanos, L., Kontoe, S. and Zdravković, L., 2015. A case study on the seismic performance of earth dams. *Géotechnique*, *65*(11), pp.923-935.

Pestana, J.M. and Nadim, F., 2000. *Nonlinear site response analysis of submerged slopes*. University of California, Department of Civil Engineering, University of California, Berkeley, Geotechnical Eng., Report No. UCB/GT/2000-04.

Popescu, R., 2002. Finite element assessment of the effects of seismic loading rate on soil liquefaction. *Canadian Geotechnical Journal*, *39*(2), pp.331-344.

Potts, D. M. and Zdravkovic, L., 1999. *Finite element analysis in geotechnical engineering: Theory*, London: Thomas Telford.

Potts, D.M., Dounias, G.T. and Vaughan, P.R., 1990. Finite element analysis of progressive failure of Carsington embankment. *Géotechnique*, *40*(1), pp.79-101.

Puzrin, A.M., Germanovich, L.N. and Kim, S., 2004. Catastrophic failure of submerged slopes in normally consolidated sediments. *Géotechnique*, *54*(10), pp.631-643.

Puzrin, A.M., Gray, T.E. and Hill, A.J., 2015. Significance of the actual nonlinear slope geometry for catastrophic failure in submarine landslides. In *Proc. R. Soc. A* (Vol. 471, No. 2175, p. 20140772). The Royal Society.

Qiu, G., Henke, S. and Grabe, J., 2011. Application of a Coupled Eulerian–Lagrangian approach on geomechanical problems involving large deformations. *Computers and Geotechnics*, *38*(1), pp.30-39.

Randolph, M.F., 2004, September. Characterisation of soft sediments for offshore applications. In *Proc. 2nd Int. Conf. on Site Characterisation, Porto* (Vol. 1, pp. 209-231).

Rathje, E.M. and Bray, J.D., 2000. Nonlinear coupled seismic sliding analysis of earth structures. *Journal of Geotechnical and Geoenvironmental Engineering*, *126*(11), pp.1002-1014.

Refahi, K., 2006. *Seismic Stability and Deformation of Waba Dam*. Master's Thesis, Carleton University, Ottawa, Ontario, Canada.

Rodríguez-Ochoa, R., Nadim, F. and Hicks, M.A., 2015. Influence of weak layers on seismic stability of submarine slopes. *Marine and Petroleum Geology*, *65*, pp.247-268.

Seed, H.B. and Martin, G.R., 1966. The seismic coefficient in earth dam design. *Journal of Soil Mechanics & Foundations Div*, *92*(Proc. Paper 4824).

Seed, H.B., Makdisi, F.I. and De Alba, P., 1978. Performance of earth dams during earthquakes. *Journal of Geotechnical and Geoenvironmental Engineering*, *104*(ASCE 13870 Proceeding).

Seed, H.B., 1979. Considerations in the earthquake-resistant design of earth and rockfill dams. *Geotechnique*, *29*(3), pp.215-263.

Soga, K., Alonso, E., Yerro, A., Kumar, K. and Bandara, S., 2016. Trends in large-deformation analysis of landslide mass movements with particular emphasis on the material point method. *Géotechnique*, *66*(3), pp.248-273.

Stewart, J.P., Blake, T.F. and Hollingsworth, R.A., 2003. A screen analysis procedure for seismic slope stability. *Earthquake Spectra*, *19*(3), pp.697-712.

Swan, C.C. and Seo, Y.K., 1999. Limit state analysis of earthen slopes using dual continuum/FEM approaches. *International Journal for numerical and analytical methods in geomechanics*, *23*(12), pp.1359-1371.

Pyke, R., 1991. Selection of seismic coefficients for use in pseudo-static slope stability analyses. *Consulting Engineer, Lafayette CA*.

Tan, D. and Sarma, S.K., 2008. Finite element verification of an enhanced limit equilibrium method for slope analysis. *Geotechnique*, *58*(6), p.481.

Taniguchi, E. and Sasaki, Y., 1985. Back analysis of landslide due to Naganoken Seibu Earthquake of September 14, 1984. In *Proc. of 11th International Conference on Soil Mechanics and Foundation Engineering, San Francisco* (pp. 1-55).

Taiebat, M., Kaynia, A.M. and Dafalias, Y.F., 2010. Application of an anisotropic constitutive model for structured clay to seismic slope stability. *Journal of Geotechnical and Geoenvironmental Engineering*, *137*(5), pp.492-504.

Terzaghi, K., 1950. Mechanisms of landslides, *Engineering Geology*, The Geological Society of America, 83-123.

Thakur, V., 2007. *Strain localization in sensitive soft clays*. PhD thesis, Norwegian University of Science and Technology, Trondheim and Norwegian Centre of Excellence: International Centre for Geohazards, Trondheim, Norway.

Tho, K.K., Leung, C.F., Chow, Y.K. and Palmer, A.C., 2011. Deep cavity flow mechanism of pipe penetration in clay. *Canadian Geotechnical Journal*, *49*(1), pp.59-69.

Trapper, P.A., Puzrin, A.M. and Germanovich, L.N., 2015. Effects of shear band propagation on early waves generated by initial breakoff of tsunamigenic landslides. *Marine Geology*, *370*, pp.99-112.

Troncone, A., 2005. Numerical analysis of a landslide in soils with strain-softening behaviour. *Geotechnique*, *55*(8), pp.585-596.

Tsai, C.C., Park, D. and Chen, C.W., 2014. Selection of the optimal frequencies of viscous damping formulation in nonlinear time-domain site response analysis. *Soil Dynamics and Earthquake Engineering*, *67*, pp.353-358.

Wakai, A., Ugai, K., Onoue, A., Kuroda, S. and Higuchi, K., 2010. Numerical modeling of an earthquake-induced landslide considering the strain-softening characteristics at the bedding plane. *Soils and foundations*, *50*(4), pp.533-545.

Wakai, A., Matsushita, K. and Fukushima, T., 2012. Numerical modeling of an earthquake-induced landslide considering the strain-softening characteristics of the clayey loam. In *15th World Conference on Earthquake Engineering (15 WCEE), Lisbon, Portugal.*

Wang, D., Randolph, M.F. and White, D.J., 2013. A dynamic large deformation finite element method based on mesh regeneration. *Computers and Geotechnics*, *54*, pp.192-201.

Wu, X., 1992. *Seismic behaviour of clay embankment dams*. PhD Thesis, Carleton University, Ottawa, Ontario, Canada.

Zabala, F. and Alonso, E.E., 2011. Progressive failure of Aznalcóllar dam using the material point method. *Géotechnique*, *61*(9), pp.795-808.

Zhai, E., Roth, W., Dawson, E. and Davis, C., 2004. Seismic deformation analysis of an earth dam–a comparison study between equivalent-linear and nonlinear effective-stress approaches. In *13th World Conference on Earthquake Engineering Vancouver, BC, Canada* (pp. 1-6).

Zheng, H., Liu, D. F., Li, C. G., 2005. Slope stability analysis based on elasto-plastic finite element method. *International Journal of. Numerical Methods Eng.*, *64*(14), pp 1871–88.

Chapter 4

Large Deformation Finite Element Modeling of Earthquake-Induced Landslides Considering Strain-Softening Behaviour of Sensitive Clay

4.1   Abstract

Large landslides in sensitive clays cannot be explained properly using the traditional limit equilibrium or Lagrangian-based finite element (FE) methods. In the present study, large deformation dynamic FE modeling of sensitive clay slope failure triggered by earthquake is performed using a coupled Eulerian-Lagrangian (CEL) FE approach. A model for post-peak degradation of undrained shear strength as a function of accumulated plastic shear strain (strain-softening) is implemented in FE analysis. The progressive development of "shear bands" (the zone of high plastic shear strains) that causes the failure of number of soil blocks is successfully simulated. Failure of slope could occur during earthquake and also at the post-quake stage until the failed soil masses come to a new static equilibrium. Upslope retrogression and downslope runout of the failed soil blocks are examined by varying geometries and soil properties. The present FE simulations can explain some of the conditions required for causing different types of seismic slope failure (e.g., spread, flowslide or monolithic slides) as observed in the field.

4.2   Introduction

Many large-scale landslides occurred in sensitive clay slopes. In Canadian sensitive clays, most of the failures were triggered by toe erosion and/or human activities; however, earthquakes are the main cause of largest landslides (Desjardins, 1980; Aylsworth and Lawrence, 2003; Locat, 2011; Brooks, 2013; Perret et al., 2013; Demers et al., 2014). Relatively small-scale landslides in sensitive clays were occurred in southern Québec due to the 1988 Saguenay earthquake (Lefebvre et al., 1992). The landslides triggered by toe erosion and human activities have been studied through post-slide investigations and development of conceptual, analytical and numerical models (Odenstad, 1951; Carson, 1977, 1979; Quinn, 2009; Locat, 2012; Dey, 2015). The authors and their co-workers presented a comprehensive review of numerical modeling techniques for large deformation slope failure under static loading elsewhere (Dey et al., 2015, 2016; Soga et al., 2016).

Based on earthquake triggered landslide history in Canadian sensitive clays, empirical relationships have been proposed for assessing large-scale landslides (Keefer, 1984; Aylsworth and Lawrence, 2003; Brooks, 2013). Keefer (1984) suggested that landslide is not expected if the earthquake magnitude (*M*) is less than 4.0. Reviewing additional failures, the threshold *M* to trigger large landslides in sensitive clays has been found between 5.9 and 6.1 (Aylsworth and Lawrence, 2003; Brooks, 2013). Quinn and Zaleski

(2015) attempted to develop relationships between ground acceleration and potential landslides; however, they found no reliable trend.

Analyzing 41 documented landslides, Mitchell and Markell (1974) categorized six general profiles where slope failures occurred in sensitive clays. In general, flowslides and spreads are the most common types of large-scale seismic landslides (Quinn and Zaleski, 2015). However, the development of a large monolithic slab (e.g., Saint Jean -Vianney landslide (Legget and LaSalle, 1978)) and formation of deep seated grabens below the upslope loaded areas (e.g., L-Street slide in the Alaska earthquake (Moriwaki et al., 1985)) have been also reported. The mechanisms of failure and landslide extent could be examined through physical and numerical modeling.

After the Alaska earthquake, small-scale physical model tests were conducted to understand the complex landslide mechanisms. The model slope consisted of an extremely weak clay layer at the level of toe. In a number of tests, failure was initiated by vibrating the model on a shaking table. Wartman et al. (2005) conducted 1g shaking table tests using kaolinite–bentonite mixture, which has strain softening behaviour, to investigate seismic slope displacement. Park and Kutter (2015) presented a series of centrifuge tests where a small amount of Portland cement was mixed with clay to create strain-softening behaviour. One of the main challenges in physical modeling is that very large displacements of the failed soil mass is required for retrogressive failure of sensitive clay slopes—as typically observed in the field—which is difficult to accommodate in laboratory setup.

The traditional limit equilibrium methods (LEM) is not suitable for analyzing large-scale landslides in sensitive clays because the LEM cannot model progressive development of failure planes due to strain-softening. The pseudostatic method, where a destabilizing horizontal body force representing the earthquake induced force is added to the gravitational driving force, is also not suitable for modeling sensitive clay slope failure because this method is applicable if the reduction in shear strength due to earthquake is not very significant (<15%, Seed, 1979; Kramer, 1996). Quinn et al. (2012) conducted seismic slope stability analysis decoupling the problem into two components: (i) the progressive development of failure planes has been modeled using the concept of linear elastic fracture mechanics and (ii) the additional stresses induced by earthquake has been calculated separately from one-dimensional wave propagation analysis using SHAKE91 (Idriss and Sun, 1991). Dynamic FE modeling of slopes considering post-peak softening of soil is very limited. Kourkoulis et al. (2010) conducted dynamic FE analyses considering linear post-peak degradation of cohesion and frictional soil parameters with plastic shear strains. Chen and Qiu (2014) showed the performance of a smoothed particle hydrodynamics (SPH) method for modeling seismic slope deformation, which has been also calibrated against the shaking table test results of Wartman (1999). However, they did not simulate the retrogression and large displacements of the failed soil blocks as observed in seismic landslides in sensitive clays.

The objective of this study is to present large deformation dynamic FE modeling of sensitive clay slope failure. Analyses are performed using Abaqus CEL implementing a

post-peak softening model for sensitive clay. The upslope retrogression and runout of failed soil are investigated by varying the soil profiles and geotechnical properties.

4.3   Problem definition

Numerical analyses are performed for the following four model geometries.

Slope-I: A 15 m high 2H:1V slope with upslope angle $\alpha=0°$ is considered (Fig. 4.1(a)). A large soil domain of 400 m long—the left and right boundaries are 150 m and 250 m, respectively, from the toe—is modeled in order to avoid any boundary effects on slope failure during dynamic loading. The soil domain consists of two clay layers and a strong base layer. The groundwater table is located at the ground surface.

Slope-II: This slope is same as the Slope-I, except for $\alpha>0°$ (Fig. 4.1(b)).

Slope-III: This slope is also same as Slope-I; however, a vertical surcharge (q) exists in the upslope area, which represents the pressure from existing structures such as building or embankment (Fig. 4.1(c)).

Slope-IV: The geometry of this slope is same as Slope-I; however, a quick clay layer of thickness H_q is placed above the level of the toe (Fig. 4.1(d)).

4.4   FE modeling

Previous studies show the advantages of FE modeling over traditional limit equilibrium methods for slope stability analysis (Duncan, 1996; Griffith and Lane, 1999). The main advantages of FE modeling are: (i) a priori definition of failure plane is not required as

LEM, instead the failure occurs through the location where shear stress reaches the shear strength; (ii) the progressive formation of failure planes can be simulated; and (iii) the deformation of failed soil can be calculated. Large deformation of the failed soil mass occurs in many sensitive clay slope failures. However, most of the existing FE programs developed in Lagrangian framework cannot simulate large deformation because of significant mesh distortions around the failure plane that causes numerical instabilities and non-convergences of the solutions (Griffith and Lane, 1999).

In the present study, the Coupled Eulerian-Lagrangian (CEL) approach in Abaqus 6.14.2 FE software is used for large deformation FE modeling of slopes subjected to earthquake loading. One of the main advantages of the CEL is that the Eulerian material (soil) flows through the fix mesh and therefore numerical issues related to mesh distortion is not encountered. Further details of mathematical formulations, CEL applications to large deformation static/quasi-static problems (e.g. onshore and offshore landslides, penetration of surface laid pipelines and spudcan foundation in seabed) and advantages of CEL over other FE formulations are available in previous studies (Benson 1992, 1995; Benson and Okazawa 2004; Henke et al., 2011; Qiu et al., 2011; Tho et al., 2011; Dassault Systèmes, 2013; Dey et al., 2015, 2016; Dutta et al., 2015; Hamman et al., 2015; Trapper et al., 2015).

Only three-dimensional modeling is allowed in CEL. Therefore, the analysis is performed with only one element length in the out-of-plane direction in order to simulate plane strain condition. The domain is discretized using 0.25 m cubical elements, except for the mesh sensitivity analyses. The soil is modeled as an Eulerian material using EC3D8R—eight-node brick elements. A void space above the ground surface is created in order to

accommodate the displaced soil mass during landslide. The Eulerian volume fraction (EVF) tool in Abaqus is used to create the initial void and soil domains. For any element, EVF=1 means that the element is filled with soil and EVF=0 means the element is void. Fractional value of EVF means that the element is partially filled with the soil.

Zero velocity boundary conditions are applied normal to the bottom and two out-of-planes in Fig. 4.1. In other words, the bottom of the model is restrained from any vertical movement while these vertical faces are restrained from any lateral movement. No boundary conditions are applied along the soil-void interface to allow the displaced soil to move in the void space when needed. Non-reflecting boundary conditions are applied to the left and right vertical faces in order to avoid reflection of wave during dynamic loading. The advantages of non-reflecting boundary conditions have been discussed elsewhere (Islam, 2017; Islam et al., 2017).

 FE modeling consists of following steps.

 (i) Gravity loading: The geostatic load is applied to establish in-situ stress condition. The slope is stable at the end of this loading step. For Slope-IV, the vertical pressure q created by increasing the unit weight of a soil block of 20 m width and 0.25 m depth (one element) at the loaded area (Fig. 4.1(c)).

 (ii) Earthquake loading: A horizontal excitation (acceleration–time) is applied at the base of the model.

 (iii) Post-quake simulation: After the completion of earthquake loading, the analysis is continued for a period of time.

Figure 4.2 shows the input acceleration–time history used in this study, which is a modified form of the 1985 Nahanni earthquake that occurred in the Northwest Territories in Canada (Wetmiller et al., 1988; PEER, 2010). The modification is performed by multiplying acceleration and time of the original accelerogram record by scale factors (Villaverde, 2009) and in this case these factors are 2.0 for acceleration and 1.0 for time.

4.5   Modeling of soil

An appropriate stress–strain model of sensitive clays that covers a wide range of strains under dynamic and monotonic loadings is equally important for successful simulation of slope failures during earthquake and post-quake phases. Most of the existing laboratory tests, such as dynamic triaxial or direct simple shear (DSS) tests, were conducted to investigate stress–strain behaviour of clays at low to medium strain ranges, or above a threshold deviatoric stress but below the peak strength to model strength degradation of clays with dynamic loading. Díaz-Rodríguez and López-Molina (2008) divided the available studies on dynamic behaviour of clays into a number of groups based on strain level and showed that experimental studies at large strains are not available. One of the main reasons is that triaxial and DSS devices cannot handle very large deformation.

During the failure of a sensitive clay slope, significantly large strains generate, especially near the failure planes. Recognizing the limitations of typical shear test apparatus for large strain tests, Tavenas et al. (1983) conducted four different types of tests—impact on a rigid surface, impact from falling objects, extrusion through a narrowing tube and shear reversals

in a large shear box—on the Champlain sea clays from 7 different sites in Quebec, Canada and showed the degradation of mobilized undrained shear strength (s_u) with strain energy. Quinn et al. (2011) reexamined Tavenas et al. (1983) test results and presented s_u degradation as a function of shear displacement. A very limited number of experimental studies on s_u degradation of sensitive clays under dynamic loadings are available in the literature (Lefebvre and LeBoeuf, 1987; Kakoli, 2005; Javed, 2011; Rasmussen, 2012; Theenathayarl, 2015). In these tests, loading/unloading occurs at stresses below the peak s_u. Theenathayarl (2015) showed large s_u reduction per cycle for stress reversal at strains after the mobilization of the peak s_u and large strain amplitudes.

4.5.1   Post-peak shear strength degradation

Figure 4.3 shows the variation of s_u of sensitive clay with accumulated plastic shear displacement (δ) used in the present study. The initial peak undrained shear strength (s_{u0}) remains constant up to δ_{pc}. The first segment of the s_u degradation curve (bcd) is modeled as,

$$s_u = \left[\frac{1}{S_t} + \left(1 - \frac{1}{S_t}\right)e^{-3\delta/\delta_{95}}\right]s_{u0} \tag{4.1}$$

where sensitivity $S_t = s_{u0}/s_{uR}$ in which s_{uR} is the value of s_u at large δ; and δ_{95} is the value of δ at which 95% reduction of (s_{u0}-s_{uR}) occurs. Equation (4.1) is a modified form of strength degradation equation proposed by Einav and Randolph (2005) but in terms of plastic shear displacement. Note that, a linear degradation of s_u with accumulated shear strains during cyclic loading has been used in previous studies (Nadim, 1998; Pestana and Nadim, 2000).

After s_{uR}, the shear strength decreases linearly to $s_{u(ld)}$ at a very large displacement (δ_{ld}). Above equation has been used for modeling T-bar/ball/offshore pipelines subjected to monotonic and cyclic loading (Zhou and Randolph, 2009; Dutta et al. 2015), and large-scale landslides (Wang et al. 2013; Dey et al., 2015, 2016).

The geotechnical parameters used in this study are listed in Table 4.1. The parameters are estimated from laboratory tests, interpretation of test data, constitutive model development and numerical studies on landslides in sensitive clays available in the literature (e.g. Shannon and Wilson, 1964; Mitchell et al., 1973; Woodward-Clyde, 1982; Tavenas et al., 1983; Idris, 1985; Moriwaki et al., 1985; Stark and Contreras, 1998; Bernander, 2000; Leroueil, 2001; Boulanger and Idris 2004, Locat et al., 2008; Quinn, 2009; Locat et al., 2011, 2013; Quinn et al., 2011).

A linearly increasing s_{u0} (kPa)=25+2z is used for the sensitive clay layer, where z is the depth from the upslope ground surface in metres. The variation of s_u with depth and plastic shear strain is implemented in Abaqus using the user defined subroutine VUSDFLD. During the failure of slope, a soil element might displace to different locations from its initial depth. In VUSDFLD, a computer program is written to ensure that the displaced soil elements carry the initial value of s_{u0}. The yield strength is given as a function of equivalent plastic shear strain ϵ_q^p (=PEEQVAVG in CEL), which can be related to plastic component of engineering shear strain (γ^p) as $\epsilon_q^p = \gamma^p/\sqrt{3}$, where $\gamma^p=\delta/t_{FE}$ for simple shear condition and t_{FE} is the length of the cubical elements (EC3D8R) used in this study.

4.5.2 Material damping

The energy dissipation primarily occurs due to frequency independent hysteretic behaviour of soil, which can be incorporated in dynamic FE analysis using nonlinear stress–strain relationship (Kwok et al., 2007; Mánica et al., 2014; Tsai et al., 2014). As elasto-plastic soil model is used in the present study, the plastic flow can simulate hysteretic damping when loading/unloading occurs from yield strength, and therefore additional damping is required only in elastic part (Zhai et al., 2004; Mánica et al., 2014). For cyclic loading inside yield surface, energy dissipation can be achieved by nonlinear variation of stiffness with Masing's rule (Masing, 1926; Chen and Qiu, 2014) and viscous damping. As the main interest of the present study is to investigate large deformation failure of sensitive clay slopes, pre-yield stiffness variation is not considered, which requires additional reliable soil model and is left for a future study. Mánica et al. (2014) compared the damping models available in FLAC (Itasca, 2012) and showed the best performance with the Rayleigh damping method for their problems. In the present study, the viscous damping is incorporated using Rayleigh damping, as previous dynamic FE modeling using Abaqus (Martino and Mugnozza, 2005; Ju and Ni, 2007; Alipour and Zareian, 2008; Jehel et al., 2014; Lindberg and Sandvik, 2015). The default bulk viscosity is used to control high frequency oscillations. Abaqus CEL neglects mass proportional damping. The stiffness proportional damping β=0.000375 is used.

4.6 FE results

The development of failure planes is explained using the formation of shear bands due to strain softening. For the soil parameters listed in Table 4.1. and t_{FE}=0.25 m, s_u degradation initiates after ϵ_q^p=0.014 ($=\delta_{pc}/(\sqrt{3}t_{FE})$) (i.e. point b in Fig. 4.3), and s_u reduces almost to s_{uR} at ϵ_q^p=0.16 ($=(2\delta_{95})/(\sqrt{3}t_{FE})$) (i.e. point d in Fig. 4.3). As the failed soil blocks displace a large distance, the zones of very high ϵ_q^p represents the failure planes.

4.6.1 Slope-I

Figure 4.4 shows the progressive development of failure surfaces during earthquake and post-quake stages for Slope-I (Fig. 4.1(a)). The first rotational slide is observed at t=8.5 s of the earthquake (Fig. 4.4(a)). Rotational failure of another soil block—shallower than previous one—occurs at t=12.25 s (Fig. 4.4(b)). During this period (t=8.5–12.25 s), the previously failed soil mass displaces a large distance in the downslope direction and broken into smaller pieces by formation of additional shear bands in it. The retrogressive failure of additional soil blocks and the displacement of failed soil mass continue with earthquake although the amplitude of acceleration decreases with time after t≈10 s (Figs. 4.4(c & d)). This is mainly because of the following reasons: (i) sufficiently large displacement of the failed soil mass reduces the support on the soil in the right side of the backscarp, (ii) relatively small earthquake accelerations after t≈10 s is enough for the failure of the soil behind steep backscarp, and (iii) kinematics of the failed soil mass is influenced by its displacement with time because of reduction of s_u along the failure planes.

Figures 4.4(e-f) show the post-quake response of the slope. Although earthquake stopped at $t \approx 18.1$ s, the failure process continues because of above mentioned reasons. The final profile of the failed slope is shown in Fig. 4.4(f) at $t=30$ s. After this, the displacements of the failed soil blocks with time are negligible.

The lateral extent of landslide (L_E) is the sum of "retrogression distance (L_R)", "slope length L_S", and "runout distance (L_U)" (Fig. 4.4(f)). In this study, L_R measures the horizontal distance from the crest of the slope to the furthest location of the shear band, which might be at the upslope ground surface on a global failure plane (e.g. point X in Fig. 4.4(f)) or at the tip of a local shear band (e.g. point Y in Fig. 4.12 (c)). In the following figures, the values of L_U and L_R at $t=30$ s are reported as shown in Fig. 4.4(f).

The rotational failure of successive soil blocks presented in Figure 4.4 is similar to typical flowslide in sensitive clays; for example, the Notre-Dame-de-la-Salette slide due to the 2010 Val de Bois earthquake (Perret et al., 2013; Demers et al., 2014)) or the Sainte Thecle and Sainte Adelphe slides due to the 1988 Saguenay earthquake (Lefebvre et al., 1992).

4.6.1.1 <u>Effect of mesh size</u>

Similar to other LDFE techniques for slope stability analysis (Soga et al., 2016), CEL analysis is computationally expensive. For example, FE modeling with 0.25 m cubical elements presented in Fig. 4.4 takes approximately 10 h with a 2.7 GHz Intel Core i7 processor and 16 GB RAM. Therefore, the use of very fine mesh is not practical, because it increases the computational time significantly. However, the simulation results is

expected to be mesh size dependent because the post-peak degradation of s_u is considered. Therefore, a computationally acceptable model can be developed using element size scaling rule (Pietruszczak and Mróz, 1981; Moore and Rowe, 1990; Andresen and Jostad, 2004; Anastasopoulos et al., 2007). Figures 4.5(a–i) show the simulations with three mesh sizes using the scaling rule proposed by Anastasopoulos et al. (2007), where γ^p for FE input is calculated scaling by element size. For example, s_{u95} mobilizes at $\gamma^p_{95} = \delta_{95}/t_{FE}$ of 3.5%, 7% and 14% for mesh sizes 1.0, 0.5 and 0.25 m, respectively, for the same $\delta_{95} = 0.035$ m.

Figures 4.5 shows that the formation of shear band at $t=8.5$ s is very similar for all three mesh sizes. For $t=17$ and 30 s, the extent of failure zone is very comparable; however, diffused plastic zones form for coarse mesh (Figs. 4.5(h–i)) while the shear bands remain distinct for small mesh size (Figs. 4.5(b–c)).

In order to show the importance of mesh regularization, simulation is also performed with 0.5 m mesh but without mesh regularization. Comparison between figures in 2nd and 4th rows of Fig. 4.5 show significantly less extent of failure if mesh regularization is not used. Except for Figs. 4.5 (d–l), all the analyses are performed with 0.25 m cubical elements.

4.6.1.2 Effect of δ_{95}

Figure 4.6 shows that, at $t=8.5$ s, the length of the shear band increases with decrease in δ_{95}, which is because of quick reduction of s_u for small δ_{95} (Eq. (4.1)) (i.e. increase in brittleness). Almost no ϵ^p_q generates at this stage for a large δ_{95} (Fig. 4.6(g)). Because of the same reason, the extent of failure at $t=17$ and 30 s decreases with increases in δ_{95}. This

trend is similar to sensitive clay slope failure due to toe erosion (Locat et al., 2013, Dey et al., 2015).

4.6.1.3 Effect of S_t

For a given s_{u0}, sensitivity increases brittleness and reduces s_{uR}. Figure 4.7(a) shows that, for a low S_t (=1.75), very small ϵ_q^p generates near the toe at t=8.5 s. A complete failure surface forms at t=13.7 s, and then the displacement of the failed soil mass causes the failure of another soil block due to earthquake loading (Fig. 4.7(b)). With time, these two soil blocks move in the downslope direction with formation of additional shear bands in the failed soil mass (Fig. 4.7(c)).

However, for higher sensitivities (S_t=3.5 and 7), a number of rotational slides occur very quickly during the earthquake. While the depth of slide becomes shallow with retrogressive failure for S_t=3.5 (Figs. 4.4), the slide depth does not reduce for S_t=7.0 (compare Figs. 4.7(e & h)). During the post-quake stage, additional soil blocks fail and displace over a large distance (Figs. 4.7(f & i)). The last two Λ- and V-shaped blocks in Fig. (4.7(h)) are similar to horst and graben, respectively, which are commonly observed in spread. Similar failure patterns—rotational flowslide followed by spread—have been observed in some cases for high sensitive clays (Geertsema et al., 2006).

4.6.1.4 Effect of slope angle

Figure 4.8 shows the results for three slope angles with a constant slope height (15 m). Global failure occurs quickly in steep slope during earthquake (Fig. 4.8(a)); however, at this time (t=8.5 s) no plastic shear strain generates in the mild slope (Fig. 4.8(g)). Retrogressive failure of a number of soil block occurs during and after seismic acceleration. Both L_R and L_U increase with increase in steepness of the slope (Fig. 4.8(c, f & i)). Locat et al. (2013) showed the increase in L_R with slope angle, except for a high coefficient of earth pressure at rest, for sensitive clay slope failure triggered by toe erosion although their definition of L_R is slightly different from the present study.

4.6.2 Slope-II: Slightly inclined upslope ground surface

Figure 4.9 shows the dynamic FE simulation results for Slope-II (Fig. 4.1b) with upslope ground surface inclination α=3°. To ensure that the slope stable under gravity load, the height of the slope considered in this case is 10 m (cf. 15 m in Slope-I, III and IV). During the initial stage of earthquake, a horizontal shear band develops (Fig. 4.9(a)). With continuation of earthquake loading, the soil mass above the horizontal shear band breaks into V- and Λ-shaped blocks forming horst and graben (Figs. 4.9(b–d)). The propagation of horizontal shear band continues during the last stage of earthquake (t=17–19.95s) and post-quake stage because of continued displacement of the failed soil mass. At t=25 s, a large monolithic slab fails causing huge retrogression, L_R=159.2 m (Fig. 4.9(e)). The failed soil blocks displace further that creates a large graben near the backscarp by formation of

another inclined shear band (Fig. 4.9(f)). Monolithic slides in sensitive clays due to earthquake have been reported in previous studies (Legget and La Salle, 1978; Desjardins, 1980). The present FE analysis can explain the mechanisms of this type of failure.

The effects of α on failure mechanisms are shown in Fig. 4.10. For small α (=1.5°), rotational failure of only one soil block occurs. For α=3°, in addition to rotational slides near the toe, a large monolithic slide occurs as discussed in previous sections. However, for α=4°, only two rotational slides occur without any monolithic slide. Significantly small retrogression occurs for α=4° (L_R=65.2 m) compared to the analysis for α=3° (L_R=159.2 m) (Figs. 4.10 (f & i)). These simulations show that, a favorable α is required for a monolithic slide, and for the conditions used here it occurs at α=3°.

4.6.3 Slope-III: With upslope distributed load

Upslope load might significantly affect the failure of slopes, which has been observed in the field and verified from numerical modeling for monotonic loading (Bernander, 2000, 2016; Dey et al. 2015, 2016(a); Wang et al., 2017) and dynamic loading (Seed and Wilson, 1967; Barnhardt et al, 2000; Kourkoulis et al., 2010). Figure 4.11 shows the formation of failure planes when a uniform surcharge q=80 kPa exists at 100 m distance from the crest. The slope is stable and there is no plastic shear strain blow the surcharge at the end of gravity step. With dynamic loading, rotational failure occurs by formation of a number of global failure planes (Figs. 4.11(a–d)). At the same time, a steep shear band generates below the surcharge (Fig. 4.11(c)). As the movement of the failed soil mass continues,

additional shear bands forms; causing retrogressive failure of the slope during earthquake and post-quake stages (Figs. 4.11(e and f)). The number of shear bands below the surcharge increases and finally a long horizontal shear band joins the two failure zones. Similar type of large graben formation below the loaded areas has been inferred from post-slide investigations of the L-Street slide due to the 1964 Alaskan earthquake (Moriwaki et al., 1985).

A parametric study is conducted varying q between 0 and 80 kPa. Figure 4.12 shows that the extent and pattern of failure for $q=0$ and 20 kPa are same. The influence of q on slope failure is found for $q=40$ kPa, which increases L_R by 8.5 m compared to no surcharge case (Figs. 4.12(c & i)). For a large q (=80 kPa), slope failure surfaces join the failure planes below the surcharge through formation of additional shear bands.

4.6.4 Slope-IV: Quick clay at toe depth

The existence of a thin weak layer has been considered as a potential reason for many large-scale landslides. After the 1964 Alaskan earthquake, tests were conducted building model slopes with a thin extremely weak soil layer at the depth of the toe to understand retrogressive failure mechanisms. Figure 4.13 shows the effects of a quick clay layer ($S_t=30$) of thickness, $H_q=3.0$ m on slope failure. The first shear band does not form horizontally through the quick clay layer, instead a curved failure plane forms along the critical location (Fig. 4.13(a)). After that, a shear band propagates almost horizontally through the quick clay layer (Figs. 4.13(b-f)). Because of the quick clay layer, the failure surfaces develop very quickly as compared to Slope-I (cf. Fig. 4.4). The horizontal shear

band through the quick layer develops rapidly and the failed soil blocks dislocate very fast in the downslope direction resulting in formation of a number of horst and grabens (Figs. 4.13(e–f)). Similar failure has been observed in the field. For example, Turnagain Heights landslide triggered by the 1964 Alaskan earthquake shows similar failure pattern (Seed and Wilson, 1967; Barnhardt et al., 2000).

Figure 4.14 shows a parametric study for the thickness of the quick clay layer, H_q (=1.0– 6.0 m). The bottom of the quick clay layer is placed at the level of the toe of the slope. As the height of the slope is same (15 m), the thickness of the overlain sensitive clay layer varies between 9.0 and 14 m. At t=8.5 s, the rotational slide of the first soil block is very similar for all three cases (Figs. 4.14(a, d & g)). The retrogression process is slow for H_q=6.0 m (Fig. 4.14(h)) compared to other two cases (Figs. 4.14(b & e), because the failure planes tend to propagate upward in the thick quick clay layer. For H_q=6.0 m, after the first rotational slide, shallow retrogressive failure occurs. However, for a thin H_q, the horizontal shear band forms first and then the inclined shear bands generate in the overlain sensitive clay after sufficient displacement of the failed soil blocks (Figs. 4.14(e & h)). At t=30 s, the maximum retrogression (L_R=180 m) is found for the thinnest case (Fig. 4.14 (c)). However, slightly more runout is found for H_q=6.0 m, because a large volume of extremely weak quick clay facilitates downslope sliding of the failed soil blocks.

4.7   Conclusions

Post-slide investigations show that many large-scale landslides in sensitive clay due to earthquake involve the failure of a number of soil blocks commonly classified as spread, flowslide and/or monolithic slides. In addition to many uncertainties, the existing empirical models simply provide a threshold magnitude of earthquake for triggering landslides. This type of landslides cannot be analyzed using the traditional limit equilibrium or Lagrangian-based FE methods because the failure surfaces develop progressively and extremely large strain generates along the failure planes that causes numerical instability in FE analysis. This paper presents large deformation FE modeling of failure of sensitive clay slopes due to earthquake using Abaqus CEL. Dynamic FE simulations are performed for four slope profiles for a given earthquake acceleration–time history. The failure initiates with a rotational slide of a soil block and then retrogresses in the upslope areas during earthquake and also in the post-quake phase. The retrogression and runout are very significant in the post-quake phase, which is similar to many post-slide field observations.

The following conclusions are drawn from this study.

a) The geometry of the slope and soil properties significantly influence failure patterns. The failure patterns obtained from the present FE analysis are comparable to field observation.

b) The rigidity of sensitive clay (i.e. low δ_{95} and high S_t) accelerates the failure process and increases the retrogression and runout distances.

c) The extent of failure increases with slope angle for the cases analyzed.

d) A large monolithic slide might occur for a favorable upslope ground surface inclination. Lesser extent of failure is found for higher or lower upslope angles than the favorable one.

e) Sufficiently large upslope surcharge exacerbates the failure. A deep seated graben form under the loaded area as observed in the field after the 1964 Alaskan earthquake.

f) A quick clay layer at the level of toe accelerates the propagation of the horizontal shear band and the extent of failure. The propagation is high for the thin quick clay layer case as compared to a thick one.

Acknowledgements

List of symbols

α Upslope ground inclination

β Stiffness proportional damping

δ Accumulated plastic shear displacement

δ_{95} δ at which s_u reduced by 95% of (s_{up}-s_{uR})

δ_{pc} δ at point b in Fig. 4.3

ϵ_q^p Generalized plastic shear strain

$\dot{\epsilon}_{ij}^p$ Plastic deviatoric strain rate tensor

γ^p Plastic shear strain

ν_u Undrained Poisson's ratio

E_u Undrained Modulus of elasticity

L_R Retrogression distance

L_S Slope length

L_U Runout distance

M Magnitude of earthquake

q Vertical surcharge load

S_t Sensitivity of clay, s_{u0}/s_{uR}

s_u Mobilized undrained shear strength

s_{u0} Initial peak undrained shear strength

s_{uR} s_u mobilized in shear band at considerable shear displacement

$s_{u(ld)}$ s_u at large displacements

t_{FE} Length of cubical elements (thickness of FE mesh size)

z Depth from upslope ground surface
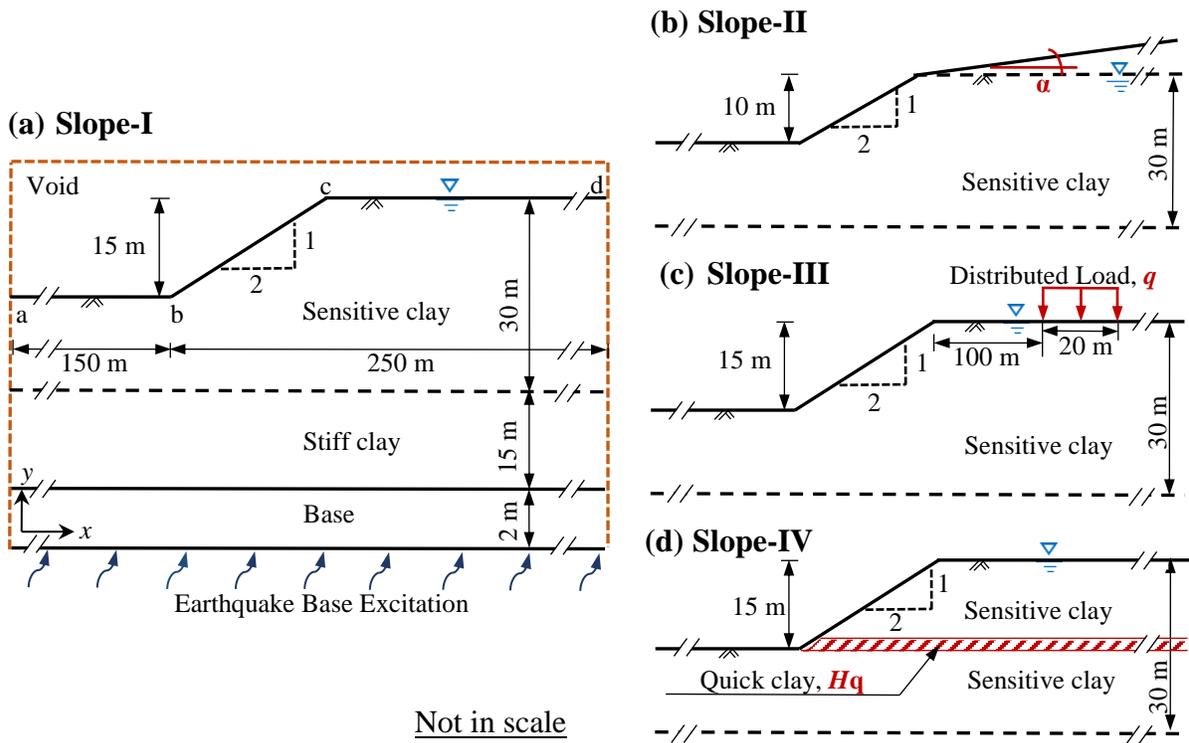
Figure 4.1: Model geometries of sensitive clay slopes (a) Slope-I:horizontal ground surface; (b) Slope- II: slightly inclined upslope ground surface; (c) Slope-III: with upslope distributed load and (d) Slope- IV: quick clay layer at toe depth
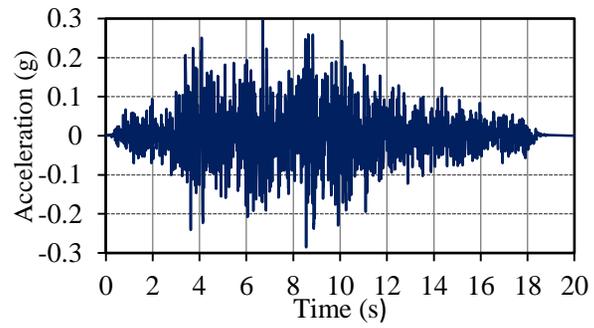
Figure 4.2: Reference acceleration time history modified from the 1985 Nahanni earthquake in Nahanni region, Northwest

Territories, Canada
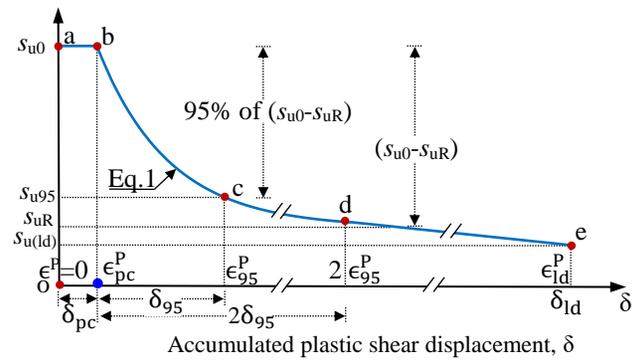
Figure 4.3: Stress strain behaviour used in FE modeling
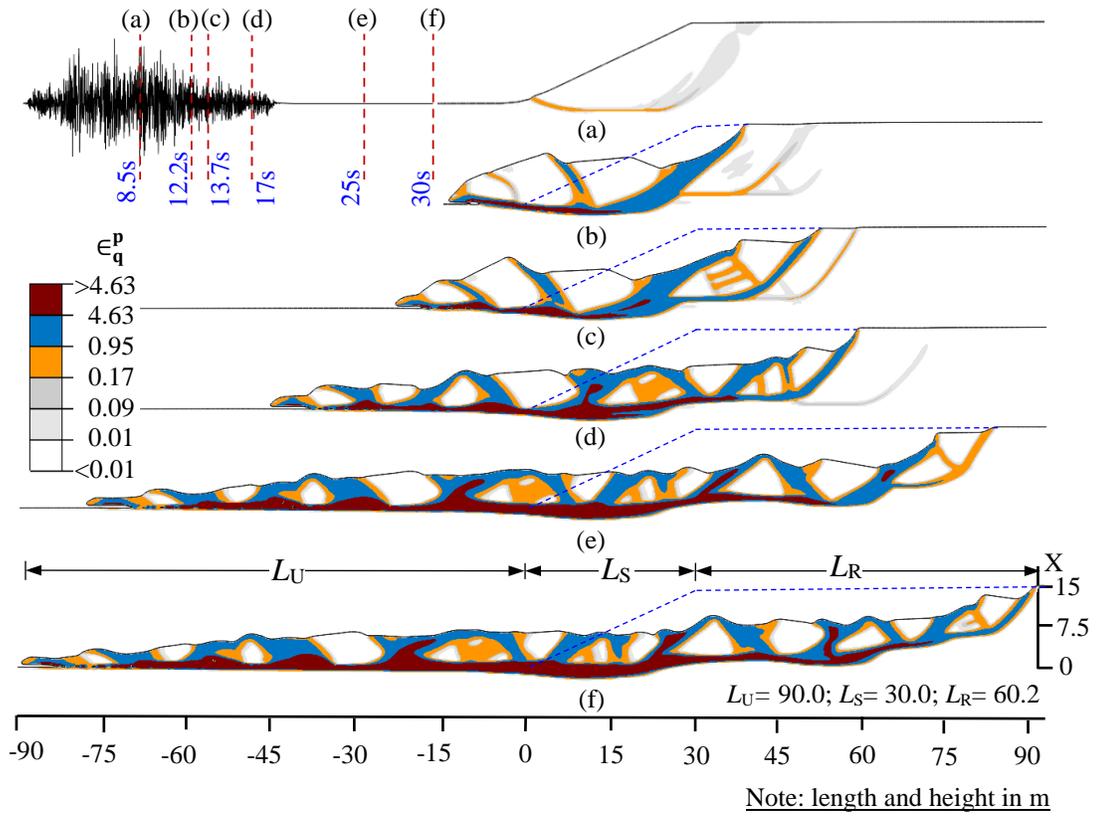
Figure 4.4: Slope-I: Development of failure surfaces

Mesh Size (m)	Time=8.5 s	ϵ_q^p	Time=17 s	Time= 30 s
0.25 (Fine)	(a)	>4.63 / 4.63 / 0.95 / 0.17 / 0.09 / 0.01 / <0.01	(b)	(c) L_U= 90.0m; L_R=60.2m
0.5 (Medium)	(d)		(e)	(f) L_U= 112.5m; L_R=60.5m
1.0 (Coarse)	(g)		(h)	(i) L_U= 129.0 m; L_R=74.0m
0.5 (Medium)	(j) Without mesh regularization		(k)	(l) L_U= 75.5m; L_R=39.0m
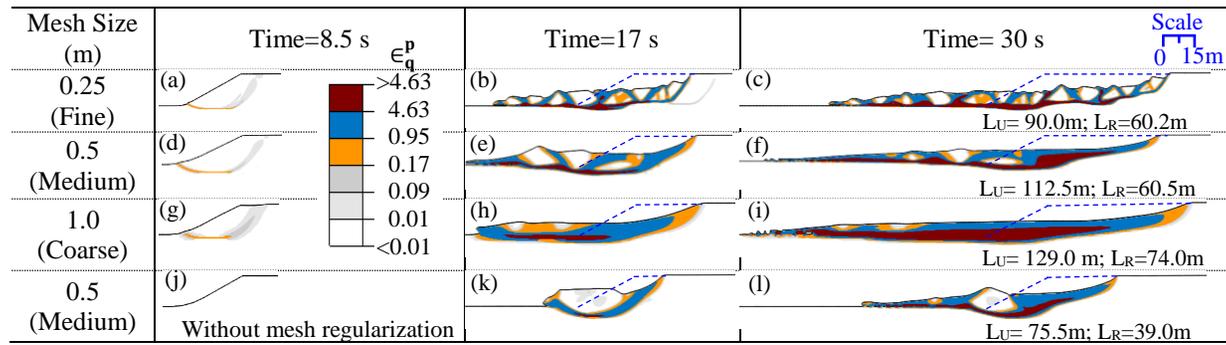
Figure 4.5: Effect of FE mesh size on the formation of failure surfaces (Slope-I)

103

δ_{95} (m)	Time=8.5 s	Time=17 s	Time= 30 s
0.035	(a)	(b)	(c) $L_U= 90.0m; L_R=60.2m$
0.07	(d)	(e)	(f) $L_U= 80.2m; L_R=51.2m$
0.10	(g)	(h)	(i) $L_U= 78.0m; L_R=42.7m$

Legend ϵ_q^p: >4.63, 4.63, 0.95, 0.17, 0.09, 0.01, <0.01

Scale 0 15m
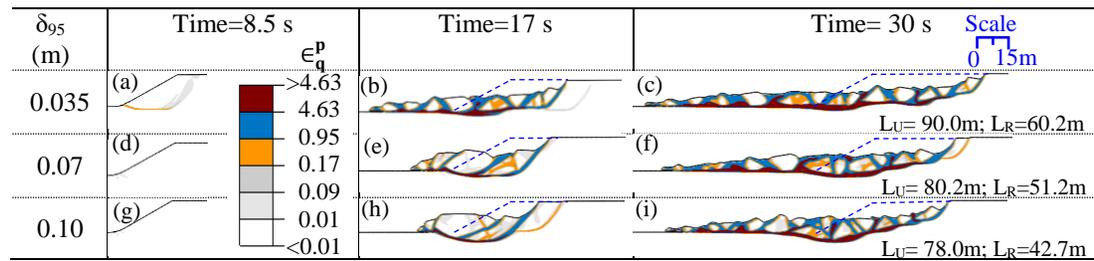
Figure 4.6: Effect of δ_{95} on failure of Slope-I

104
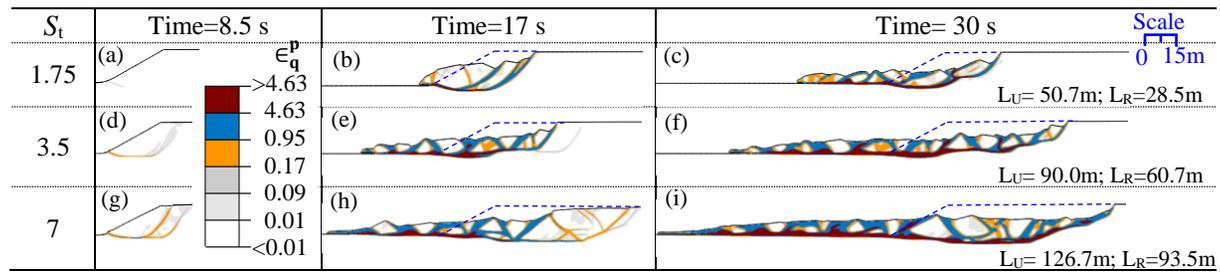
Figure 4.7: Effect of sensitivity on failure of Slope-I

Slope	Time=8.5 s ϵ_q^p	Time=17 s	Time= 30 s	Scale
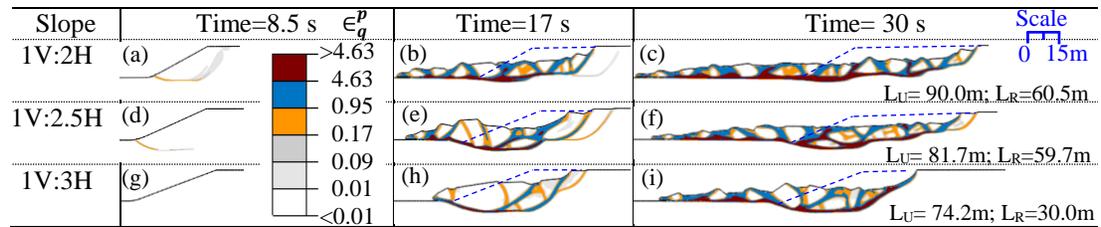
Figure 4.8: Effect of slope inclination on failure of Slope-I
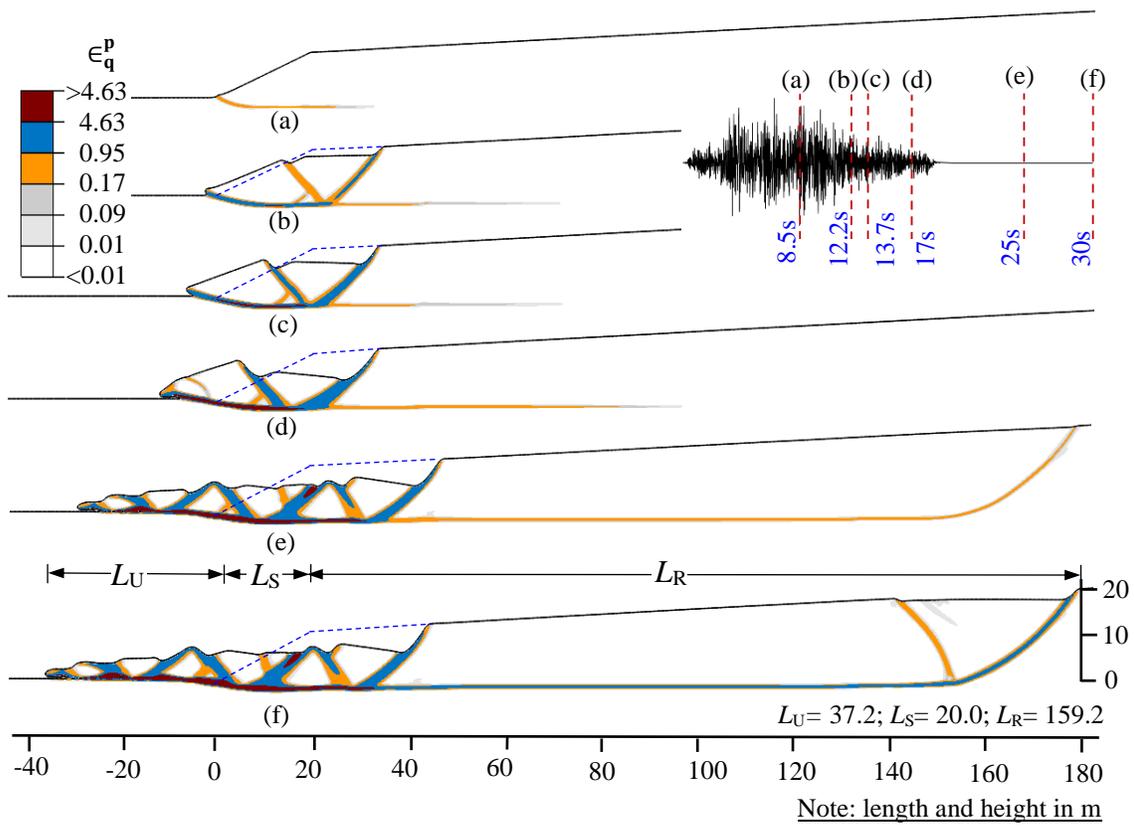
Figure 4.9: Slope-II: Development of failure surfaces
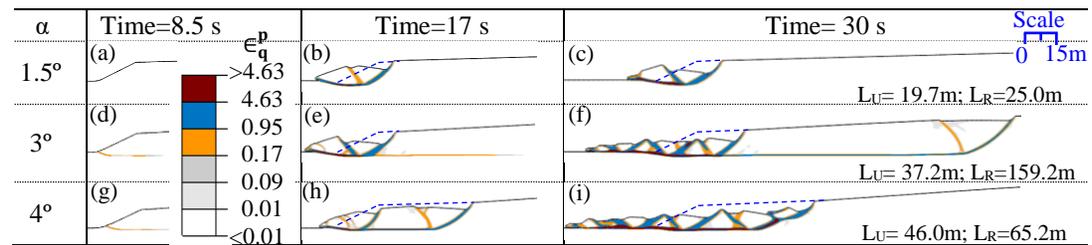
**Figure 4.10:** Effect of upslope inclination on failure of Slope-II
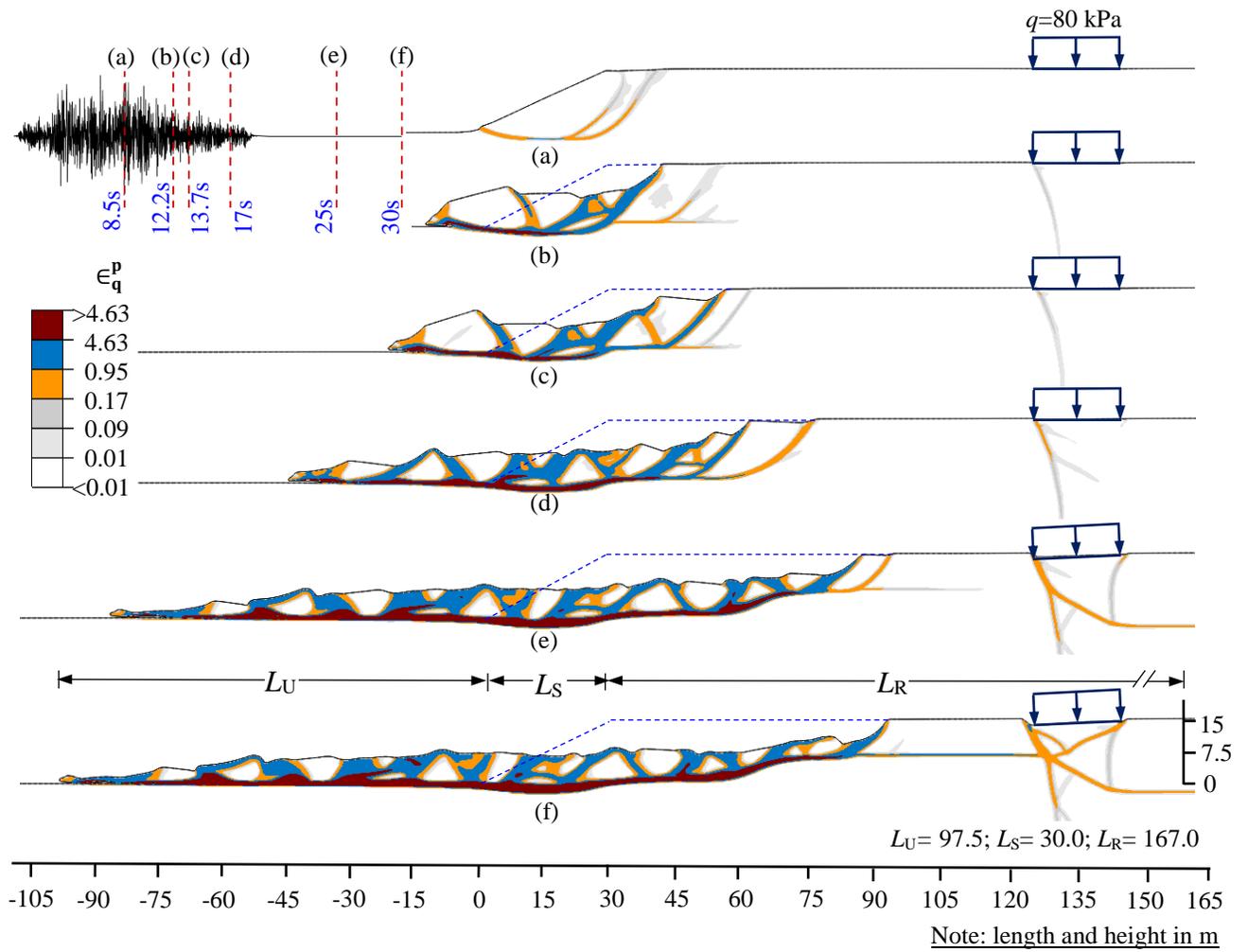
Figure 4.11: Slope-III: Development of failure surfaces

Note: length and height in m

L_U= 97.5; L_S= 30.0; L_R= 167.0
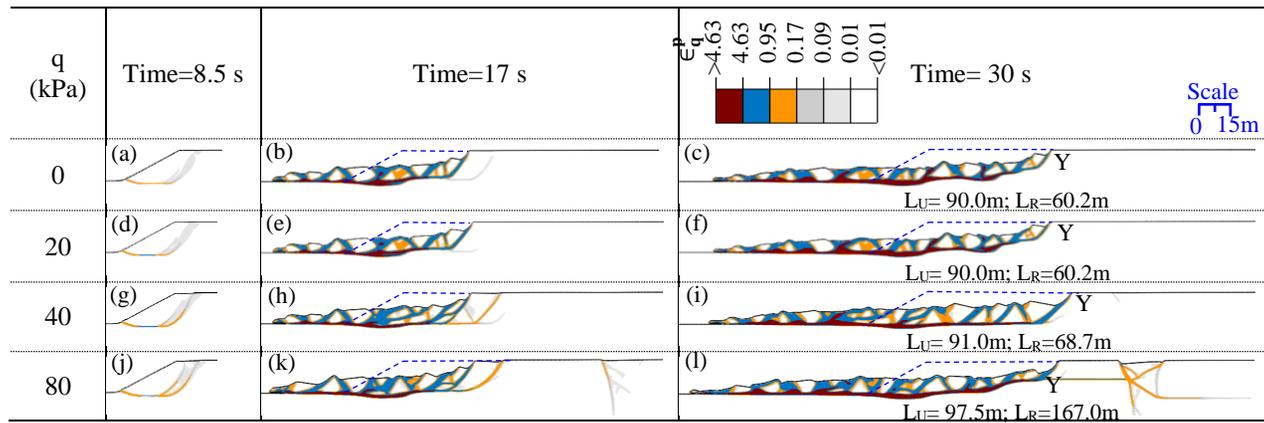
Figure 4.12: Slope-III: Effect of variation in distributed loads
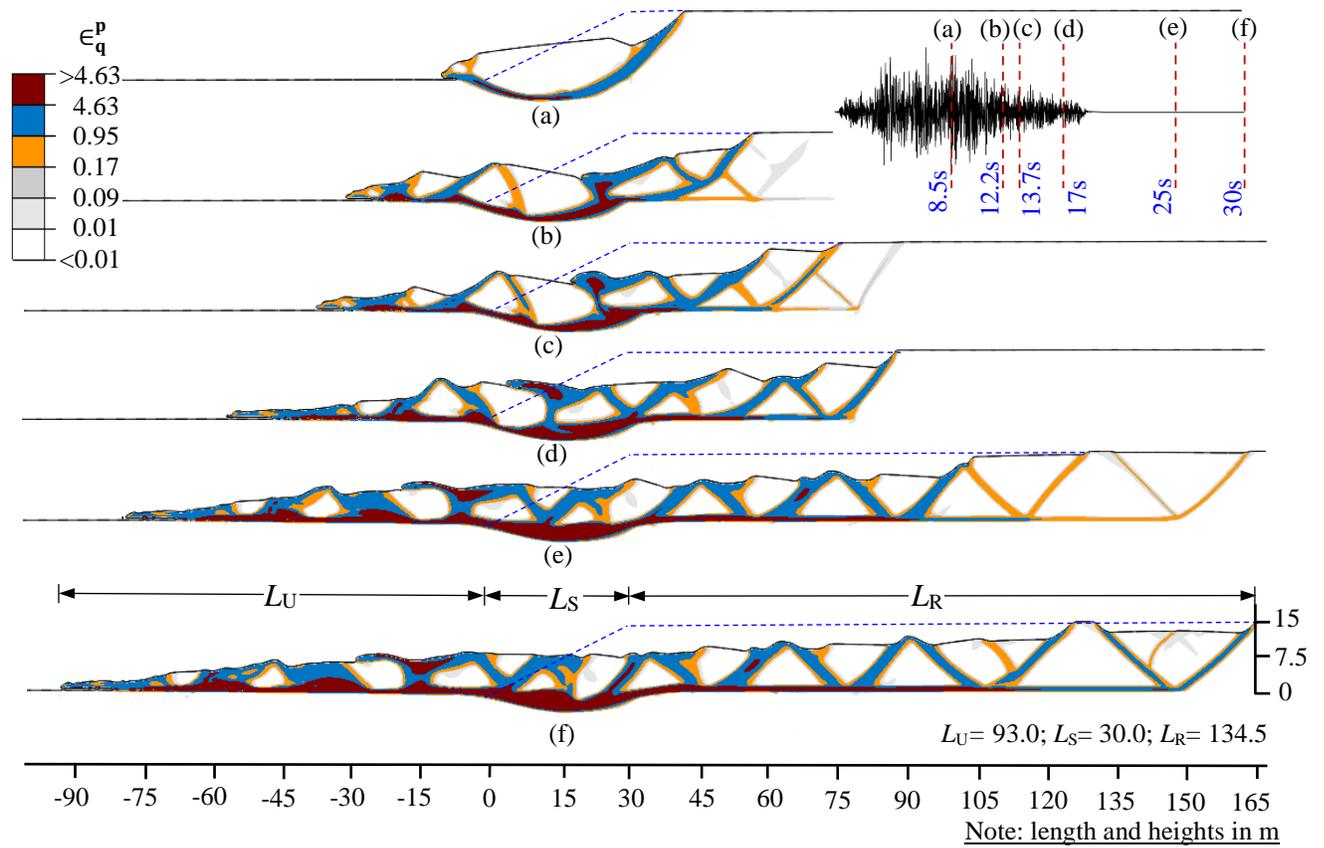
Figure 4.13: Slope-IV: Development of failure surfaces
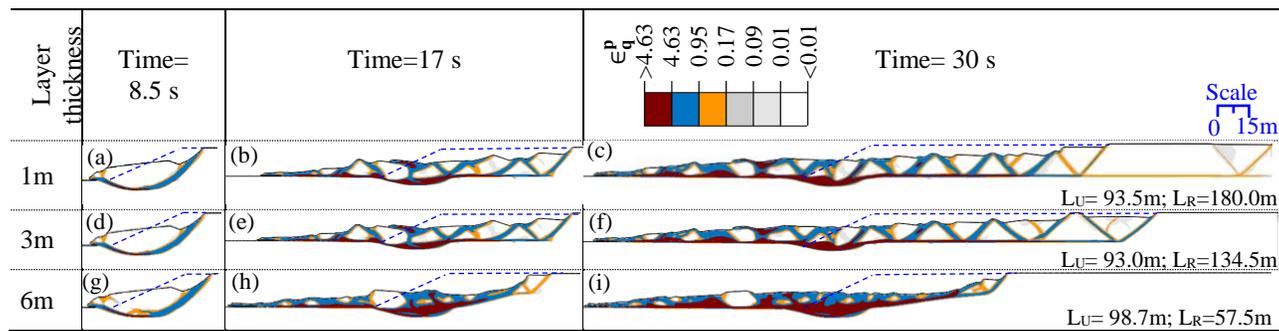
Figure 4.14: Slope-IV: Effect of change in quick clay layer thickness

Table 4.1: Soil Properties used in Finite Element Analyses

Parameters	Values			
	Sensitive Clay	Stiff Clay	Base	Quick Clay (Case4)
Undrained Young's Modulus, E_u (Mpa)	10	10	100	10
Poisson's ratio, ν_u	0.495	0.495	0.495	0.495
Peak undrained shear strength, s_{u0} (kPa)	25-85	85-300	-	55
Residual undrained shear strength, s_{uR} (kPa)	$s_{up}/3.5$	-	-	$s_{up}/30$
Large displacement undrained shear strength, s_{uld} (kPa)	$s_{up}/16$	-	-	$s_{up}/50$
Plastic shear displacement for initiation of softening, δ_{pc} (m)	0.006	-	-	0.006
Plastic shear displacement for 95% degradation of soil strength, δ_{95} (m)	0.035	-	-	0.01
Plastic shear displacement for large displacement undrained shear strength, δ_{ld} (m)	2	-	-	2
Unit weight of soil, γ_{sat} (kN/m^3)	20	20	20	20
Parameter for Damping (β)	0.000375	0.000375	-	0.000375

Bibliography

Alipour, A. and Zareian, F., 2008. Study Rayleigh damping in structures; uncertainties and treatments. In *Proceedings of 14th World Conference on Earthquake Engineering, Beijing, China*.

Anastasopoulos, I., Gazetas, G., Bransby, M.F., Davies, M.C.R. and El Nahas, A., 2007. Fault rupture propagation through sand: finite-element analysis and validation through centrifuge experiments. *Journal of Geotechnical and Geoenvironmental Engineering*, *133*(8), pp.943-958.

Andresen, L. and Jostad, H.P., 2004. Analyses of progressive failure in long natural slopes. *Numerical Models in Geomechanics: Proceedings of NUMOG IX, Ottawa, Ontario, Canada*, pp.25-27.

Aylsworth, J.M. and Lawrence, D.E., 2003. Earthquake-induced landsliding east of Ottawa: a contribution to the Ottawa Valley Landslide Project. In *Geohazards 2003, 3rd Canadian Conference on Geotechnique and Natural Hazards, Edmonton, Alberta; CA*

Barnhardt, W.A. and Kayen, R.E., 2000. Radar structure of earthquake-induced, coastal landslides in Anchorage, Alaska. *Environmental Geosciences*, *7*(1), pp.38-45.

Benson, D.J., 1992. Computational methods in Lagrangian and Eulerian hydrocodes. *Computer methods in Applied mechanics and Engineering*, *99*(2), pp.235-394.

Benson, D.J., 1995. A multi-material Eulerian formulation for the efficient solution of impact and penetration problems. *Computational Mechanics*, *15*(6), pp.558-571

Benson, D.J. and Okazawa, S., 2004. Contact in a multi-material Eulerian finite element formulation. *Computer methods in applied mechanics and engineering*, *193*(39), pp.4277-4298.

Bernander, S. 2000. *Progressive failure in long natural slopes: formation, potential extension and configuration of finished slides in strain-softening soils*. MSc thesis, Luleå University of Technology, Luleå, Sweden.

Bernander, S., Kullingsjö, A.A., Gylland, A., Bengtsson, P.E., Knutsson, S., Pusch, R., Olofsson, J. and Elfgren, L., 2016. Downhill progressive landslides in long natural slopes. triggering agents and landslide phases modeled with a finite difference method. *Canadian Geotechnical Journal*, *53(*10*)*, pp 1565-1582.

Boulanger, R.W. and Idriss, I.M., 2004. *Evaluating the potential for liquefaction or cyclic failure of silts and clays: Report UCD*. CGM-04/01, Center for Geotechnical Modeling, Department of Civil and Environmental Engineering, University of California, Davis, CA.

Brooks, G.R., 2013. A massive sensitive clay landslide, Quyon Valley, southwestern Quebec, Canada and evidence for a paleoearthquake triggering mechanism. *Quaternary Research*, *80*(3), pp.425-434.

Carson, M.A., 1977. On the retrogression of landslides in sensitive muddy sediments. *Canadian Geotechnical Journal*, *14*(4), pp.582-602.

Carson, M.A., 1979. Le glissement de Rigaud (Québec) du 3 Mai 1978: Une interprétation du mode de rupture d'après la morphologie de la cicatrice. *Géographie physique et Quaternaire*, *33*(1), pp.63-92.

Chen, W. and Qiu, T., 2014. Simulation of earthquake-induced slope deformation using SPH method. *International Journal for Numerical and Analytical Methods in Geomechanics*, *38*(3), pp.297-330.

Dassault Systèmes 2013. Abaqus user manual, version 6.14-EF2.Waltham, MA, USA, Dassault Systèmes.

Demers, D., Robitaille, D., Locat, P. and Potvin, J., 2014. Inventory of large landslides in sensitive clay in the province of Quebec, Canada: preliminary analysis. *Landslides in Sensitive Clays*, pp.77-89.

Desjardins, R., 1980. Tremblements de terre et glissements de terrain: Corrélation entre des datations au 14C et des données historiques à Shawinigan, Québec. *Géographie physique et Quaternaire*, *34*(3), pp.359-362.

Dey, R., 2015. *Analytical and numerical modeling of progressive failure of onshore and offshore slopes with sensitive clay layer,* Doctoral dissertation, Memorial University of Newfoundland.

Dey, R., Hawlader, B., Phillips, R. and Soga, K., 2015. Large deformation finite element modeling of progressive failure leading to spread in sensitive clay slopes. *Géotechnique*, *65*(8), pp.657-668.

Dey, R., Hawlader, B., Phillips, R. and Soga, K., 2016a. Numerical modeling of combined effects of upward and downward propagation of shear bands on stability of slopes with sensitive clay. *International Journal for Numerical and Analytical Methods in Geomechanics*.

Dey, R., Hawlader, B., Phillips, R. and Soga, K., 2016b. Modeling of large-deformation behaviour of marine sensitive clays and its application to submarine slope stability analysis. *Canadian Geotechnical Journal*, *53*, pp.1-18.

Dey, R., Hawlader, B., Phillips, R. and Soga, K., 2016c. Numerical modeling of submarine landslides with sensitive clay layers. *Géotechnique*, *66*, pp.454-468.

Díaz-Rodríguez, J.A. and López-Molina, J.A., 2008, Strain thresholds in soil dynamics. In *The 14th World Conference on Earthquake Engineering*, pp. 12-17.

Duncan, J.M., 1996. State of the art: limit equilibrium and finite-element analysis of slopes. *Journal of Geotechnical engineering*, *122*(7), pp.577-596.

Dutta, S., Hawlader, B. and Phillips, R., 2015. Finite element modeling of partially embedded pipelines in clay seabed using Coupled Eulerian–Lagrangian method. *Canadian Geotech. Journal*, *52*(1), pp.58-72.

Einav, I. and Randolph, M.F., 2005. Combining upper bound and strain path methods for evaluating penetration resistance. *International Journal for Numerical Methods in Eng.*, *63*(14), pp.1991-2016.

Geertsema, M., Cruden, D.M. and Schwab, J.W., 2006. A large rapid landslide in sensitive glaciomarine sediments at Mink Creek, northwestern British Columbia, Canada. *Engineering Geology*, *83*(1), pp.36-63.

Griffiths, D.V. and Lane, P.A., 1999. Slope stability analysis by finite elements. *Geotechnique*, *49*(3), pp.387-403.

Hamann, T., Qiu, G. and Grabe, J., 2015. Application of a Coupled Eulerian–Lagrangian approach on pile installation problems under partially drained conditions. *Computers and Geotechnics*, *63*, pp.279-290.

Hashash, Y.M.A., Musgrove, M.I., Harmon, J.A., Groholski, D.R., Phillips, C.A. and Park, D., 2015. DEEPSOIL 6.1, User manual. *Board of Trustees of University of Illinois at Urbana-Champaign, Urbana*.

Henke, S., Hamann, T. and Grabe, J., 2011. Coupled Eulerian-Lagrangian simulation of the deep vibration compaction process as a plastodynamic problem. In *Proceedings of the 8th international conference on structural dynamics, EURODYN* (pp. 482-489).

Idriss, I.M., 1985. Evaluating seismic risk in engineering practice. *Proceedings of The Eleventh International Conference On Soil Mechanics and Foundation Engineering, San Francisco, 12-16 AUGUST 1985. Publication of: Balkema (AA)*.

Idriss, I.M., and Sun, J.I., 1991. *Users' manual for SHAKE91: a modified version of SHAKE for conducting equivalent linear seismic response analyses of horizontally layered soil deposits*. Centre for Geotechnical Modelling, University of California, Berkeley, California.

Islam, N., 2017. *Numerical implementation and modeling of earthquake induced landslides for slopes with soft and sensitive clay layers*. Master of Engineering Thesis, Memorial University of Newfoundland, Canada.

Islam, N., Hawlader, B., Wang, C. and Soga, K., 2017. Implementation of a large deformation finite element modeling technique for seismic slope stability analyses. *(To be submitted for consideration in an international journal)*

Itasca, 2012. FLAC3D. Fast lagrangian analysis of continua in 3-dimensions, version 5.0, manual. Itasca, Minnesota

Javed, K., 2011. *Behavior of Sensitive Clay Subjected to Static and Cyclic Loading* , Doctoral dissertation, Concordia University, Montreal, Quebec, Canada.

Jehel, P., Léger, P. and Ibrahimbegovic, A., 2014. Initial versus tangent stiffness-based Rayleigh damping in inelastic time history seismic analyses. *Earthquake Eng. & Structural Dynamics*, *43*(3), pp.467-484.

Ju, S.H. and Ni, S.H., 2007. Determining Rayleigh damping parameters of soils for finite element analysis. *Int. Journal for Numerical and Analytical Methods in Geomechanics*, *31*(10), pp.1239-1255.

Kakoli, S.T.N., 2005. *Behaviour of sensitive clay under cyclic loading*, Master Thesis, Concordia University, Montreal, Quebec, Canada.

Karlsrud, K., Aas, G. and Gregersen, O., 1985. *Can we predict landslide hazards in soft sensitive clays? Summary of Norwegian practice and experiences*. Norges geotekniske institutt.

Keefer, D.K., 1984. Landslides caused by earthquakes. *Geological Society of America Bulletin*, *95*(4), pp.406-421.

Kourkoulis, R., Anastasopoulos, I., Gelagoti, F. and Gazetas, G., 2010. Interaction of foundation− structure systems with seismically precarious slopes: Numerical analysis with strain softening constitutive model. *Soil Dynamics and Earthquake Engineering*, *30*(12), pp.1430-1445.

Kramer, S.L., 1996. *Geotechnical earthquake engineering*. Pearson Education.

Kwok, A.O., Stewart, J.P., Hashash, Y.M., Matasovic, N., Pyke, R., Wang, Z. and Yang, Z., 2007. Use of exact solutions of wave propagation problems to guide implementation of nonlinear seismic ground response analysis procedures. *Journal of Geotechnical and Geoenvironmental Engineering*, *133*(11), pp.1385-1398.

Lefebvre, G. and Leboeuf, D., 1987. Rate effects and cyclic loading of sensitive clays. *Journal of Geotechnical Engineering*, *113*(5), pp.476-489.

Lefebvre, G., Leboeuf, D., Hornych, P. and Tanguay, L., 1992. Slope failures associated with the 1988 Saguenay earthquake, Quebec, Canada. *Canadian Geotechnical Journal*, *29*(1), pp.117-130.

Legget, R.F. and LaSalle, P., 1978. Soil studies at Shipshaw, Quebec: 1941 and 1969. *Canadian Geotechnical Journal*, *15*(4), pp.556-564.

Leroueil, S., 2001. Natural slopes and cuts: movement and failure mechanisms. *Géotechnique*, *51*(3), pp.197-243.

Lindberg, S. and Sandvik, P., 2015. *A comparison of finite element formulations for analysis of the converting process of packaging materials*. Master's Thesis, Chalmers University of Technology, Göteborg, Sweden

Locat, A., Leroueil, S., Bernander, S., Demers, D., Locat, J. and Ouehb, L., 2008. Study of a lateral spread failure in an eastern Canada clay deposit in relation with progressive failure: the Saint-Barnabé-Nord slide. In *Proceedings of the 4th Canadian conference on geohazards: from causes to management*, Québec, Canada, pp. 89–96.

Locat, A., Leroueil, S., Bernander, S., Demers, D., Jostad, H.P. and Ouehb, L., 2011. Progressive failures in eastern Canadian and Scandinavian sensitive clays. *Canadian Geotech. Journal*, *48*(11), pp.1696-1712.

Locat, A., 2012. *Rupture progressive et étalements dans les argiles sensibles*. PhD Thesis. Université Laval, Québec, Canada.

Locat, A., Jostad, H. P. and Leroueil, S., 2013. Numerical modeling of progressive failure and its implications for spreads in sensitive clays. *Can. Geotech. J., 50*(9), pp 961–978

Mánica, M., Ovando, E. and Botero, E., 2014. Assessment of damping models in FLAC. *Computers and Geotechnics*, *59*, pp.12-20.

Martino, S. and Mugnozza, G.S., 2005. The role of the seismic trigger in the Calitri landslide (Italy): historical reconstruction and dynamic analysis. *Soil Dynamics and Earthquake Eng.*, *25*(12), pp.933-950.

Masing G., 1926.Eigenspannungen and verfertigung beim messing [Fundamental stresses and strengthening with brass]. In *Proceeding of 2ⁿᵈ International Congress on Applied Mechanics*, *Zurich*, 332–335.

Mitchell, J. K., Houston, W. N., Yamane, G., 1973. *Sensitivity and geotechnical properties of bootlegger cove clay, The Great Alaska Earthquake of 1964*, Committee on the Alaska Earthquake of the division of earth sciences, National Research Council.

Mitchell, R.J. and Markell, A.R., 1974. Flowsliding in sensitive soils. *Canadian Geotechnical Journal*, *11*(1), pp.11-31.

Moore, I. D. and Rowe, R. K., 1990. Scaling rule for localized plasticity in strain-softening continua. In *Proceedings of the 1ˢᵗ International Conference on Computer Aided Assessment of Localized Damage*, Portsmouth, *2*, pp. 99–112.

Moriwaki, Y., Vicente, E.E., Lai, S.S. and Moses, T.L., 1985. *A Re-evaluation of the 1964. Street Slide,* State of Alaska, Department of Transportation and Public Facilities.

Nadim, F., 1998. *Slope stability under earthquake loading*. Appendix F in Seabead project. NGI Report 982512-2.

Odenstad, S., 1951. The landslide at Skottorp on the Lidan River February 2, 1946. *Proceedings of the Royal Swedish Geotechnical Society*, *4, pp* 5-39.

Park, D.S. and Kutter, B.L., 2015. Static and seismic stability of sensitive clay slopes. *Soil Dynamics and Earthquake Engineering*, *79*, pp.118-129.

Perret, D., Mompin, R., Demers, D., Lefebvre, G. and Pugin, A.J.M.,2013. *two large sensitive clay landslides triggered by the 2010 Val-Des-Bois Earthquake*, Quebec (Canada) Implications for Risk Management.

PEER, 2010. Pacific Earthquake Engineering Research Center (PEER) ground motion database; *http://peer.berkeley.edu/smcat/*

Pestana, J.M. and Nadim, F., 2000. *Nonlinear site response analysis of submerged slopes*. Department of Civil Engineering, The University of California – Berkeley.

Pietruszczak, S.T. and Mroz, Z., 1981. Finite element analysis of deformation of strain-softening materials. *International Journal for Numerical Methods in Engineering*, *17*(3), pp.327-334.

Qiu, G., Henke, S. and Grabe, J., 2011. Application of a Coupled Eulerian–Lagrangian approach on geomechanical problems involving large deformations. *Computers and Geotechnics*, *38*(1), pp.30-39.

Quinn, P., 2009. *Large landslides in sensitive clay in eastern Canada and the associated hazard and risk to linear infrastructure*. PhD Thesis, Queen's University, Kingston, Ontario, Canada.

Quinn, P.E., Diederichs, M.S., Rowe, R.K. and Hutchinson, D.J., 2011. A new model for large landslides in sensitive clay using a fracture mechanics approach. *Canadian Geotech. Journal*, *48*(8), pp.1151-1162.

Quinn, P.E., Diederichs, M.S., Rowe, R.K. and Hutchinson, D.J., 2012. Development of progressive failure in sensitive clay slopes. *Canadian Geotechnical Journal*, *49*(7), pp.782-795.

Quinn, P. E. and Zaleski, M., 2015. Co-seismic large landslides in sensitive clay in eastern Canada, a search for an initiation threshold. *The 68th Canadian Geotechnical Conference, GeoQuébec, 2015, Québec, Canada*

Rasmussen, K.K., 2012. *An Investigation of Monotonic and Cyclic Behaviour of Leda Clay*, Doctoral dissertation, The University of Western Ontario, Canada.

Seed, H.B. and Wilson, S.D., 1967. The Turnagain heights landslide, Anchorage, Alaska. *Journal of Soil Mechanics & Foundations Division.*

Seed, H.B., 1979. Considerations in the earthquake-resistant design of earth and rockfill dams. *Geotechnique*, *29*(3), pp.215-263.

Shannon and Wilson , 1964. *Anchorage Area Soil Studies*, U.S. Army Engr. Dist., Alaska, Corps of Engineers.

Soga, K., Alonso, E., Yerro, A., Kumar, K. and Bandara, S., 2016. Trends in large-deformation analysis of landslide mass movements with particular emphasis on the material point method. *Géotechnique,66*(3), pp.248-273.

Stark, T.D. and Contreras, I.A., 1998. Fourth Avenue landslide during 1964 Alaskan earthquake. *Journal of Geotechnical and Geoenvironmental Engineering*, *124*(2), pp.99-109.

Tavenas, F., Flon, P., Leroueil, S. and Lebuis, J., 1983. Remolding energy and risk of slide retrogression in sensitive clays. In *Proceedings of the Symposium on Slopes on Soft Clays. Swedish Geotechnical Institute, Linkoping, Sweden. Report*, No. 17, pp. 423-454.

Theenathayarl, T., 2015. *Behaviour Of Sensitive Leda Clay Under Simple Shear Loading* , Doctoral dissertation, Carleton University, Ottawa,Canada.

Tho, K.K., Leung, C.F., Chow, Y.K. and Palmer, A.C., 2011. Deep cavity flow mechanism of pipe penetration in clay. *Canadian Geotechnical Journal*, *49*(1), pp.59-69.

Trapper, P.A., Puzrin, A.M. and Germanovich, L.N., 2015. Effects of shear band propagation on early waves generated by initial breakoff of tsunamigenic landslides. *Marine Geology*, *370*, pp.99-112.

Tsai, C.C., Park, D. and Chen, C.W., 2014. Selection of the optimal frequencies of viscous damping formulation in nonlinear time-domain site response analysis. *Soil Dynamics and Earthquake Engineering*, *67*, pp.353-358.

Villaverde, R., 2009. *Fundamental concepts of earthquake engineering*. CRC Press.

Wang, D., Randolph, M.F. and White, D.J., 2013. A dynamic large deformation finite element method based on mesh regeneration. *Computers and Geotechnics*, *54*, pp.192-201.

Wang C. and Hawlader B., 2017. Numerical modeling of three types of sensitive clay slope failures. In *Proceedings of the 19th International Conference on Soil Mechanics and Geotechnical Engineering, Seoul, South Korea* (on review).

Wartman J.,1999. *Physical model studies of seismically induced deformation in slopes*. Ph.D. Dissertation, The University of California – Berkeley.

Wartman, J., Seed, R.B. and Bray, J.D., 2005. Shaking table modeling of seismically induced deformations in slopes. *Journal of Geotechnical and Geoenvironmental Engineering*, *131*(5), pp.610-622.

Wetmillier, R. J., Horner, R. B., Hasegawa, H. S., North, R. G., Lamontagne, M., Weichert, D. H. and Evans, S. G., 1998. An analysis of the 1985 Nahanni earthquakes, *Bulletin of the Seismological Society of America, 78*(2), pp.590-616

Woodward-Clyde, 1982. *Anchorage Office Complex*, Geotechnical Investigation, Anchorage, Alaska.

Zhai, E., Roth, W., Dawson, E. and Davis, C., 2004. Seismic deformation analysis of an earth dam–a comparison study between equivalent-linear and nonlinear effective-stress approaches. In *13th World Conference on Earthquake Engineering Vancouver, BC, Canada*, pp. 1-6.

Zhou, H. and Randolph, M.F., 2009. Numerical investigations into cycling of full-flow penetrometers in soft clay. *Géotechnique*, *59*(10), pp.801-812.

Chapter 5

Conclusions and Future Recommendations

5.1   Conclusions

Many earthquakes induced landslides in soft and sensitive clays reported to be retrogressive or progressive in nature and occurred during earthquake and post-quake stages under undrained loading condition. Attempts have been taken in the past to understand the complex mechanisms of these large-scale landslides, which include post-slide site investigations, estimation of possible failure surfaces based on post-slide investigations, development of conceptual models and numerical modeling. Unfortunately, conventional pseudostatic method of slope stability analysis based on limit equilibrium principle cannot explain these large-scale landslides. Very limited number of physical model tests were conducted. However, physical modeling of this process is extremely difficult and might be expensive because significantly large retrogression and deformation of failed soil mass needs to be accommodated in laboratory setup. Finite element modeling using typical Lagrangian-based techniques also cannot simulate this process because of significant mesh distortion around the failure planes that causes numerical issues.

Finite element modeling of clay slopes subjected to earthquake loading is presented in this thesis. The main focus of this study is to develop a large deformation FE modeling

technique for sensitive clay slope failure. The Coupled Eulerian Lagrangian (CEL) approach in Abaqus FE software is used for large deformation FE modeling. As this is the first attempt of using CEL approach for dynamic FE analysis of sensitive clay slopes, the CEL models are developed after systematic calibration of its performance against other FE modeling approaches and earthquake loading. FE modeling techniques based on implicit and explicit solution schemes have been used in the past for dynamic analysis. Some of these studies implemented the earthquake load using the empirical pseudostatic coefficient. However, in some studies, complete dynamic analyses have been performed.

In the first part of the present study, the performance of CEL approach is compared with FE simulations based on implicit and explicit schemes for both pseudostatic and dynamic loading conditions. It is found that at small strains all three approaches give similar results, which confirm that CEL models have been properly developed for successful simulation of seismic landslides. However, at large displacements, implicit and explicit schemes cannot provide acceptable solution because of mesh distortion. However, CEL can simulate very large deformation without any numerical issues related to mesh distortion.

The second part of the thesis focused on the dynamic large dynamic FE modeling of sensitive clay slope using Abaqus CEL. Depending upon geometry and soil properties, FE results shows different failure patterns—flowslide, spread, monolithic slide, deep seated grabens—as commonly observed in sensitive clay slope failure due to earthquake. Upslope retrogression and downslope runout are also successfully simulated.

In summary, numerical techniques developed in the present study using Abaqus CEL can successfully simulate large deformation behaviour of clay slope failure due to earthquake loading. The above conclusions illustrate the general overview of the thesis. However, problem specific conclusions are presented at the end of Chapters 3 and 4 and also in Appendix-A.

5.2 Future Recommendations

The presented study showed the importance of large deformation FE analysis to explain potential mechanisms involved in large-scale landslides in soft and sensitive clays. Some of the limitations of this study are discussed in Chapters 3 and 4. In addition, the following issues could be investigated in future studies:

- Initial effective stress condition might influence the failure of the slope. Analysis should be performed for varying earth pressure coefficient at rest.

- The model parameters for post-peak shear strength degradation are estimated from limited number of laboratory tests results available in the literature. The performance of this model could be further verified developing advanced laboratory test method and conducting tests on different sensitive clays.

- Additional parametric study is required. For example, in Chapter 4, the simulation is performed for a surcharge load located at 100 m from the crest of the slope. Analyses could be performed for varying distance of the surcharge

from the crest. However, it is to be noted here that CEL analysis is computationally expensive as discussed in Chapter 4.

REFERENCES

Abbo, A.J. and Sloan, S.W., 2000. *SNAC, User manual, Version 2.0*. Department of Civil, Surveying and Environmental Engineering, University of Newcastle, Callaghan, Australia.

Abbott, P. L., 1996, *Natural Disasters*. Wm. C. Brown Publishing Co., 438 pp

Abramson, L.W., Lee, T.S., Sharma, S. and Boyce, G.M., 2002. *Slope Stability and Stabilization Methods*, 2nd ed., John Wiley & Sons, Inc., New York, NY, USA.

Aryal, K.P., 2006. *Slope stability evaluations by limit equilibrium and finite element methods*. PhD Thesis, Norwegian University of Science and Technology, Norway.

Azizian, A. and Popescu, R., 2006. Three-dimensional seismic analysis of submarine slopes. *Soil Dynamics and Earthquake Engineering*, *26*(9), pp.870-887.

Ambraseys, N.N. and Srbulov, M., 1994. Attenuation of earthquake-induced ground displacements. *Earthquake engineering & structural dynamics*, *23*(5), pp.467-487.

Barnhardt, W.A. and Kayen, R.E., 2000. Radar structure of earthquake-induced, coastal landslides in Anchorage, Alaska. *Environmental Geosciences*, *7*(1), pp.38-45.

Bray, J.D. and Travasarou, T., 2007. Simplified procedure for estimating earthquake-induced deviatoric slope displacements. *Journal of Geotechnical and Geoenvironmental Engineering*, *133*(4), pp.381-392.

Bray, J.D. and Travasarou, T., 2009. Pseudostatic coefficient for use in simplified seismic slope stability evaluation. *Journal of Geotechnical and Geoenvironmental Engineering*, *135*(9), pp.1336-1340.

Cai, Z. and Bathurst, R.J., 1995. Seismic response analysis of geosynthetic reinforced soil segmental retaining walls by finite element method. *Computers and Geotechnics*, *17*(4), pp.523-546.

California Division of Mines and Geology, 1997. *Guidelines for evaluating and mitigating seismic hazards in California*. DMG Special Publication 117.

Chen, W. and Qiu, T., 2014. Simulation of earthquake-induced slope deformation using SPH method. *International Journal for Numerical and Analytical Methods in Geomechanics*, *38*(3), pp.297-330.

Demers, D., Robitaille, D., Locat, P. and Potvin, J., 2014.Inventory of Large Landslides in Sensitive Clay in the Province of Québec, Canada: Preliminary Analysis. *Landslides in Sensitive Clays: From Geosciences to Risk Management*, Advances in Natural and Technological Hazards Research 36, J.-S. L'Heureux et al. (eds.), Springer.

Desjardins, R., 1980. Tremblements de terre et glissements de terrain: Corrélation entre des datations au 14C et des données historiques à Shawinigan, Québec. *Géographie physique et Quaternaire*, *34,* 359-362.

Díaz-Rodríguez, J.A. and Santamarina, J.C., 2001. Mexico City soil behavior at different strains: Observations and physical interpretation. *Journal of Geotechnical and Geoenvironmental Engineering*, *127*(9), pp.783-789.

Díaz-Rodríguez, J.A. and López-Molina, J.A., 2008, Strain thresholds in soil dynamics. In *The 14th World Conference on Earthquake Engineering* (pp. 12-17).

Filion, L., Quinty, F., and Begin, C., 1991. A chronology of landslide activity in the valley of Rivière du Gouffre, Charlevoix, Québec. *Canadian Journal of Earth Sciences,28,* 250-256.

Fine, I.V., Rabinovich, A.B., Bornhold, B.D., Thomson, R.E. and Kulikov, E.A., 2005. The Grand Banks landslide-generated tsunami of November 18, 1929: preliminary analysis and numerical modeling. *Marine Geology*, *215*(1), pp.45-57.

GeoStudio 2016, GEOSLOPE International Ltd. Calgary, AB, Canada.

Ghobrial, F. and Karray, M., 2015. Development of spectral pseudo-static method for dynamic clayey slope stability analysis, *GEOQuebac2015*, Québec, Canada.

Hansen, W.R., 1965. *Effects of the earthquake of March 27, 1964, at Anchorage, Alaska*. US Government Printing Office.

Houston, W.N. and Herrmann, H.G., 1980. Undrained cyclic strength of marine soils. *Journal of Geotechnical and Geoenvironmental Engineering*, *106* (ASCE 15503).

Hsu, C.C. and Vucetic, M., 2004. Volumetric threshold shear strain for cyclic settlement. *Journal of geotechnical and geoenvironmental engineering*, *130*(1), pp.58-70.

Hsu, C.C. and Vucetic, M., 2006. Threshold shear strain for cyclic pore-water pressure in cohesive soils. *Journal of Geotechnical and Geoenvironmental Engineering*, *132*(10), pp.1325-1335.

Hynes-Griffin, M.E. And Franklin, A.G., 1984. *Rationalizing The Seismic Coefficient Method* (No. Wes/Mp/Gl-84-13). Army Engineer Waterways Experiment Station, Vicksburg Ms Geotechnical Lab.

Idriss, I.M., 1985. Evaluating seismic risk in engineering practice. In *Proceedings of The Eleventh International Conference On Soil Mechanics and Foundation Engineering*, *San Francisco, 12-16 August 1985. Publication of: Balkema (AA).*

Jibson, R.W., 1993. Predicting earthquake-induced landslide displacements using Newmark's sliding block analysis. *Transportation research record*, pp.9-9.

Jibson, R.W., 2011. Methods for assessing the stability of slopes during earthquakes—A retrospective. *Engineering Geology*, *122*(1), pp.43-50.

Kourkoulis, R., Anastasopoulos, I., Gelagoti, F. and Gazetas, G., 2010. Interaction of foundation− structure systems with seismically precarious slopes: Numerical analysis with strain softening constitutive model. *Soil Dynamics and Earthquake Engineering*, *30*(12), pp.1430-1445.

Kramer, S.L., 1996. *Geotechnical earthquake engineering*. Pearson Education.

Kramer, S.L. and Smith, M.W., 1997. Modified Newmark model for seismic displacements of compliant slopes. *Journal of Geotechnical and Geoenvironmental Engineering*, *123*(7), pp.635-644.

Lade, P., Updike, R.G. and Cole, D.A., 1988. *Cyclic triaxial tests of the Bootlegger Cove formation, Anchorage, Alaska*. US Government Printing Office.

Lamontagne, M., 2008. Earthquakes in Eastern Canada: A threat that can be mitigated. In *Comptes rendus de la 4e Conférence canadienne sur les géorisques: des causes à la gestion. Presse de l'Université Laval, Québec*.

Lefebvre, G., LeBoeuf, D. and Demers, B., 1989. Stability threshold for cyclic loading of saturated clay. *Canadian Geotechnical Journal*, *26*(1), pp.122-131.

Lefebvre, G., Leboeuf, D., Hornych, P. and Tanguay, L., 1992. Slope failures associated with the 1988 Saguenay earthquake, Quebec, Canada. *Canadian Geotechnical Journal*, *29*(1), pp.117-130.

Lefebvre, G., 1996. *Soft sensitive clays. In: Turner AK, Schuster RL (eds) Landslides: investigation and mitigation*, Special report 247, Transportation Research Board. National Academy Press, Washington, DC, pp 607–619.

Li, X., 2007. Finite element analysis of slope stability using a nonlinear failure criterion. *Computers and Geotechnics*, *34*(3), pp.127-136.

Loukidis, D., Bandini, P. and Salgado, R., 2003. Stability of seismically loaded slopes using limit analysis. *Geotechnique*, *53*(5), pp.463-480.

Makdisi, F.I. and Seed, H.B., 1977, December. Simplified procedure for estimating dam and embankment earthquake-induced deformations. In *ASAE Publication No. 4-77. Proceedings of the National Symposium on Soil Erosion and Sediment by Water, Chicago, Illinois, December 12-13, 1977.*

Marcuson, W.F. III., 1981. Moderator's report for session on 'Earth dams and stability of slopes under dynamic loads'. *Proceedings, International Conference on Recent Advances in Geotechnical Earthquake Engineering and Soil Dynamics*, St. Louis, Missouri, Vol.3, p. 1175

Marcuson, W.F. and Franklin, A.G., 1983. *Seismic design analysis and remedial measures to improve the stability of existing earth dams, Corps of Engineers Approach, Seismic Design of Embankments and Caverns*. TR Howard (ed) New York, ASCE.

Marcuson, W.F.I., Hynes, M.E. and Franklin, A.G., 1992. Seismic stability and permanent deformation analyses: the last twenty five years. In *Stability and Performance of Slopes and Embankments II* (pp. 552-592).

Marcuson, W.F., Hynes, M.E. and Franklin, A.G., 2007. Seismic design and analysis of embankment dams: the state of practice. In *Proceedings of the 4th Civil Engineering Conference in the Asian Region, June 25-28, Taipei.*

Matsuo, M., Itabashi, K. and Sasaki, Y., 1984, March. Study on a seismicity of earth structures by inverse analyses of actual cases. In *Proceedings Of The Japan Society Of Civil Engineers* (Vol. 1984, No. 343, Pp. 25-33). Japan Society of Civil Engineers.

Melo, C. and Sharma, S., 2004, August. Seismic coefficients for pseudostatic slope analysis. In *13th World Conference on Earthquake Engineering, Vancouver, BC, Canada, Paper* (No. 369).

Mitani, Y., Wang, F., Okeke, A.C. and Qi, W., 2013. Dynamic analysis of earthquake amplification effect of slopes in different topographic and geological conditions by using ABAQUS. *Progress of Geo-Disaster Mitigation Technology in Asia*, pp.469-490.

Moormann, C. and Hamad, F., 2015. MPM dynamic simulation of a seismically induced sliding mass. In *IOP Conference Series: Earth and Environmental Science* (Vol. 26, No. 1, p. 012024). IOP Publishing.

Moriwaki, Y., Vicente, E.E., Lai, S.S. and Moses, T.L., 1985. *A Re-evaluation of the 1964. Street Slide,* State of Alaska, Department of Transportation and Public Facilities.

Newmark, N. M. 1965 Effects of earthquakes on dams and embankments. *Geotechnique, 15 (2)*: 139–160

Okur, D.V. and Ansal, A., 2007. Stiffness degradation of natural fine grained soils during cyclic loading. *Soil Dynamics and Earthquake Engineering*, *27*(9), pp.843-854.

Park, D.S. and Kutter, B.L., 2015. Static and seismic stability of sensitive clay slopes. *Soil Dynamics and Earthquake Engineering*, *79*, pp.118-129.

Perret, D., Mompin, R., Demers, D., Lefebvre, G. and Pugin, A.J.M., 2013. *Two Large Sensitive Clay Landslides Triggered by the 2010 Val-Des-Bois Earthquake*, Quebec (Canada) Implications for Risk Management.

PLAXIS, 2004. *Finite Element Code for Soil and Rock Analyses*. PLAXIS-2D Version 8, Reference Manual, Edited by Brinkgreve, et al., DUT, the Netherlands.

Potts, D. M. and Zdravkovic, L., 1999. *Finite element analysis in geotechnical engineering: Theory*. London: Thomas Telford.

Prevost, J.H., 1981. *DYNA-FLOW: a nonlinear transient finite element analysis program*. Department of Civil Engineering, School of Engineering and Applied Science, Princeton University.

Rathje, E.M. and Bray, J.D., 2000. Nonlinear coupled seismic sliding analysis of earth structures. *Journal of Geotechnical and Geoenvironmental Engineering*, *126*(11), pp.1002-1014.

Roscoe, K. and Burland, J.B., 1968. *On the generalized stress-strain behaviour of wet clay. Engineering plasticity*, Cambridge University Press, Cambridge, UK, 553–609.

Seed, H.B. and Wilson, S.D., 1967. The Turnagain heights landslide, Anchorage, Alaska. *Journal of Soil Mechanics & Foundations Division.*

Seed, H. and Idriss, I., 1969. Influence of soil conditions on ground motions during earthquake. *Journal of the Engineering Mechanics Division, ASCE*, *95*, pp.99-127.

Seed, H.B., 1979. Considerations in the earthquake-resistant design of earth and rockfill dams. *Geotechnique*, *29*(3), pp.215-263.

Seed, H.B. and Martin, G.R., 1966. The seismic coefficient in earth dam design. *Journal of Soil Mechanics & Foundations Div.*, *92*(Proc. Paper 4824).

Seed, H.B., Makdisi, F.I. and De Alba, P., 1978. Performance of earth dams during earthquakes. *Journal of Geotechnical and Geoenvironmental Engineering*, *104* (ASCE 13870 Proceeding).

Shannon and Wilson, 1964. *Report on Anchorage area soil studies, Alaska*, Rep. prepared for U.S. Army Engineer District, Anchorage, Alaska, Contract No. DA-95-507-CIVENG-64-18.

Stark, T.D. and Contreras, I.A., 1998. Fourth Avenue landslide during 1964 Alaskan earthquake. *Journal of Geotechnical and Geoenvironmental Engineering*, *124*(2), pp.99-109.

Syvitski, J.P.M., and Schafer, C.T., 1996. Evidence for an earthquake-triggered basin collapse in Saguenay Fjord, *Canada. Sedimentary Geology, 104*, 127-153.

Stark, T. D., and Contreras, 1. A., 1996. Constant volume ring shear apparatus. *Geotech. Testing J.,* American Society for Testing and Materials, *19*(1), pp. 3-11.

Taiebat, M., Kaynia, A.M. and Dafalias, Y.F., 2010. Application of an anisotropic constitutive model for structured clay to seismic slope stability. *Journal of Geotechnical and Geoenvironmental Engineering*, *137*(5), pp.492-504.

Tan, D. and Sarma, S.K., 2008. Finite element verification of an enhanced limit equilibrium method for slope analysis. *Geotechnique*, *58*(6), p.481.

Taniguchi, E. and Sasaki, Y., 1985. Back analysis of landslide due to Naganoken Seibu Earthquake of September 14, 1984. In *Proc. of 11th International Conference on Soil Mechanics and Foundation Engineering, San Francisco* (pp. 1-55).

Tavenas, F., 1984. Landslides in Canadian sensitive clays–a state-of-the-art. In *Proceedings of the 4th International Symposium on Landslides, Toronto, Ont* (pp. 16-21).

Terzaghi, K., 1950. Mechanisms of landslides, *Engineering Geology (Berdey) Volume*, The Geological Society of America, pp. 83-123.

Corps of Engineers, 1970. *Stability of earth and rock-fill dams*, Engineer Manual 1110-2-1902, U.S. Army Corps of Engineers, Washington D.C., USA.

Wartman, J., Seed, R.B. and Bray, J.D., 2005. Shaking table modeling of seismically induced deformations in slopes. *Journal of Geotechnical and Geoenvironmental Engineering*, *131*(5), pp.610-622.

Woodward-Clyde (Consultants), 1982. *Anchorage office complex, geotechnical investigation, Anchorage, Alaska*. Rep. to Alaska Dept. of Transp. and Public Facilities, Des. and Constr., Anchorage, Alaska.

APPENDIX A

Appendix A is prepared as per the conference paper format. This part of the research has been published and presented as:

Islam, N. and Hawlader, B., 2016. Pseudostatic Seismic Slope Stability Analyses using a Large Deformation Finite Element Modeling Technique. In *The 69th Canadian Geotechnical Conference, Geovancouver 2016*, *Vancouver, B. C.,Canada, Oct 2-5.*

Most of the research work presented in this paper was conducted by the first author. He also prepared the draft manuscript. The second author supervised the research and reviewed the manuscript.

Pseudostatic Seismic Slope Stability Analyses using a Large Deformation Finite Element Modeling Technique

Naveel Islam & Bipul Hawlader
Memorial University of Newfoundland, St. John's, Newfoundland, Canada

ABSTRACT

Pseudostatic method is widely used to analyze the stability of slopes subjected to earthquake loading. While the limit equilibrium (LE) methods are mainly used in the industry, the application of finite element (FE) methods has increased in recent years. The pseudostatic coefficient (k_h) has also been implemented in some of these FE programs. However, most of the FE programs developed in Lagrangian framework cannot handle large deformation of slopes during failure. In the present study, slope stability analyses are performed implementing k_h in Abaqus CEL, which can model large deformation behaviour. Analyses are performed for undrained loading conditions. In order to show the comparison, analyses are performed using Abaqus/Standard, which is based on implicit solution scheme. Comparison of FE results are also done with LE analyses results using Slope/W software. It is shown that, Abaqus CEL can simulate the response better including the gradual formation of failure planes, strain localization and kinematics of failed soil mass.

RÉSUMÉ

Méthode pseudo-statique est largement utilisé pour analyser la stabilité des pentes soumises à une charge sismique. Bien que la limite d'équilibre (LE) méthodes sont principalement utilisées dans l'industrie, l'application des éléments finis (FE) des méthodes a été augmenté ces dernières années. Le coefficient pseudostatique (k_h) a également été mis en œuvre dans certains de ces programmes FE. Cependant, la plupart des programmes FE développés dans le cadre lagrangien ne peut pas gérer une déformation importante des pentes en cas de panne. Dans la présente étude, les analyses de stabilité des pentes sont effectuées la mise en œuvre k_h dans Abaqus CEL, qui peut modéliser le comportement à grande déformation. Les analyses sont effectuées pour les conditions de chargement non drainées. Afin de montrer la comparaison, les analyses sont effectuées en utilisant Abaqus / Standard, qui est basé sur le schéma de solution implicite. Comparaison des résultats FE ont également été fait avec LE analyse les résultats en utilisant Slope/W logiciel. Il est démontré que, Abaqus CEL peut simuler la meilleure réponse, y compris la formation progressive des plans de rupture, la localisation des déformations et la cinématique de masse de sol échoué.

1   INTRODUCTION

Pseudostatic method is commonly used in engineering practice to check the likelihood of failure of slopes subjected to earthquake loading. In this method, instead of comprehensive dynamic analysis of actual response of the slope due to ground motion, a single parameter "pseudostatic coefficient (k_h)" is used. The coefficient k_h, represents the ratio between representative seismic acceleration and gravitational acceleration. In most of the design, the vertical component of earthquake effect is neglected and the horizontal component k_h is assumed to be constant with depth.

Majority of the slope stability analyses are still performed using the traditional limit equilibrium (LE) approach. In LE method, in addition to other loads, a static horizontal inertial force is applied at the center of the soil mass above the potential failure plane. The inertial force is calculated as the product of k_h and weight of soil above the failure plane. Although it has been widely used, the pseudostatic method should not be used when the soil softens considerably under cyclic loading (Loukidis et al. 2003; Bray and Travasarou 2009). In that case, complete dynamic analyses with advanced soil constitutive model for stress–strain behaviour of soil is required.

Significant displacements might occur during the failure of slopes due to earthquake. For example, Seed (1979) evaluated the performance of this method for earth dams with seismic displacement of 1 m as an acceptable criterion. Moreover, during earthquake, the failure planes generally forms progressively. Therefore, some segments of the failure plane might undergo large relative displacements. If the soil along the failure plane has post-peak softening behaviour, strain localization occurs.

Post-peak softening, strain localization and progressive development of sliding surface cannot be modeled using the traditional LE method. Instead, the LE method provides only factor of safety assuming that the complete failure plane develops at once.

Finite element (FE) method could be an alternative approach for analyses of stability of slopes. It can provide the zone of high shear strains, which could be interpreted as the failure plane. Recently a number of researchers conducted FE analyses to calculate the stability of slopes for various soil profiles and loading conditions (Griffith and Lane 1999). Tan and Sharma (2008) conducted a series of FE analyses using the Imperial College Finite Element Program (ICFEP) (Potts and Zdravković 1999) with pseudostatic approach. Loukidis et al. (2003) used Abaqus/Standard to calculate the critical horizontal acceleration required to cause the failure of homogeneous

slopes. It has been shown that, considerable mesh distortions occur in the above mentioned FE analyses formulation and non-convergence has been considered as an indicator of failure in addition to other failure criteria.

As significant strain might generate in the zone of failure, FE programs that can handle large deformation behaviour could better model the failure of slopes. In the present study, the Coupled Eulerian Lagrangian approach available in Abaqus (Abaqus CEL) is used to simulate large deformation behaviour during the failure of clay slopes subjected to earthquake loading. Analyses are also performed using Abaqus/Standard to show the advantages of Abaqus CEL for modeling of slopes. In addition, LE analyses are performed using Slope/W software and thereby compared with FE simulation results.

2   PROBLEM DEFINITION

The geometry of the slope used in the present FE modelling is shown in Fig. 1. A 15 m high 2H:1V slope is considered in this study. The boundaries are placed at sufficiently large distance from the slope and therefore no significant effect on stability and potential failure mechanisms is expected, which has been verified placing the boundaries at further distances. The ground surface to the right side of the crest is horizontal. The groundwater table is assumed at the ground surface. Two idealized soil layers are considered. The base layer consists of relatively strong soil and therefore it is modeled as elastic material. The behaviour of the upper clay layer is discussed in the following sections.

The failure of a slope could occur both in drained or undrained conditions. However, earthquake effects in general necessitates considerations for a short-term loading condition. Therefore, all the analyses are conducted for undrained loading conditions.
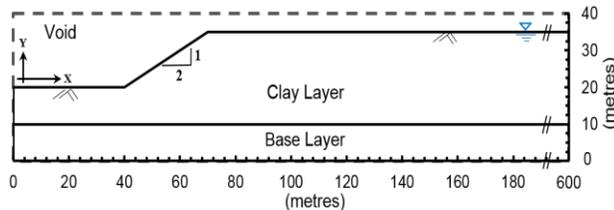

Figure 1. Geometry of the slope used in Finite Element (FE) modeling

The following cases are analyzed in this study.

Case 1: Analyses are performed for an uniform undrained shear strength (s_u=60 kPa) of the upper clay layer.

Case 2: The undrained shear strength of the upper clay layer is increased linearly from 55 kPa at the ground surface to 65 kPa at the bottom of the clay layer.

Case 3: The undrained shear strength of the upper clay layer is decreased linearly as a function of plastic shear strain (γ_p) from the peak value (s_{uP}) of 65 kPa at γ_p=0 to a residual value (s_{uR}) of 55 kPa at γ_p= 0.20.

3   FINITE ELEMENT MODELING

3.1   Numerical Technique

For numerical analyses, Abaqus 6.14.2 is used in which both implicit and explicit solution schemes are available. In general, the implicit scheme is more efficient for solving linear and smooth nonlinear problems, while the explicit scheme is more suitable for dynamic problems. However, for large deformation, large model size and quasi-static problems, explicit approach could be a better choice.

Static analyses of slopes has been performed in the past using the FE methods developed in Lagrangian framework based on implicit solution scheme (Griffith and Lane 1999; Troncone 2005). Earthquake loadings have also been incorporated in some studies using the pseudostatic coefficients (k_h) in this type of FE modeling (Swan and Seo 1999; Loukidis et al. 2003; Li 2007; Tan and Sharma 2008; Khosravi et al. 2013). The authors of these studies showed that, significant mesh distortion occurs at large displacement that results in convergence issues. In fact, some of these studies considered the un-converged condition at large displacements as the failure of the slope (Griffith and Lane 1999; Tan and Sharma 2008).

It is better to consider un-convergence as numerical issue instead of failure condition. The failure might be better explained by displacement and/or formation of failure plane through accumulation of plastic shear strains. Therefore, FE modeling techniques that can simulate large strain/deformation is required.

In the present study, in order to overcome mesh distortion issues, FE simulation is performed using the Abaqus CEL approach that has been developed taking the advantages of both Lagrangian and Eulerian formulation. The success of Abaqus CEL for modeling large deformation slope failure problems has been discussed in some previous studies (e.g. Dey et al. 2015, 2016; Trapper et al. 2015).

Although the main focus of the present study is to show the FE simulation of earthquake loading using Abaqus CEL, analyses are also performed using Abaqus/Standard for comparison of results from different solution schemes.

3.2   Abaqus CEL modeling

The FE model in Abaqus CEL consists of two parts: (i) soil and (ii) void space (to accommodate the displaced soil mass). The soil is modeled as an Eulerian material using EC3D8R elements, which are eight-node linear brick elements with reduced integration and hourglass control. Soil and void spaces for the initial conditions are created in the Eulerian domain using the Eulerian Volume Fraction (EVF) tool in Abaqus. EVF=0 for void spaces (i.e. no soil in the void space) and EVF=1 for the elements below the ground surface (i.e. filled with soil as Eulerian material).

CEL can model only three-dimensional condition. Therefore, the plain strain condition is simulated using model thickness of one element in the out of plane direction. Uniform mesh of 0.5 m x 0.5 m is used for all CEL analyses.

Zero velocity boundary conditions are applied normal to the bottom and along all the vertical faces (Fig. 1) to make sure that the Eulerian material remains within the domain. In other words, the bottom of the model shown in Fig. 1 is restrained from any movement in the vertical direction, while the vertical sides are restrained from any lateral movement. No boundary conditions are applied at the soil-void interface.

3.3 Modeling with Abaqus/Standard

In the implicit analyses using Abaqus/Standard, only the soil domain in Figure 1 is modeled (without the void part). The plane strain condition is simulated modeling the soil as Lagrangian material using the CPE4R elements in Abaqus which are 4-node bilinear, reduced integration and hourglass control elements.

Roller supports are used for the left and right vertical faces, while at the bottom hinge supports are used.

3.4 Loading steps

FE modeling consists of two loading steps. At first, the geostatic loading is applied to bring the soil to in-situ stress conditions. As discussed in the following sections that the slope is globally stable after geostatic step for all the cases simulated in the present study. In the second step, the effect of earthquake is applied to the soil elements by increasing the body force in the horizontal direction as a function of pseudostatic coefficient (k_h). The value of k_h is gradually increased with time. In order to avoid numerical issues, the rate of increase of k_h is reduced further when the failure planes are formed by the development of large plastic shear strains. The rate of increase of k_h is low enough to maintain quasi-static conditions, which is one of the requirements of CEL analyses in this type of problem. This has been verified from a number of analyses with slower rate than above, which shows no significant change in the failure patterns.

It is planned to increase k_h to a maximum value of 0.1. All the CEL analyses continue up to this targeted value. However, some analyses using Abaqus/Standard stop before k_h=0.1 because of significant mesh distortion as discussed in the following sections.

3.5 Modeling of Soil

The analyses were performed for undrained condition by modeling soil as elasto-plastic material. The undrained shear strength of soil (s_u) is defined in Abaqus as a function of depth or plastic shear strain, depending upon the case of analyses listed in Section 2. The Tresca yield criterion is adopted in this study. The soil parameters used in the analyses are shown Table 1, unless otherwise mentioned.

4 RESULTS

In the following sections, the development of failure planes is explained using the formation of shear bands in which shear strain concentration occurs. The equivalent plastic shear strain, PEEQ in Abaqus/Standard and PEEQVAVG

in Abaqus CEL is used. Note that, PEEQ and PEEQVAVG represent the plastic shear strain ($= \sqrt{\frac{2}{3}\varepsilon^{pl}:\varepsilon^{pl}}$, where ε^{pl} =plastic shear strain) except in PEEQVAVG weighted average of volume fraction is considered. When an element is completely filled with an Eulerian material (e.g. clay) PEEQVAVG= PEEQ.

Table 1. Geotechnical parameters used in the analyses

| Parameters	Values		Base Layer
	Clay Layer		
Undrained shear strength, s_u (kPa)	Case :1 (Uniform)	60	-
	Case : 2 (Linear increase with depth)	55 to 65	-
	Case : 3 (Linear decrease with γ_p)	65 to 55	-
Undrained Young's Modulus, E_u (MPa)	10		50
Poisson's ratio, ν_u	0.495		0.495
Saturated unit weight, γ_{sat} (kN/m³)	20		20

4.1 Case-1

Figure 2 (a) shows the equivalent plastic shear strains at the end of geostatic loading. Very small plastic shear strains develop at the interface between the clay and base layer below the middle of the slope. However, the slope is stable under this loading condition. Limit equilibrium analyses has also been performed for this slope under geostatic loading (k_h=0) using Slope/W software. The minimum factor of safety (FOS) from the LE analysis is 1.24 that corresponds to the critical slip circle shown in Fig. 2(a). As shown, the critical circle from LE method also passes through the zone where plastic shear strains are calculated from FE analysis and intersects the ground surfaces at point D and E.

With increase in k_h, the FOS gradually decreases (Fig. 2b–f). Figure 2(b) shows that the equivalent plastic strain distribution for k_h=0.07. The shear band reaches the ground surface at point D and at the same time another distinct shear band BF also forms. The zone of plastic shear strain also increases in the right side of point A. The limit equilibrium analysis with Slope/W gives a FOS=1.0 at this level of k_h. The value of k_h that gives FOS=1 is commonly known as the yield coefficient (k_y) (Li 2007, Jibson 2011; Nadi et al. 2014). A comparison of critical circles in Fig. 2(a) & 2(b) shows that the zone of potential failure is higher in Fig. 2(b). FE results are consistent with LE analysis. Moreover, FE analysis could explain the formation of failure planes. In this case, with increase in k_h starting from point A, the failure surface propagates mainly to the downslope and forms the segment AD and then to the upslope and forms the segment AE. Note that, LE methods cannot explain the gradual development of the failure plane.

Finite element analysis of the same problem has been performed using Abaqus/Standard (Lagrangian framework and implicit solution scheme). Plastic shear strains obtained from this analysis at k_h=0.07 is shown in Fig. 2(c). A comparison of strains in Fig. 2(b) and 2(c) shows that, plastic shear strains calculated in Abaqus/Standard are significantly higher than Abaqus CEL.

In order to examine it further, the accumulation of plastic shear strain of a soil element near point A in Fig. 2(a) is considered. Figure 3 shows that the plastic shear strains at this point at low value of k_h is comparable in Standard and CEL; however, the difference between calculated strain suddenly starts to increase at larger value of k_h when mesh distortion occurs.

The inset of Fig. 2(c) shows the distorted mesh at k_h=0.07. Extremely large distortion of soil elements near and the left side of point A occurs in this implicit analysis, although analysis did not stop at this level because of convergence issue. As mentioned before, some authors (e.g. Griffith and Lane 1999; Tan and Sharma 2008) considered the non-convergence of the solution as an indication of failure. Therefore, care must be taken when the non-convergence condition is defined as failure, because it might be only a numerical issue.

Analysis using Abaqus/Standard for k_h>0.07 is not shown because the results may not be acceptable as significant mesh distortion occurs. However, there is no mesh distortion issues in Abaqus CEL and therefore the results for higher values of k_h (0.075, 0.08 and 0.0825) are shown in Fig. 2(d–f). The zone of plastic shear strain increases with k_h and at k_h=0.08 it reaches the ground surface at point E, which is at 30 m right of the crest of the slope, forming a complete failure plane DBAE. In addition, due to movement of the soil elements above this failure plane, another quasi-horizontal shear band AC develops. Considerable heaving also occurs near the toe of the slope (DF in Fig.2).
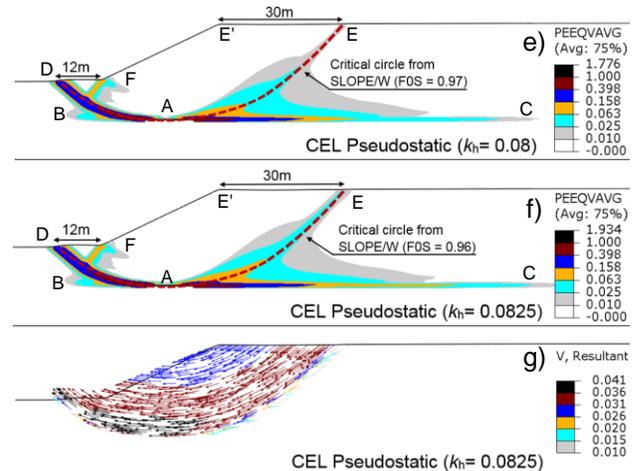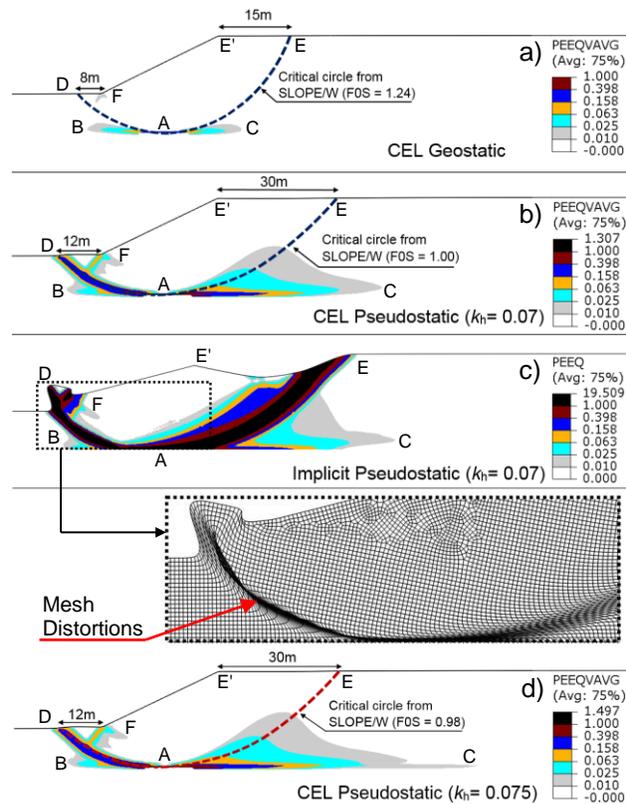

Figure 2. Formation of shear bands and failure planes for uniform undrained shear strength of clay (Case-1)

The instantaneous velocity vector plot at k_h=0.0825 in Fig. 2(g) shows that, the velocity of the soil particle just above the failure plane is higher than the velocity of soil elements far from it (e.g. near the crest) which shows the rotation of the failed soil mass.
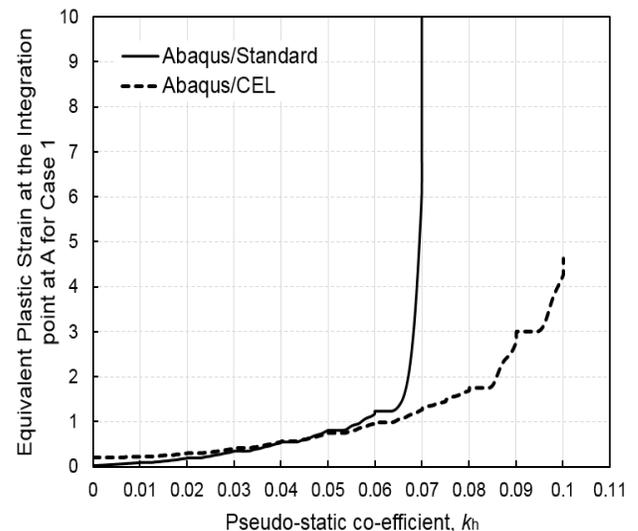

Figure 3. Comparison of Equivalent plastic strain at the Integration point near point A (in Fig. 2) with variations of pseudostatic coefficients (k_h).

Based on the above analyses it can be concluded that, Abaqus CEL can successfully simulate the failure and large deformation of homogeneous clay slopes subjected to earthquake load.

4.2   Case-2

In this case, a linearly increasing s_u profile of clay layer is considered. Figure 4(a), shows the results at the end of the geostatic step. Similar to Case-1, small plastic shear strains develop at the interface between clay layer and base layer under the slope. However, the slope is globally

stable. Slope/W analysis gives the critical slip circle DAE with a FOS=1.29. The yield co-efficient k_y is 0.085, which is slightly higher than that in Case-1.

Figures 4(b)–4(d) shows the development of plastic shear strains with increase in k_h. The failure surface forms gradually with increase in earthquake loading. The shear band AD in the downslope direction forms first and then the shear band AE forms at high k_h (Fig. 4c and 4d). The distance between the point of intersection of the failure plane with ground surface (D, E) from the toe (F, E′) are similar those shown for Case-1 (Fig. 2), which indicates that this slight variation of s_u with depth does not change the failure pattern significantly. Therefore, in the following section uniform initial undrained shear strength is used to investigate the effect of other parameters. Figure 4(e) shows that, once the complete failure plane DBAE develops, mainly the soil element above this plane displaces. The instantaneous velocity vector (in Fig. 4e) also shows rotational movement of the failed soil mass. Moreover, although the shear band AC forms, the instantaneous velocity of soil elements above this band is very small compared to the velocity of soil elements above the failure plane DBAE.
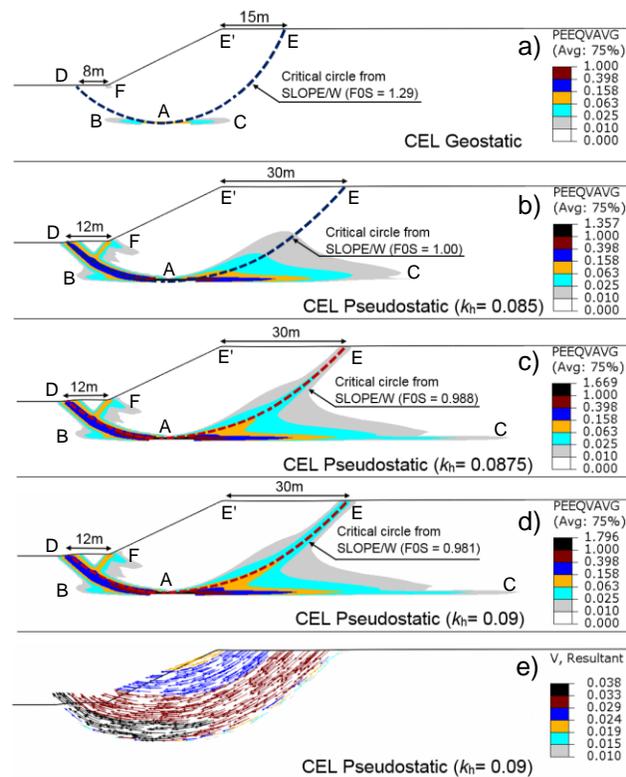

Figure 4. Shear strains and instantaneous velocity for undrained shear strength variations with depth of clay (Case-2)

4.3   Case -3

Field observation and experimental studies show that, during large earthquakes of long duration a significant loss of undrained shear strength could occur in fine grained saturated soils that could lead to large displacement or instability (Yasuhara et al. 2004; Donahue and Bray 2014). The effect of s_u degradation on stability of slope is investigated in this section. Instead of modeling the complete process of strength degradation with cyclic loading, the s_u is reduced by 15% as a linear function of accumulated plastic strain as discussed in Section 2. Note that, the pseudostatic method for slope stability (Seed 1979) was originally developed for earth dams where soil does not undergo significant strength loss (Bray and Travasarou 2009).

Similar to previous cases, Fig. 5(a) shows that at the end of the geostatic step, small shear strains develop near the interface between top clay and strong bottom layer but the slope is globally stable. With the increase in k_h the length of the shear band increases. Figure 5(b) shows that, at k_h=0.06 a complete shear band in the downslope direction (AD) develops. However, in the upslope direction (right side of point A), mainly the zone of plastic shear strain increases by formation of a number of potential shear bands (AE, AH and AG). In order to compare with implicit analysis, the plastic shear strains obtained from Abaqus/Standard is plotted in Fig. 5(c), which shows that a complete failure plane develops at this value of k_h. As discussed before, Abaqus/Standard calculates higher strains than Abaqus CEL.

Figures 5(d), 5(f) and 5(g) shows the shear strains with increase in value of k_h. At k_h=0.075, the shear band reaches the ground surface (Fig. 5d). The extent of failure (i.e. length of DF and EE′) is less than the values obtained for Case-1 or Case-2, because s_u degradation is considered in this case. The instantaneous velocity vector (Fig. 5e) is similar to the previous cases. With the increase in k_h, a clear and distinct circular failure surface, DAE forms (Fig. 5f). After the formation of the circular failure surface, the horizontal shear band AC starts propagating towards the right. At k_h=0.1, another failure surface DAH forms (Fig. 5g). The failure pattern shown in Fig. 5(g) is similar to typical flowslide reported from post-slide observation after earthquake. For example, flowslide at Notre-Dame-de-la-Salette in Québec 2010 formed by successive rotational failure of soil blocks having post-peak strength degradation behaviour (Perret et al. 2013; Demers et al. 2014). The present LDFE analyses could somehow explain this failure pattern.

In Slope/W analyses, s_u degradation with strain cannot be modeled. In order to show some comparison between LE and FE analyses, Slope/W analyses are performed with constant value of s_u=65 kPa (peak) and s_u=55 kPa (residual). The critical circles obtained from these analyses are shown in Fig. 5(g). As expected, FOS reduces with
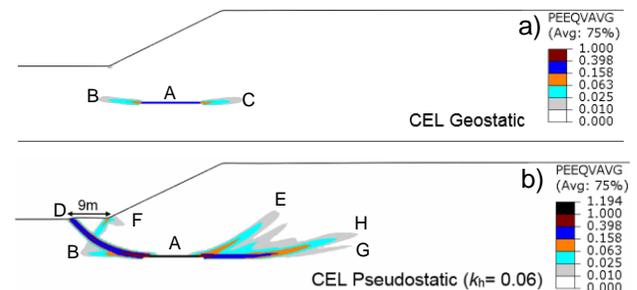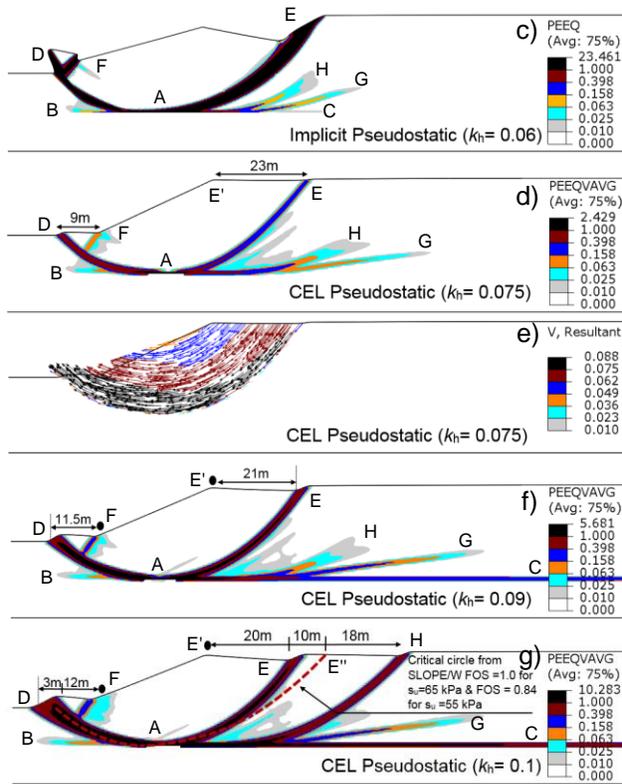
Figure 5. Analyses with post-peak degradation of undrained shear strength of clay (Case-3)

decrease in s_u; however, the location of the critical failure plane does not change. The extent of the failure plane obtained from LE method is larger than that of FE analyses. The critical circle intersects the ground surface at E″ which is 10 m far from E′ obtained from FE analyses.

5   CONCLUSIONS

In this study, the pseudostatic approach is implemented in Abaqus CEL for modeling large deformation behaviour during the formation of failure planes in a clay slopes. Comparison of results obtained from Abaqus CEL and Abaqus/Standard shows that the Lagrangian FE model with Implicit solution scheme over predicts the strains at failure planes when considerable mesh distortion occurs. However, at small strains both solution schemes give similar results. The initial failure planes obtained from CEL analyses are comparable with those obtained from LE analyses using Slope/W software. The CEL analyses could explain the subsequent formation of shear band and failure planes as reported from post-slide investigations, which cannot be explained using the conventional LE method.

REFERENCES

Abaqus 2013. Analysis user manual. Abaqus 6.13.1. Simulia Inc., Dassault Systemes.

Bray, J. D. and Travasarou, T. 2009. Pseudostatic co-efficient for use in simplified seismic slope stability evaluation. *Journal of Geotechnical and Geoenvironmental Engineering*, Technical Notes, ASCE,135: 1336-1340

Demers, D., Robitaille, D., Locat, P. and Potvin, J. 2014. Inventory of Large Landslides in Sensitive Clay in the Province of Québec, Canada: Preliminary Analysis. *Landslides in Sensitive Clays: From Geosciences to Risk Management*, Advances in Natural and Technological Hazards Research 36, J.-S. L'Heureux et al. (eds.), Springer.

Dey, R., Hawlader, B., Phillips, R. and Soga, K. 2015. Large deformation finite element modeling of progressive failure leading to spread in sensitive clay slopes. *Géotechnique*.

Dey, R., Hawlader, B., Phillips, R. and Soga, K. 2016. Numerical modelling of submarine landslides with sensitive clay layers, *Géotechnique.*

Donaque, J. L. and Bray, J. D. 2014. Seismic displacements for the Downtown Anchorage seismic risk assessment. *10th U.S National Conference on Earthquake Engineering*, Frontiers of Earthquake Engineering, Anchorage, Alaska, July 21-25

Griffiths, D. V. and Lane, P. A. 1999. Slope stability analysis by finite elements, *Géotechnique*, 49(3): 387–403.

Jibson, R. W. 2011. Methods for assessing the stability of slopes during earthquakes-A retrospective, *Engineering Geology*,122: 43-50.

Khosravi, M., Leshchinsky, D., Meehan, C. L. and Khosravi, A. 2013. Stability Analysis of Seismically Loaded Slopes Using Finite Element Techniques, *Geo-Congress 2013, ASCE.*

Kovacevic, N., Hight, D. W., Potts, D. M. and Carter, I. C. 2013. Finite-element analysis of the failure and reconstruction of the main dam embankment at Abberton Reservoir, Essex, UK, *Géotechnique*, 63(9): 753–767

Li, X. 2007. Finite element analysis of slope stability using a non-linear failure criterion., *Computers and Geotechnics*, 34: 127-136.

Loukidis, D., Bandini, P. and Salgado, R. 2003. Stability of seismically loaded slopes using limit analysis, *Géotechnique*, 53(5): 463–479.

Nadi, B., Askari, F. and Farzaneh, O. 2014. Seismic performance of slopes in pseudostatic designs with different safety factors. *Iranian Journal of Science & Technology (IJST)*, Transactions of Civil Engineering, 38(C2): 465-483

Perret, D., Mompin, R., Demers, D., Lefebvre, G. and Pugin, A. J. 2013. Two large sensitive clay landslides triggered by the 2010 Val-Des-Bois earthquake, Quebec (Canada), *Implications for risk management* (*AIGTAS IWLC*)

Potts, D. M. and Zdravković, L. 1999. Finite Element Analysis in Geotechnical Engineering: Theory, 1st Edition, ICE Publishing, Thomas Telford Ltd.

Seed, H. B. 1979. Considerations in the earthquake-resistant design of earth and rockfill dams. *Geotechnique*, 293: 215–263.

SLOPE/W 2007, 4th ed. GEOSLOPE International Ltd. Calgary, AB, Canada.

Swan, C. C. and Seo, Y. K. 1999. Limit state analysis of earthen slopes using dual continuum/FEM approaches. *International Journal for Numerical and Analytical Methods in Geomechanics*, 23(12): 1359-1371

Tan, D. and Sarma, S. K. 2008. Finite element verification of an enhanced limit equilibrium method for slope analysis, *Géotechnique*, 58(6): 481–487.

Trapper, P. A., Puzrin, A. M. and Germanovich, L. N. 2015. Effects of shear band propagation on early waves generated by initial breakoff of tsunamigenic landslides, *Marine Geology*, 370: 99–112

Troncone, A. 2005. Numerical analysis of a landslide in soils with strain-softening behaviour, *Géotechnique*, 55 (8): 585–596

Yasuhara, K., Murukami, S. and Hyde, A. F. L. 2004. Post-cyclic degradation of saturated plasticity silts. *Cyclic Behaviour of Soils and Liquefaction Phenomena,* Triantafyllidis (ed), Taylor & Francis Group, London, ISBN 90 5809 620 3.